Delft University of Technology

Thesis

Density wave amplification during long horizontal slurry transport

Experimental studies exploring mechanisms

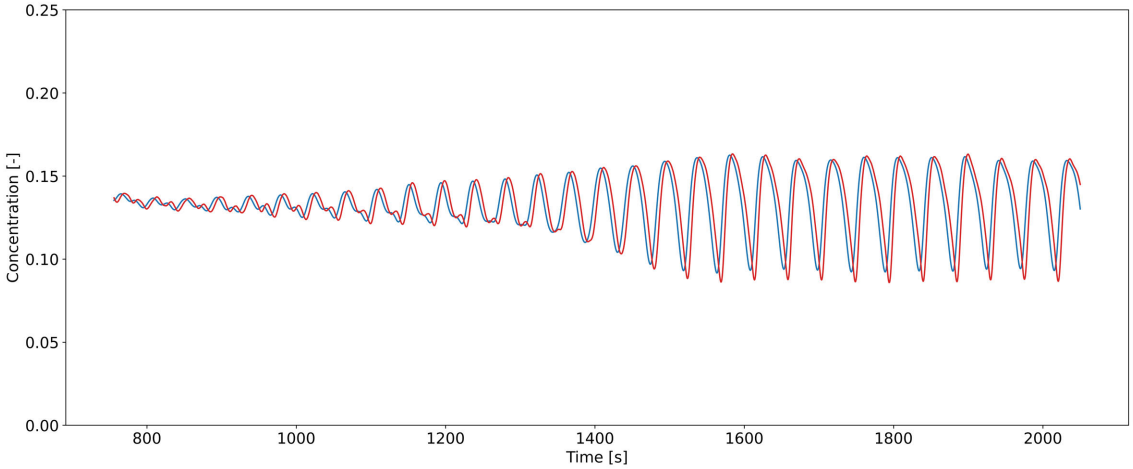

Author:
Oscar van der Ven (4594851)

February 6, 2023

Section of Dredging Engineering

Thesis Committee:
Prof. dr. ir. C. van Rhee
dr. ir. A.M. Talmon

Company supervisor:
ir. E. de Hoog

TU Delft Delft University of Technology

Royal IHC

Abstract

This study is the first to experimentally show two wave mechanisms regarding density wave amplification with long horizontal slurry transport. There is bed-driven and suspended-driven density wave amplification, in which the grain size determines which mechanism is dominant.

Density wave amplification in hydraulic pipeline transport causes significant risk during operation with the consequences of blockage. Current design methodology for pipeline transport considers mixture velocity and density constant over space and time. However, these conditions are only possible in laboratory circuits where conditions can be controlled carefully. In real-world conditions, concentration varies significantly over time due to the natural dredging process in which a dredging vessel takes slurry from the seabed. Density wave amplification can be differentiated into two different flow categories. Both long horizontal transport and a combination of vertical and horizontal transport. With the first category, there are two main theories that explain the amplification of density waves: 'erosion and sedimentation imbalance' and 'the unstable slip point of the bed'. Here, density wave amplification only occurs in the present of a bed. In the second category, there is one theory called the: 'transient accumulation theory' which is applicable to a combination of horizontal and vertical transport. With this density wave, amplification can occur far above the deposit limit velocity. Mixture velocities change when density waves travel from horizontal to vertical orientation and vice versa. When mixture velocity changes density will change. The influence of grain size, concentration and the centrifugal pump on density wave amplification has not been researched yet.

A test loop has been built with an inner diameter of 46mm and a length of 46 meters. The goal of this laboratory circuit is to investigate the mechanisms that result in the amplification of density waves. Two types of density waves were measured: bed-driven density waves occurring with coarse sediments (Dorsilit 7; d_{50} = 1040 μm & Dorsilit 8; d_{50} = 619 μm) and suspended driven density waves occurring with fine sediments (Dorsilit 9; d_{50} = 316 μm & Zilverzand; d_{50} = 240 μm). With bed-driven density waves, there is fast amplification and multiple sharp waves which can result in areas where no concentration is left. With suspended-driven density waves, there is one smooth wave, and amplification takes multiple loop lengths.

Contents

Nomenclature

α	Slip ratio	[–]
α_s	Slip ratio suspension	[–]
ΔP	Differential pressure	[Pa]
Δ	specific density $\frac{\rho_s - \rho_w}{\rho_w}$	[–]
ϵ	Absolute wall roughness	[m]
η	Efficiency pump	[–]
γ	Bed area/pipe area	[–]
$\overline{C}$	Cross sectional averaged concentration	[–]
ρ	density	[kg m^{-3}]
τ_A	Wall shear stress in ascending pipe	[N m^{-2}]
τ_B	Wall shear stress in descending pipe	[N m^{-2}]
A	Area of the inner pipe	[m^2]
B	Width of the bed surface	[m]
C	Concentration	[–]
C_b	suspended load concentration close to the bed layer	[–]
c_w	Wave celerity	[m s^{-1}]
$C_{v,A}$	Volumetric concentration of ascending vertical pipe	[–]
$C_{v,B}$	Volumetric concentration of descending vertical pipe	[–]
C_{vd}	Delivered volumetric solids concentration	[–]
C_{vi}	spatial volumetric solids concentration	[–]
D	Inner diameter pipe	[m]
d_{50}	Particle diameter at 50% in the cumulative distribution	[μm]/[mm]
E	Erosion flux	[kg s^{-1}]
f	Darcy–Weisbach friction coefficient	[–]
f_c	Stepanoff's factor	[–]
g	Gravitational acceleration	[m s^{-2}]
H	Head	[m]
h	Sediment bed height	[m]

I	Moment of inertia	[m^4]
kD	Wavenumber	[–]
L	Length pipeline	[m]
n	Richardson and Zaki (1954)/Garside & Al-Dibouni (1977) settling exponent	[–]
n_0	Porosity of the bed layer	[–]
P	Pressure	[Pa]
R_s	Slip ratio	[–]
Re_p	Reynolds particle number	[–]
S_s	Relative solids concentration	[–]
U	Mean flow velocity	[m s^{-1}]
v_m	Mixture velocity	[m s^{-1}]
v_s	Solids velocity	[m s^{-1}]
v_t'	Hindered settling velocity	[m s^{-1}]
v_{bed}	Upward velocity of the bed surface	[m s^{-1}]
v_{dl}	Deposition limit velocity	[m s^{-1}]
W	Weight	[kg]
w_0	Settling velocity of a single particle	[m s^{-1}]
w_s	Fall velocity of particles in high concentration	[m s^{-1}]

List of Figures

List of Tables

1. Introduction

Pipeline design is based on empirical steady-state models from pipeline energy losses and energy characteristics of centrifugal pumps. Controlled laboratory conditions determine these characteristics, and any concentration fluctuations are allowed to attenuate. In slurry transport pipeline design often the deposition limit velocity v_{dl} is used as a lower limit for safe transport. Research on accurately determining the deposition limit velocity is still undergoing. Ensuring these conditions, however, does not guarantee stability, and varying concentrations could amplify which can result in density wave amplification.

The research topic of density waves in slurry transport first came to attention at the construction of the Prins Clausplein highway junction, where the equally named 10 km long Prins Clausplein pipeline was in operation. This pipeline was 650 mm in diameter and had a total of 3 booster stations, transporting medium to fine sand. During operation fluctuations in density were observed at the booster stations where density and flow measurements were taken. Fluctuations in density are typical in slurry transport due to the dredging process (Matoušek, 1996). However, it was unusual that the fluctuations in density took the form of amplification of density waves. This phenomenon was first investigated by Matoušek (1995, 1996), where the conclusion was made that the effect of amplifying density waves is a product of the variable slip ratio, see Equation 1.1.

$$R_s = \frac{v_s}{v_m} \tag{1.1}$$

Where v_s is the velocity of the particles and v_m the velocity of the mixture. By which the slip ratio increases with increasing slurry density, and therefore the solids flow brings instability into the pipeline, even when the slurry flow rate is approximately constant.
The conclusion that the amplifying density waves were a product of the slip ratio was later rejected by Talmon (1999).

$$\frac{\partial \overline{C}}{\partial t} + \frac{\partial \alpha U \overline{C}}{\partial x} - \frac{\partial \epsilon \frac{\partial \overline{C}}{\partial x}}{\partial x} = 0 \tag{1.2}$$

With a 1D mass continuity equation (Figure 1.2) a model was made to investigate the effects of the slip ratio on the density waves. The first term is the time dependency of the concentration, $\overline{C}$. The second term is the advection of particles by the flow, depended on $\overline{C}$, the mixture velocity U and the integration coefficient α. The third term is the longitudinal dispersion of particles by the flow (with a diffusion coefficient ϵ). The variable slip was assumed to be a linear function of the local cross-sectional averaged concentration, which makes the advection term non-linear. Imputing a periodic wave function for the concentration resulted in sawtooth shape waves relatively fast, which decreased in amplitude over time (see Figure 1.1a). The conclusion was made that density wave amplification can not be explained by variable slip, and thus Talmon (1999) refuted the conclusion made by Matoušek (1995,1996).

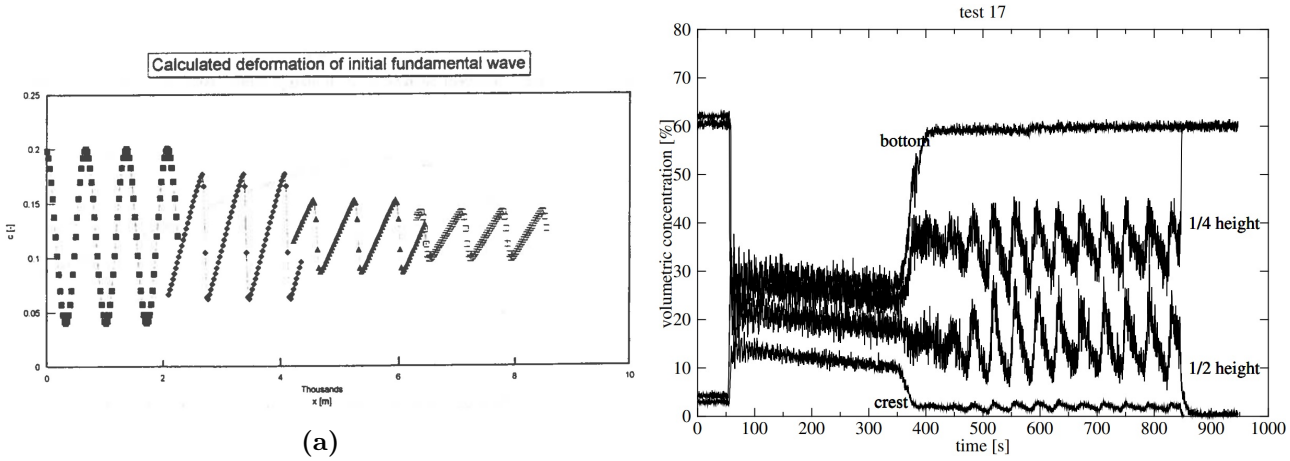

Figure 1.1: (a): Simulated concentration fluctuations to see the effect of the slip ratio on density wave amplification (Talmon, 1999), (b): examples of concentration fluctuations during an experiment (Talmon et al., 2007).

The new hypothesis was that the disequilibrium of erosion and sedimentation, occurring at the interface between the bed layer and the suspended layer is the cause of density wave amplification. At low concentrations, the sedimentation flux increases with concentration, and at high suspended load concentrations the sedimentation flux decreases due to hindered settling. This adverse process could favour density wave amplification due to the net transfer of sand from the bed layer to the suspension layer. The disequilibrium of erosion and sedimentation was hypothesised as the cause of density wave amplification using a linear stability analysis of stationary bed conditions, where in section 2.2.1 it is discussed in more depth. Matoušek (2001) re-evaluated the original data of 1981 of the Prins Clausplein pipeline and showed that the amplification occurred both in stationary bed regime and sliding bed regime. Talmon (2002) showed that also the sliding bed regime is caused by the disequilibrium of erosion and sedimentation using linear stability analysis of wave development conditions.

Talmon et al. (2007) further investigated the phenomena of density wave amplification with a test loop experiment trying to validate the linear theory described above. During the experiment amplifying density waves were observed and successfully measured. A thin bed layer is sufficient for density wave development to commence. At low concentrations the limiting velocities for a stationary deposit and full suspension nearly coincide. At high concentrations corresponding flow velocities differ more because of a widening of the intermediate regime with sliding patches of grains. As well as in the linear analysis of sliding abd stationary bed conditions the observation of sawtooth-shaped waves was also observed in the experiment. According to Talmon (1999, 2002), the cause of the sawtooth-shaped waves is due to variable slip (see Figure 1.1b). The amplification, however, is explained by the disequilibrium of erosion and sedimentation, due to hindered settling. It is concluded that for amplifying density waves to occur a bed layer is necessary.

Matoušek and Krupicka (2013) studied the unsteady flow of solids in a laboratory slurry pipe loop, with horizontal and vertical sections. Amplifying density waves were observed, wave celerity and wavelength were estimated from differential pressure signals (DP-signals), torque of the centrifugal pump and pressure at the outlet of the centrifugal pump (outlet pressure). It was deduced that there were four waves circulating through the loop, no matter whether the loop was short or long (extended). The theory of why density wave amplification occurred differed from the previously mentioned theory of the disequilibrium between erosion and sedimentation. Matoušek and Krupicka (2013) argued that the amplification was due to the unstable slip point of the bed. Meaning that, at low concentrations the transition between stationary- to sliding bed regime is smooth. However, at high concentration, a large volume of eroded deposit, and consequently a high hydraulic gradient ($\frac{\Delta P}{\rho_f g L}$), results in an unstable slip point. This can cause the sediment bed to shake or fully erode, further amplifying density waves. Also, the theory of restratification effect was mentioned, where above a certain mixture velocity the flow exhibits a gradual restratification under the further increasing of the mixture velocity (Matoušek, 1997). This restratification is the signature of a standing wave in a heterogeneous transport regime. Further information about restratification can be found in section 2.2.2.

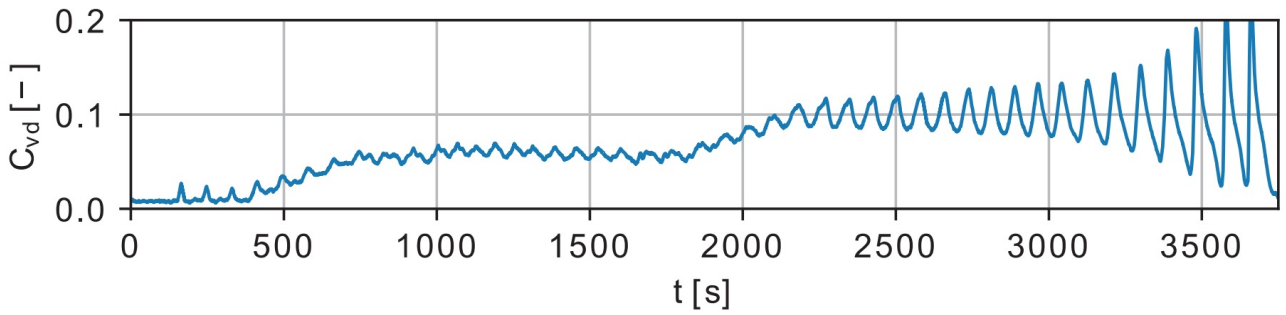

Figure 1.2: An example of a data set recorded in the Freiberg experiment circuit. $D = 150\text{mm}, d_{50} = 600\ \mu\text{m}, c = 0.05, 0.1$ (de Hoog et al., 2021a).

In 2017 a large-scale experiment was performed by Royal IHC and TU Bergakedemie Freiberg, in Halsbrücke, Germany. A 150 mm diameter loop was partially constructed in a vertical mine shaft, with a total vertical length of 242 meters, and 57 meters in horizontal length. During the experiment density wave amplification was common (see Figure 1.2), and tests had to be ended prematurely due to growing density waves that lead to excessive power requirements. It is hypothesised that in this circumstance the cause of density wave amplification was caused by a different process than the sedimentation erosion imbalance described by Talmon (1999). De Hoog et al. (2021a) explained a different process with transient accumulation, where the difference in particle velocity between horizontal and vertical pipelines with similar mixture velocities is thought to contribute to the amplification of density waves. Again, this process is explained by the slip ratio, and thus is thought again to be playing a role in density wave amplification. See section 2.2.3 where it is discussed in further depth.

1.1 Problem definition

The topic of density wave amplification has not been researched widely. Experimental data are limited, and real-world pipeline data are even more scarce. The data that are available are already analysed and researched. An experimental study into the system dynamics of density waves could therefore be beneficial to further develop knowledge about density wave amplification. More specific, the influence of the pump on density wave amplification on long horizontal transport could be investigated, an influence which has not yet been researched. The Freiberg data (discussed in 2.2.3) and model reveal that the pump has an instrumental part in the formation of density waves. The pump could therefore possibly also have an effect on growing density waves with a bed layer present. If the mixture density changes,

the operating point of the pump shifts, resulting in mixture velocity variations. These mixture velocity variations can change the bed height if stratified conditions are present or arise. With the formation of a bed, unstable density wave amplification could develop. Also, the grain size has an important role in the amplification of density waves, which current research has not investigated extensively. The theory of the "unstable slip point of the bed causing amplification" by Matoušek and Krupicka (2013) and the theory of the "imbalance between erosion and sedimentation" by Talmon et al. (2007) are two different theories explaining amplification of density waves for long horizontal transport. Could both theories be right, by which grain size is dominate in determining which theory is correct? Therefore there are two main questions that could be investigated: 1. What effect do grain size and concentration have on density wave amplification? 2. Could the centrifugal pump play an essential role in the development and amplification of density waves, which was the case in the Freiberg experiments (de Hoog et al., 2021b) This thesis focuses on the first research question.

1.2 Research questions

Main-research question thesis:

1. What is the effect of concentration, grain size and mixture velocity on density wave amplification?

   Sub-questions thesis:

   (a) What system dynamics play a role in amplifying density waves?
   (b) What is the influence of the centrifugal pumps on density wave amplification?

Main-research question of the literature study:

2. What is the current state of amplifying density wave research?
   Sub-questions literature study:

   (a) What is the best design approach for a test loop to further develop knowledge about density wave amplification?
   (b) What is the governing physical process that causes amplifying density waves?

2. Literature

2.1 Basic slurry transport

In this chapter some of the fundamentals of slurry transport are explained.

2.1.1 Mixture flow

Mixture flow consists of a combination between solids and liquid. Volumetric concentration can be described by the following equations:

$$\rho_m U_m = \rho_f U_f + \rho_s U_s \tag{2.1}$$

Where ρ is the density of the mixture, fluid and solids respectively. Considering that $U_m = U_s + U_f$ and $C_v = \frac{U_s}{U_m}$, Equation 2.2 derives to the following equation:

$$C_v = \frac{\rho_m - \rho_f}{\rho_s - \rho_f} \tag{2.2}$$

For flowing mixtures the concentration must be further specified because the delivered concentration may be different than the spatial volumetric concentration (see Equation 2.3 and 2.4).

$$C_{vi} = \frac{U_s}{U_m} \tag{2.3}$$

$$C_{vd} = \frac{Q_s}{Q_m} \tag{2.4}$$

Where Q_s and Q_m are the flow rates of the solid and mixture, respectively. Differences in delivered concentration in mixture flow can be explained by the different flow regimes that occur in slurry transport in a pipeline. These regimes explained by Matoušek and Talmon (2021) are visualised in figure 2.1.

2.1.2 Flow regimes

These flow regimes are caused by certain flow transitions, like the critical velocity and the deposition limit velocity. The critical velocity is described by van der Berg and Stam (2013) as: "the minimum velocity required for transport of solid material through a pipeline without any particle deposition". The critical velocity should not be confused with the deposition limit velocity defined by Wilson et al. (2006). Where it is defined as the transitional velocity when a stationary bed occurs.

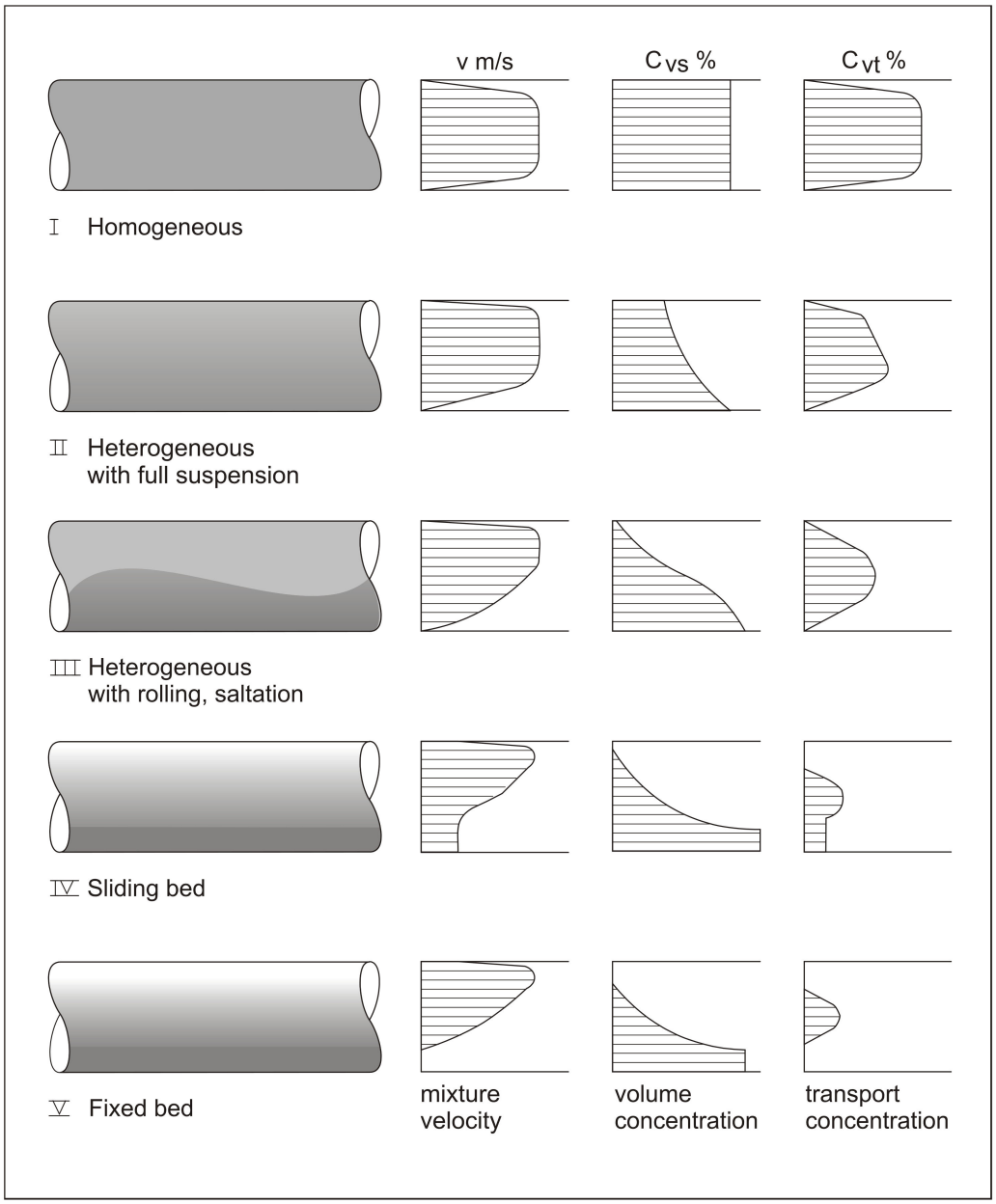

Figure 2.1: Different mixture flow regimes (Miedema, 2019).

Homogeneous flow

Fully homogeneous flow occurs with non-Newtonian mixtures like clay, silt and coal-ash mixtures in high concentrations. Also with sand homogeneous flow can occur at very high mixture velocities. Turbulent flux dominates the flow with respect to deposition processes.

Heterogeneous flow with full suspension

With coarse silts or fine sand mixtures, heterogeneous flow can occur, and velocities need to be significantly higher than the deposition limit velocity. Particles are not fully suspended, and higher concentrations occur near the bottom of the pipe.

Heterogeneous flow with rolling saltation

Stratified conditions are developing. A combination of creep, saltation and a full suspension occurs. This creates dynamic dunes moving at the bottom of the pipe. There is enough turbulence to suspend some of the smaller particles.

Sliding bed

Fully stratified flow occurs, mixture velocity is below the critical velocity and the sliding bed phenomena occurs. The large majority of the concentration moves in the bed, and the very fine particles are in suspension depending on particle size distribution (PSD).

Fixed bed

Flow is below the deposition limit velocity, which causes the majority of the particles to settle. There is not enough shear stress caused by the flow for a sliding bed. Depending on the particle distribution very fine particles could still be in suspension.

2.1.3 Settling velocity

In slurry transport sediments are transported in water, the mixture of sediment and water consists of small suspended particles. These single particles have a settling velocity (see equation 2.5) that depend on local conditions like particle size, specific density and viscosity.

$$\omega_0 = \sqrt{\frac{4\Delta g d}{3C_d}} \tag{2.5}$$

Where Δ is the specific density, g the gravitational acceleration, d the particle diameter and C_d the drag coefficient which is dependent on the particle Reynolds number.

$$\begin{aligned} Re_p < 1 &\longrightarrow C_d = \frac{24}{Re_p} \\ 1 < Re_p < 2000 &\longrightarrow C_d = \frac{24}{Re_p} + \frac{3}{\sqrt{Re_p}} + 0.34 \\ Re_p > 2000 &\longrightarrow C_d = 0.4 \end{aligned} \tag{2.6}$$

When the concentration of a mixture is very high, the settling velocity of a single particle is reduced. This is due to the displacement of water flowing up as the particles move down, thus increasing drag on the nearby particles. This hindered settling velocity is can be described with the following equation (Richardson & Zaki, 1954):

$$\omega_s = \omega_0(1 - C)^n \tag{2.7}$$

$$n = \frac{4.7 + 0.41 Re_p^{0.75}}{1 + 0.175 Re_p^{0.75}} \tag{2.8}$$

Where exponent n in Equation 2.7 is a function of the particle Reynolds number, defined as: $Re_p = \frac{\omega_0 * d}{\nu}$.

2.1.4 Two-layer model

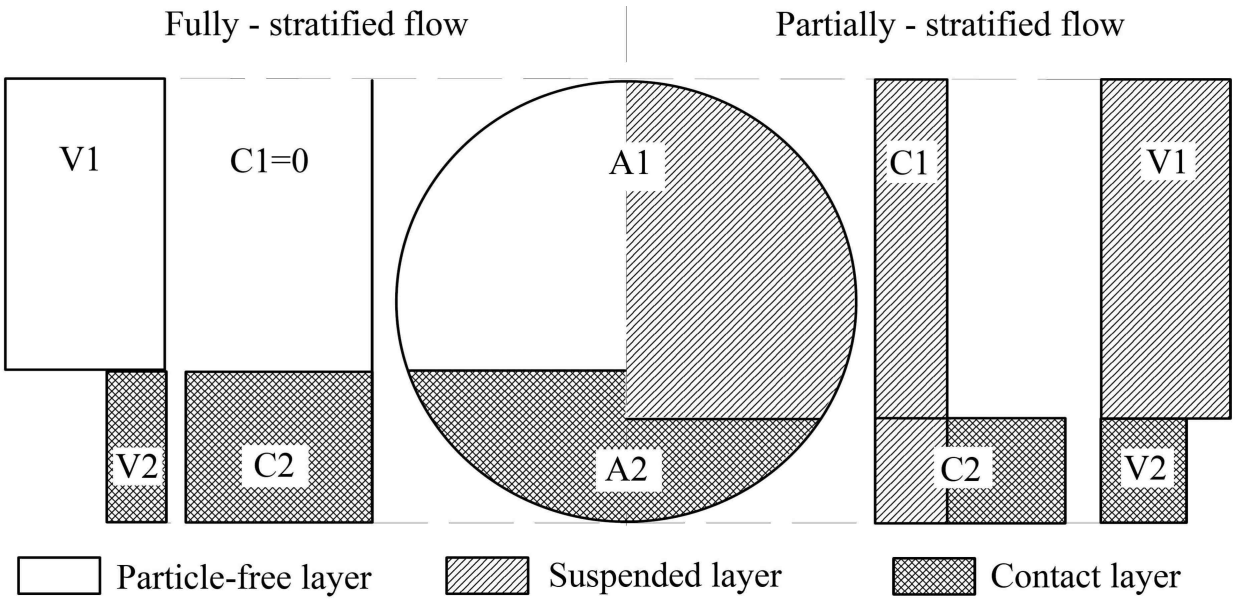

Figure 2.2: Schematic cross section of the two-layer model (Matoušek & Talmon, 2021).

The different flow regimes that are discussed where stratified or partially stratified conditions are present are frequently modelled by a simplified two-layer model. Originally the model comes from Wilson (1992). In this model fully stratified and partially stratified flows are modelled (see Figure 2.3). For fully stratified conditions there is a particle-free layer and a contact layer (bed layer). For partially stratified conditions there is a suspended layer and a contact layer (bed layer). Some important assumptions made by the model is that the suspended particles have no contact with other particles and flow boundaries. Furthermore, the velocity distribution is simplified to a uniform flow for both layers. There are two physical mechanisms for solids flowing through a pipeline, interparticle contact (bed layer), and particle suspension in the carrying liquid (Matoušek & Talmon, 2021). The force balance between the two layers (driving and resisting forces) governs the behaviour of the flow.

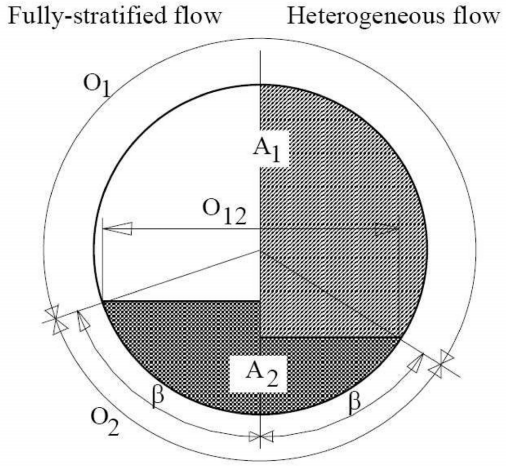

Figure 2.3: Schematic cross section of the two-layer model (Matoušek & Talmon, 2021).

Mathematical formulation of the two-layer model

The two-layer model consists of conservation of mass and momentum equations for both layers. The mass balance brings the following equation:

$$V_m A = V_1 A_1 + V_2 A_2 \tag{2.9}$$

Where V is the velocity, and A the inner area of the of the pipe, depending on the subscripts explained in Figure 2.2 and 2.3. The momentum balance for the two layers is different depending on the suspended or bed layer. For the suspended layer the momentum balance is:

$$\Delta P A_1 = \tau_1 O_1 L + \tau_{12} O_{12} L \tag{2.10}$$

Where O is the circumference, L the length of the pipe and τ the Coulombic interparticle shear stress between the suspension and the bed. The bed layer has the following momentum equation:

$$\Delta P A_2 + \tau_{12} O_{12} L = (\tau_{2f} + \tau_{2s}) O_2 L \tag{2.11}$$

Here the notable difference between the two momentum equations is that the bed layer has shear stress that describes the mechanical friction between the wall and the particles (τ_{2s}). Both layers have shear stress terms that describe the viscous shear stress at the flow boundaries (τ_1, τ_2 and τ_{2f}). Combining Equation 2.10 and 2.11 gives the force balance for the whole pipeline section:

$$\Delta P A = \tau_1 O_1 L + (\tau_{2f} + \tau_{2s}) O_2 L \tag{2.12}$$

Figure 2.2 and 2.3 gives an schematic view of the variables and used subscripts of Equations 2.9, 2.10, 2.11 and 2.12.

2.2 Literature of density wave amplification

There are three scientists that have the biggest contribution towards density wave amplification research: Prof. dr. Ir. Václav Matoušek, dr. Ir. Arno Talmon, and Ir. Edwin de Hoog. These main research contributions are summarised in this chapter.

2.2.1 Prins Clausplein pipeline

With the construction of the highway intersection Prins Clausplein in 1981 near The Hague sand-water slurry was transported in an equally named Prins Clausplein pipeline. The 10 km long pipeline, with 650 mm diameter transported medium to fine sand. Using a cutter suction dredger and three additional booster pump stations sand was transported through the pipeline. The density was measured at the cutter suction dredge, and at two additional booster stations (1,886m, Jagerplas and 6538m, Duinjager). Matoušek (1996) first investigated the occurrence of density waves that were measured, see Figure 2.4.

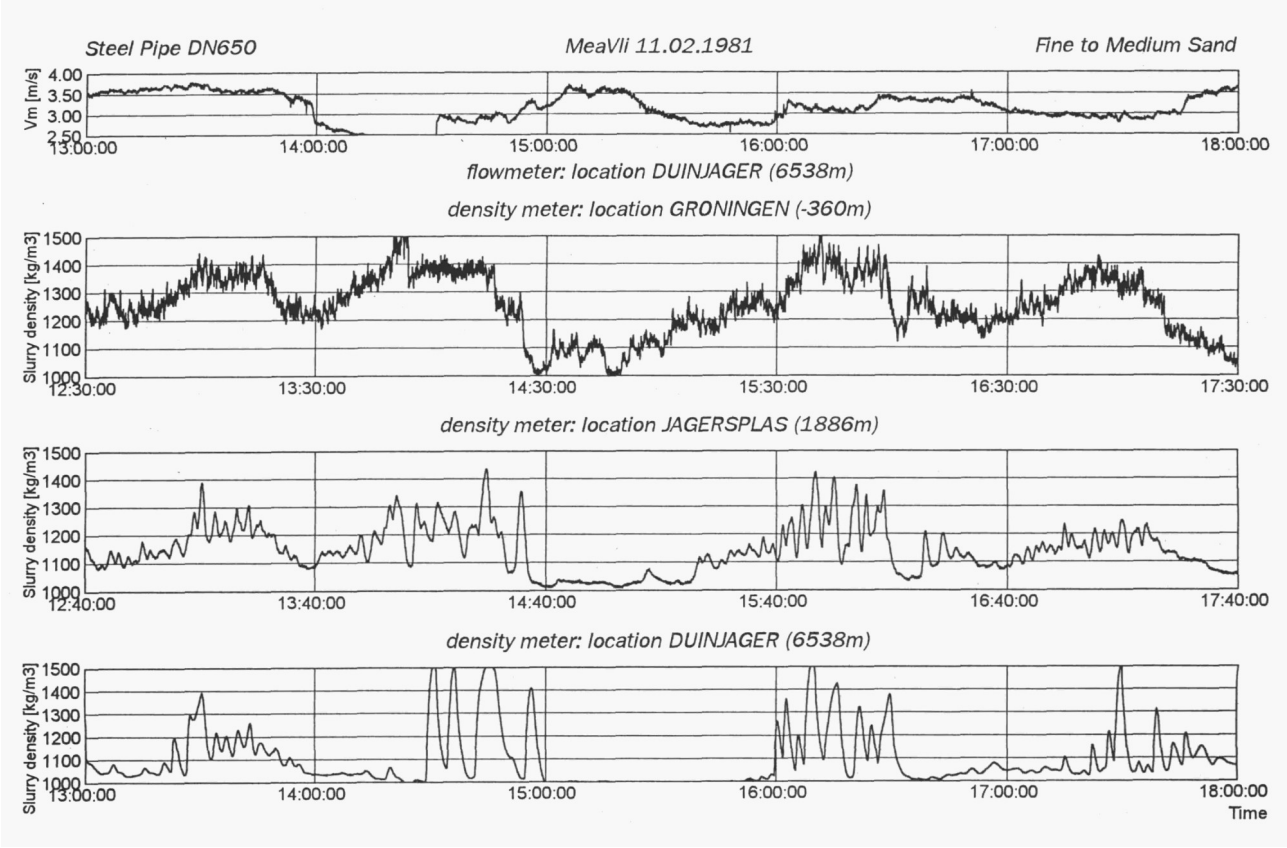

Figure 2.4: Density waves measured along DN650 pipeline (11/02/81 13:00-18:00), first graph: measured mixture velocity, other graphs are mixture density measurements (Matoušek, 1996).

The figures are shifted in time to visualise the development of the density waves. It can be seen that between 14:30 and 15:30 a low-density mixture enters the pipe, and is relocated to other parts of the flow. At Duinjager the same flow consists almost only of water. The mixture accumulates in density waves, where peaks of 1000 kg/m^3 and 1500 kg/m^3 are measured (the limit of the density meter). The deposition limit velocity was not determined during operation, however later it was determined by Matoušek (2001) to be just above the deposition limit velocity. Matoušek (1996) made the conclusion that density wave amplification was caused by the variation of axial slip. At high mixture velocities, the variation of axial slip becomes smaller comparatively than at low mixture velocities. This was later refuted by Talmon (1999) with the use of the Burgers equation (see Equation 2.13).

$$\frac{\partial \overline{C}}{\partial t} + \frac{\partial \alpha U \overline{C}}{\partial x} - \frac{\partial \epsilon \frac{\partial \overline{C}}{\partial x}}{\partial x} = 0 \tag{2.13}$$

where α is the slip ratio. Talmon (1999,2007) proved that with Equation 2.13 the linear and non-linear model of the slip ratio always leads to decreasing sawtooth-shaped waves. It is however assumed that the mixture velocity is based on the average velocity of all the particles in the mixture. In specific circumstances (dominant advection) small particles overtake larger particles which could result in amplifying density waves. However in natural sediments advection does not dominate the transport process over axial dispersion, and thus the effect of density wave amplification or plug forming due to difference in mixture velocity does not occur (van Wijk et al., 2015).

Talmon (1999) argued that the variable slip is not unique to pipeline transport. And that it also occurs in open channel flow, flow in rivers and in estuaries, but at much lower sand concentrations levels. In these situations, the amplification in concentration occurs through the disequilibrium of erosion and sedimentation (Talmon, 1992), and not variable slip. Talmon (1999) further validates his hypothesis

by using a mass continuity equation for the suspended load.

$$\frac{\partial A\overline{c}}{\partial t} + \frac{\partial \alpha_s AU\overline{C}}{\partial x} = \frac{\partial A\epsilon \frac{\partial \overline{C}}{\partial x}}{\partial x} + (-w_s C_b + E_{erob} - v_{bed} C_b)B \tag{2.14}$$

$$v_{bed} = \frac{w_s C_b - E_{er}}{1 - n_0 - C_b} \tag{2.15}$$

Where α_s is the slip ratio of the suspension, C_b the suspended load concentration near the bed layer, B the width of the bed surface, E_{erob} the erosion flux of the bed, E_{er} the erosion due to turbulence and $n0$ the porosity of the bed. Equation 2.15 calculates the vertical velocity of the bed. The sedimentation and erosion flux are linearly approximated, resulting in a linear approximation of the vertical velocity of the bed surface. The mass continuity Equation 2.14 also gets linearised. In the numerical solution, the calculated wave complex celerities are displayed as a function of the dimensionless wavenumber, see Figure 2.5. It can be seen that with a dimensionless wavenumber of 0.006 amplification is the largest, which results in a wavelength of 640 meters. This is comparable to the field data presented by Matoušek (1996), further confirming the hypotheses of the disequilibrium that exists between erosion and sedimentation causing density wave amplification.

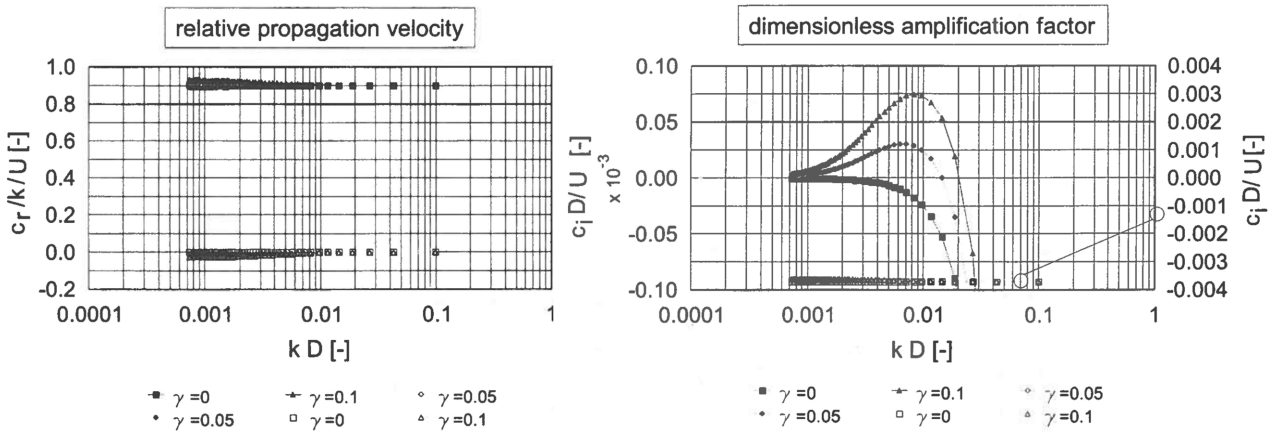

Figure 2.5: Complex celerities of density waves as a function of the wavenumber (Talmon, 1999).

Interestingly Matoušek (2001) states that the influence of the pump performance has been observed to be negligible according to the data analysis of the Prins Clausplein pipeline.

2.2.2 Laboratory Loops

There are three laboratory loops made with published articles that researched amplifying density waves. Talmon et al. (2007), Matoušek & Krupicka (2013), de Hoog et al. (2021b). Van Wijk et al. (2022) and van Wijk et al. (2015) also made two laboratory loops, however, density wave amplification was not the main research focus. Furthermore, the research was primarily about manganese nodules and vertical transport which is only partly applicable to this research, see section 2.2.3 for more information on vertical transport.

A.M. Talmon laboratory loop

Talmon et al. (2007) used a horizontal loop, with several pressure meters, a radioactive density meter and a flow meter (see Figure 2.6). The laboratory circuit had a diameter of 100 mm and a total length of 52 meters. Sand of d_{50} = 200 μm and d_{85}/d_{50} = 1.9 was used. Several perplex observation sections were made to observe the bed on the bottom of the pipe, and its character (stationary or sliding).

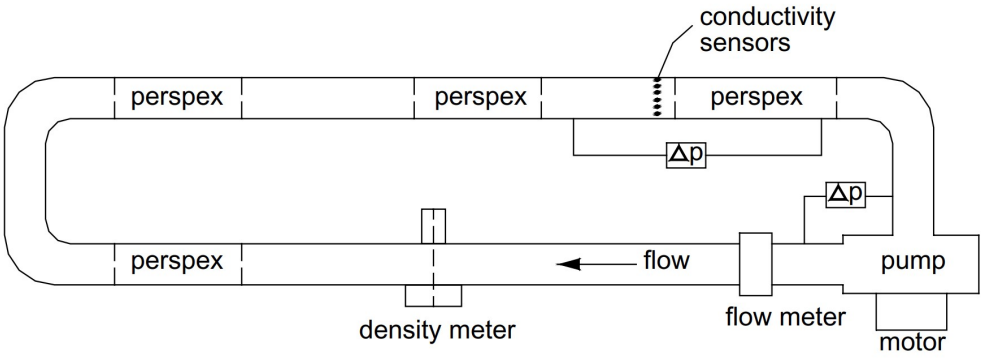

Figure 2.6: Sketch of the laboratory circuit, not to scale (Talmon et al., 2007).

Mean solids concentrations of [14,18,25,30] percent volumetric concentration were first tested with a flow velocity of U = 0.5-6 m/s, by stepwise increasing pump rpm. This was done to determine the flow resistance and identify the transition of flow characteristics, like full suspension transition. Critical flow velocity for density wave development was also determined (see Table 2.1). Notice that the flow rate at which incipient density waves form is lower than the flow rate at which there is a bed present. In long horizontal configurations, density wave amplification can only occur if there is a bed present.

Table 2.1: Characteristic flow velocities of the laboratory loop used in Talmon et al. (2007).

	Incipient density wave development U_{cr} (m/s)	Transition: stationary bed layer/thin layer of sliding grains U (m/s)	Full suspension U(m/s)
14 v%	1.93	2.04	2.14
18 v%	1.81	2.01	2.21
25 v%	1.6	2.01	2.27
30 v%	1.25	1.86	2.25

When flow velocity was near the point of incipient instability, small amplitude harmonic density variations developed into larger amplitude sawtooth-shaped density waves. These sawtooth-shaped waves were predicted by Talmon (1999), and are caused by variable slip (the shape of it, not amplification). Wave periods observed had a period equal to the circulation time of the flow. Bed height was observed to vary with the passage of a density wave. At the approach of a density wave the bed height increases and at the passage the bed height decreases. Interestingly it is stated that the pressure variations over the pump are small, and wave celerity has been observed to be lower than the mixture velocity (50-95%).

At low concentrations the limiting velocities for a stationary deposit and "full suspension" nearly coincide. At the highest concentrations corresponding flow velocities differ more, because of a widening of the intermediate regime with sliding patches of grains (Talmon et al., 2007). The development of density waves is caused by the adverse relation between settling flux and solids concentration including the presence of a sliding/stationary bed layer.

Matoušek 2013 laboratory loop

The loop used in Matoušek and Krupicka (2013) was comparable in length (52 meters length and 100 mm diameter) with the previous loop of Talmon et al. (2007), and could be extended with an additional 41 meters. Overall the loop is more complex with a combination of vertical, horizontal and

inclinable sections (see Figure 2.7). Ballotini with d_{18} = 0.45 mm, d_{50} = 0.53 mm and d_{84} = 0.6 mm with specific gravity of S_s = 2.46 was used as a sediment.

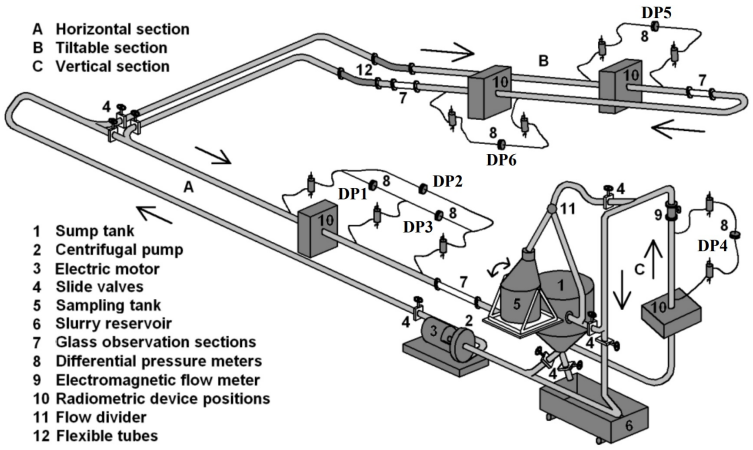

Figure 2.7: Schematic sketch of the laboratory loop (Matoûsek & Krupicka, 2013).

The hydraulic gradient was measured using the different pressure sensors (see Figure 2.7 and 2.8). The development of the hydraulic gradient for DP2 is rather different than that of DP4. Matoušek calls it the restratification effect. Where normally one expects that an increase in mixture velocity results in a decrease of stratification, but with certain mixture velocities an increase in flow exhibits gradual restratification (Matoûsek, 1997). This theory of restratification was later further investigated by Talmon et al. (2019) and it was concluded that the restratification effect appears when internal structure and fluid pressures are measured close to a disturbance such as a bend.

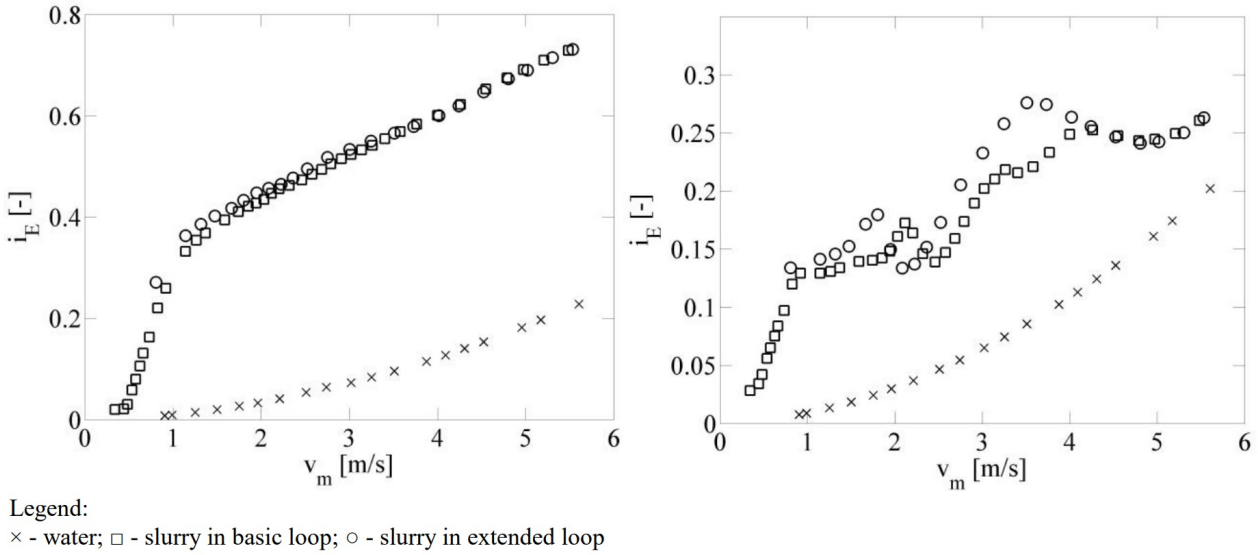

Figure 2.8: Measured hydraulic gradient of DP4 (left) and DP2 (right) (Matoûsek & Krupicka, 2013).

From the tests performed it was deduced that there were four density waves circulating through the loop, and extending the loop did not have any effect on the number of waves present. The wave celerity was estimated from the DP-signals, torque of the pump, and outlet pressure. In vertical sections the wave celerity was approximately the same as the mixture velocity ($c \approx v_m$) while at horizontal pipe sections $c \approx 1.3$ m/s and $v_m = 0.83$ m/s, due to the presence of deposits below the discharge area (Matoûsek & Krupicka, 2013). Using fast Fourier transform the periodicity of the waves in the loop

was determined (12.5 seconds and 21.5 seconds for the extended loop). With the combination of wave celerity and periodicity, the number of waves could be determined. At some velocities, a passing wave caused a local sliding bed. As to why there was amplification of density waves Matoušek argued that the amplification was due to the unstable slip point of the bed, where higher concentrations erode the bed.

It is remarkable that the wave celerity deduced is higher than the mixture velocity flowing in the pipe system. Also four waves in one loop are higher than what was observed in Talmon et al. (2007). In section 2.3 these phenomena are discussed in more detail.

It is concluded that strong density waves developed near the deposition limit velocity. The number of waves appeared to be independent of the length of the loop. And that it is unclear where the waves were generated.

De Hoog 2021 laboratory loop

De Hoog et al. (2021b) conducted a flow loop test with larger particles compared with the other laboratory loops discussed. The diameter of the pipe was also 100 mm. Maximum flow loop length was 26.7 meters, and two different gravels were tested, d_{50} = 6.3 mm and d_{50} = 12 mm. Deposition limit velocity for horizontal pipe orientation for both gravels were determined to be 0.75 m/s and 1.28 m/s respectively. Deposits were detected in the lower part of the s-bend (see the red ellipse in Figure 2.9) at 1.9-1.8 m/s. This means that the lower bend of the s-bend dictates the deposition limit velocity for the entire system.

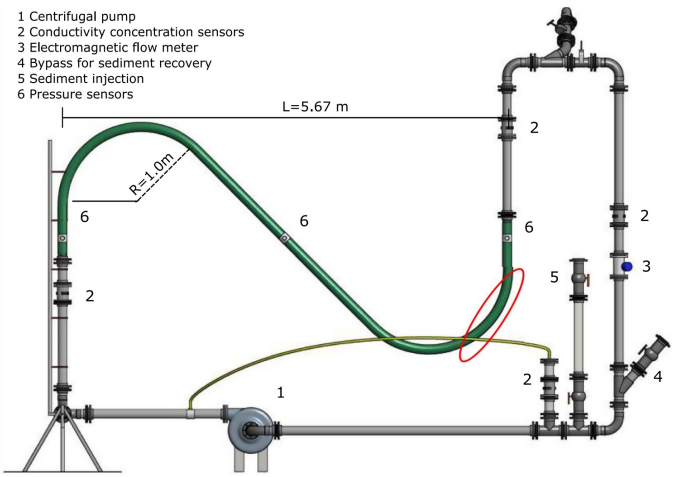

Figure 2.9: Sketch of the laboratory loop used by de Hoog (de Hoog et al., 2021b).

With the small gravel, density wave amplification occurred above its horizontal deposition limit velocity of 0.75 m/s. The wavelength was observed to be the entire length of the system. Density wave growth was however significantly lower than observed by Talmon et al. (2007), this can be explained by the presence of vertical pipe sections where deposits cannot settle. Half the loop consists of these vertical sections where density waves cannot amplify. At high mixture velocity, density wave amplification is hardly noticeable, but over a long time span it can be seen that amplification occurs, see Figure 2.10(d). At lower mixture velocities, amplification is more apparent, see 2.10(b). Axial dispersion is low for gravels in vertical pipes (van Wijk et al. 2014), with fine sands axial dispersion can cause smoothing which could create damping effects. Again as observed by Talmon et al. (2007) wave crests of density waves eroded deposits, and grew again in the passing tail. This 'caterpillar wave' behaviour substantiates the erosion and sedimentation imbalance theory. Above an average mixture velocity of 2.2 m/s there was no density wave amplification because there was no bed present. De Hoog et al. (2021b) confirmed that the stability of the system is directly related to the deposition limit velocity, and if there is even a small local deposit in the system, stability could be compromised due to growing density waves.

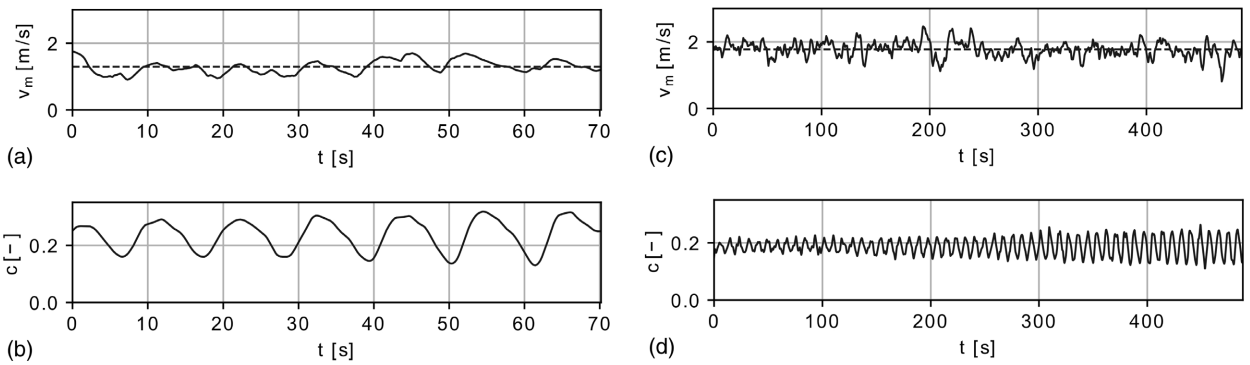

Figure 2.10: Density wave amplification in de Hoog et al. (2021b): (a) density wave growth: low mixture velocity over time, d_{50} = 6.3 mm; (b) density wave growth (low mixture velocity): concentration over time, d_{50}= 6.3 mm; (c) density wave growth: high mixture velocity over time, d_{50}= 6.3 mm; and (d) density wave growth (high mixture velocity): concentration over time, d_{50}= 6.3 mm (de Hoog et al., 2021b).

2.2.3 Freiberg loop

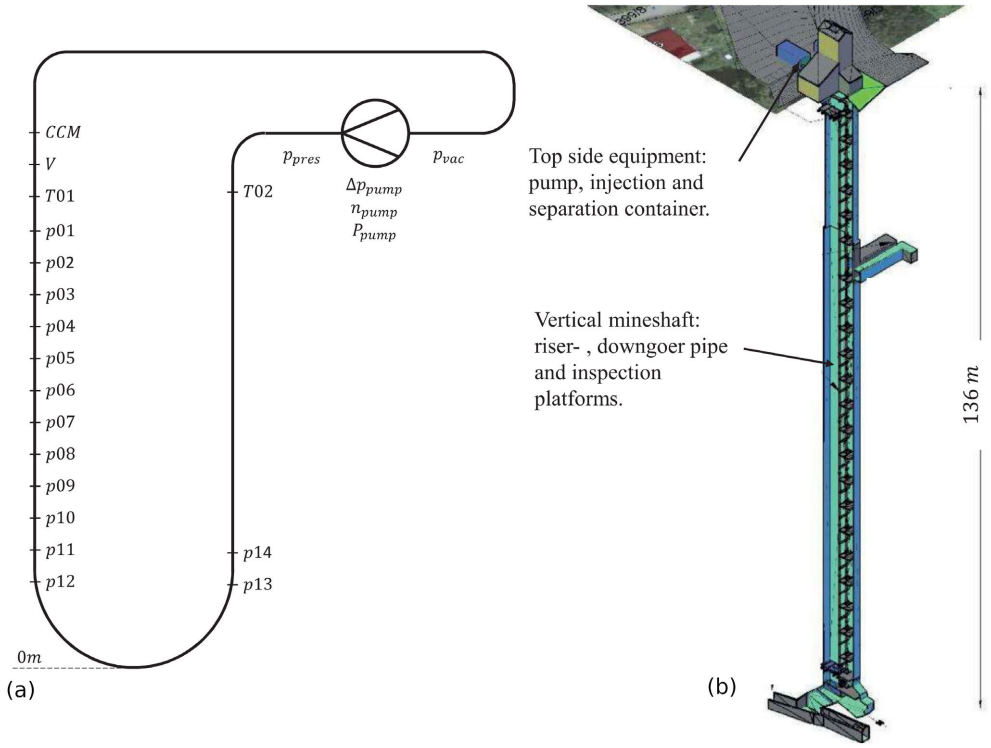

Figure 2.11: (a): A schematic overview with sensors, flow direction is clockwise; (b): detailed illustration with topside equipment (de Hoog et al., 2021a).

For the development of vertical transport technology to be used in deep-sea mining applications a long vertical transport system was designed and built in an old mine shaft in Halsbrücke, Germany (see Figure 2.9(a),(b)). The 297 meter (150 mm diameter) long vertical pipeline system had a 121 meter vertical downgoer and riser. Connected by 57 meter horizontal pipes at the top of the loop. Two sediments were used, d_{50} = 0.6 mm sand and d_{50} = 11.2 mm gravel. concentrations were 5%, 10% and 15%.

During testing density wave amplification was a common occurrence. At higher concentrations the system required too much power from the pump drive and therefore tests had to be ended prematurely, due to density wave growth (see Figure 2.12(b)). The aim of the test was to acquire data at several constant mixture velocities by varying the rpm of the pump at intervals. However with a constant rpm, the mixture velocities still fluctuated as density waves kept growing with each circulation through the loop. The sand tested was stable at 5% and high velocity, however when the concentration was increased to 10% density wave amplification commenced (see Figure 2.12(d)). The alarming aspect of these density waves in the Freiberg system was that the mixture velocity was far above the deposit limit velocity and critical velocity. Whereas in the other experiments density wave amplification stops above the critical velocity and thus suggests another process was causing density wave amplification.

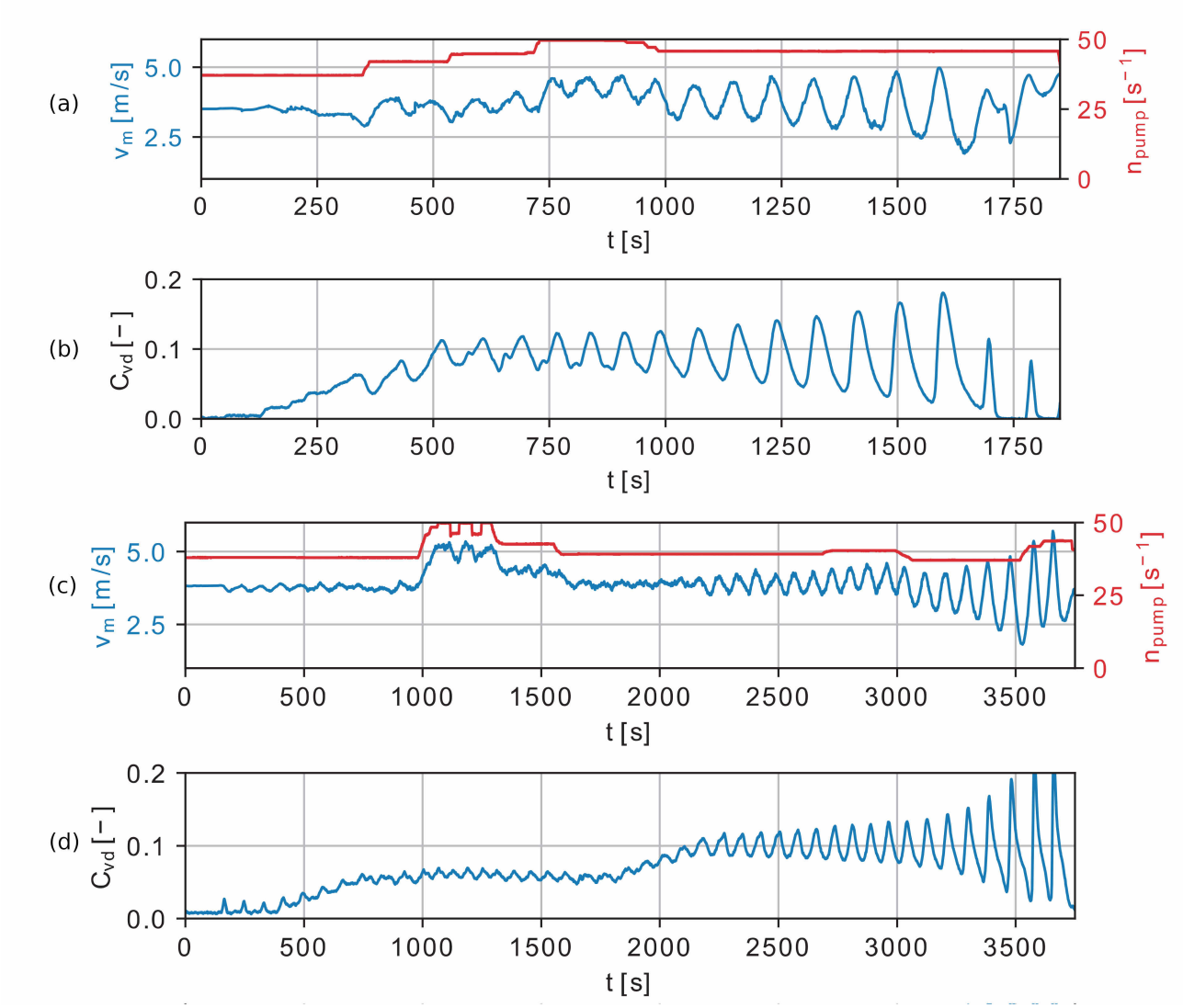

Figure 2.12: (a): Mixture velocity and pump revolutions over time, d_{50} = 11.2 mm; (b): delivered concentration over time (bottom of the loop), d_{50} = 11.2 mm; (c): mixture velocity and pump revolutions over time, d_{50} = 600 μm; (d): delivered concentration over time (bottom of the loop), d_{50} = 600 μm; (de Hoog et al., 2021a).

This different process causing density wave amplification is the 'transient accumulation' theory. This theory is currently still a hypothesis and where again the burgers equation is used (see Equation 2.13). The continuity equation simplifies to the following equation:

$$\frac{\partial \overline{C}}{\partial t} + \frac{\partial}{\partial x}(v_s \overline{C}) - \epsilon \frac{\partial \frac{\partial \overline{C}}{\partial x}}{\partial x} = 0 \longrightarrow \underbrace{\frac{\partial}{\partial x}(v_s \overline{C}) = 0}_{\text{Low diffusion and temporal steady-state}} \tag{2.16}$$

Particle velocity is different depending on pipe orientation, for horizontal pipe orientation the slip ratio model of Sobota and Kril (1992) is used. For vertical pipe orientation is modeled according to Richardson & Zaki (1954):

$$v_s = v_m - w_{ts}(1 - C)^n \tag{2.17}$$

Where w_{ts} is the terminal settling velocity of a single particle, and n is the Richardson & Zaki (1954) settling exponent. For illustrative purposes n and w_{ts} are modeled according to Garside & Al-Dibouni (1977) and Ferguson & Church (2004) respectively (de Hoog et al., 2021a).

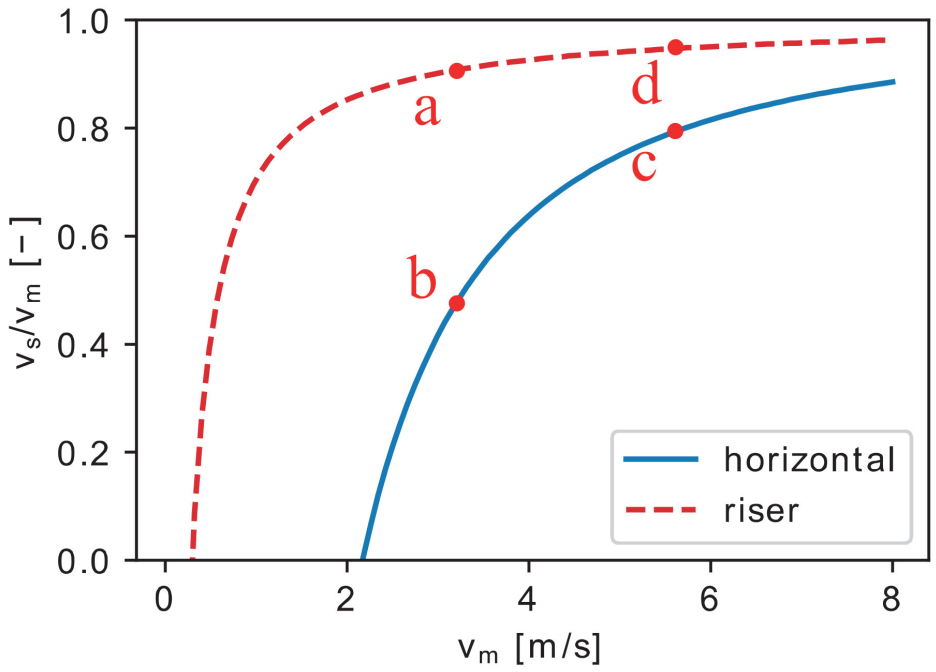

Figure 2.13: (a): Slip ratio over mixture velocity for horizontal and vertical pipe orientation. D = 150 mm and d_{50} = 600 μm (de Hoog et al., 2021a).

To understand Figure 2.13, assume the mixture velocity is steady in time, and all density variations are damped, except for the density wave. The density wave flows from the riser to the horizontal pipe, resulting in a particle decrease (see a → b). When particle velocity decreases the continuity equation (see Equation 2.16) imposes that concentration increases. This concentration increase is only temporal because when flow travels in the vertical riser again concentration will decrease. The essential part to understand density wave amplification as observed in Freiberg is that the mixture velocity will increase if the density wave flows out of the riser and into the horizontally orientated pipe. The centrifugal pump does not create a constant mixture velocity, even if the revolutions of the pump are constant. When the density wave flows from the riser into the horizontal pipe, the load of the pump decreases, due to the decreasing hydrostatic gradient (de Hoog et al., 2021a). This will cause the particle velocity to go from a → b → c. When the flow travels from the horizontal pipe to the vertically oriented pipe, particle velocity will go from c → d, which consequently is a part of the increased concentration remains (de Hoog et al., 2021a).

2.3 Discussion on density wave amplification research

In this part of the section, a critical review is given of the literature that was assessed in sections 2.2.1 - 2.2.3. Contradictions within the literature are analysed and discussed. All together this section focuses the main research question of the literature study as well as literature research question 2b.

Matoušek (2001)

Firstly Matoušek (2001) directly states that: 'from analysis of MeaVli pumps data the influence of a pump performance on density wave transformation has been observed to be negligible'. This statement directly contradicts the hypothesis that the centrifugal pump plays a role in density wave amplification. The new research theory: 'transient accumulation theory' of de Hoog et al. (2021a,2021b) is based upon the principle that the density wave affects the performance of the pump. Also, van Wijk et al. (2022) state that a batch (density wave) that moves downward helps the pump accelerate the entire mixture. Furthermore van Wijk et al. (2022) state that certain circumstances causes the pump to attenuate or increase peak concentration. In specific sand with a Stokes number smaller than 1, attenuation of the concentration peaks was measured over the pump section. And gravel with a Stokes number larger than 1 a growth in concentration was measured over the pump section. Both research of de Hoog et al. (2021a,2021b) and van Wijk et al. (2022) are based upon a combination of vertical and horizontal transport while the Prins Clausplein pipeline discussed by Matoušek (2001) is based on purely horizontal transport. Furthermore it is known that when the density of a mixture increases, more frictional losses occur in the centrifugal pump, and mixture velocity decreases (Wilson et al., 2006). When mixture velocity decreases, a bed layer could grow or form, and it is known that density wave amplification cannot occur without a bed present when considering horizontal transport (Talmon et al., 2007).

If the flow rate is close to the critical velocity (which was the case with the Prins Clausplein pipeline), a mixture concentration disturbance could cause the pump to temporally decrease mixture velocity and make density wave amplification possible. This decrease in mixture velocity depends on the working point of the centrifugal pump. Figure 2.14a & 2.14b are based on a closed loop system and are great examples of what happens when a density wave flows through a centrifugal pump. The constant rpm curve leads to a constant torque curve. When a density wave flows through the centrifugal pump, the constant torque curve will shift according to Stepanoff's approximation (added frictional resistance in the pump due to sediments). which results in a lower rpm.

$$f_c = 1 - C_{vd} * (0.8 + 0.6 * log(d_{50}) = \frac{P_{man,m}}{P_{man,f}} * \frac{\rho_f}{\rho_m} \tag{2.18}$$

Where C_{vd} is the delivered concentration, d_{50} the corresponding particle size when the cumulative percentage reaches 50 percent, $P_{man,m}$ the pressure difference caused by the pump using a mixture and $P_{man,f}$ the pressure difference caused by the pump using water. The mixture resistance curve will not shift significantly in a flow loop, because a local change in density does not change the density over the whole system. In open end-to-end slurry transport, however, the mixture resistance curve could change. When suddenly high-density waves appear, the frictional resistance increases which leads to an increase in the resistance curve and makes it more narrow. In Figure 2.14a the working point is still far from the maximum power the pump can provide (point 1). So when a density wave passes through the centrifugal pump, the pressure of the pump will increase. This increase in pressure shifts the working point resulting in a temporarily higher mixture velocity (point 2). In figure 2.14b the working point is close to the maximum power the centrifugal pump can provide (point 3). When a density wave flows through the centrifugal pump the new working point (point 4) will shift to a constant torque line. The pump pressure will decrease, resulting in a temporarily lower mixture velocity.

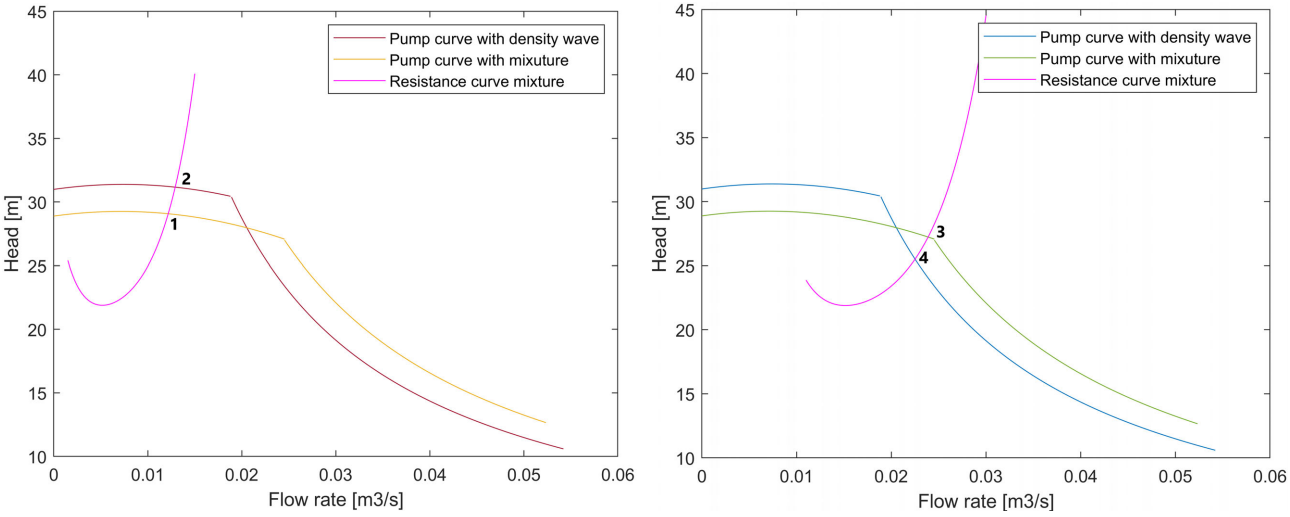

Figure 2.14: (a): Modelled constant rpm curve to constant torque curve with Stepanoff's correction and a stable working point (b): Modelled constant rpm curve to constant torque curve with Stepanoff's correction and an unstable working point.

It is important to distinguish between the 'erosion sedimentation imbalance' and the 'transient accumulation' theory. In Freiberg the mixture velocity was far above the deposit limit velocity, and thus no bed layer was present, still density wave amplification occurred. Personal communication with Prof. dr. ing. V. Matoušek verified that there was no extensive research done on the influence of the centrifugal pump on density wave amplification.

Matoušek (2013)

Matoûsek and Krupicka (2013) stated that in the horizontal sections of the test loop (see Figure 2.7) the wave celerity and mixture velocity, c = 1.3 m/s and v_m = 0.83 m/s was respectively. And that the wave celerity at the vertical sections the same was as the mixture velocity. It seems unusual that the wave celerity is higher than the mixture velocity, furthermore other research does not seem to replicate this behaviour. Talmon et al. (2007) measured a wave celerity of 50-95% of the mean flow velocity depending on concentration. Personal communication with Matoušek brought a possible explanation for this unusually high wave celerity. It is probably due to the way the mixture velocity and the wave celerity are measured. In vertical sections the wave celerity was the same as the mixture velocity, while in horizontal sections it was higher, this could be due to the bed layer. When a stationary bed is present, and mixture velocity is measured the mixture velocity is relatively lower due to the bed that is stationary. When a density wave passes, the bed starts sliding. Thus resulting in relatively higher wave celerity compared to the mixture velocity.

What is also unusual is the number of waves present in the loop, which is four. Currently, all the density waves measured in test loops measure a wavelength about the same length as the loop. Talmon et al. (2007) had a loop length of 52 meters, with a corresponding wavelength. This is because the largest wave is most amplified, while the smaller size waves are attenuated. Matoušek measured 4 waves, with a loop length of also 52 meters that could extend with an additional 41 meters. Including the extension had no effect on the number of waves. With the combinations of pressure sensors and torque of the pump Matoûsek and Krupicka (2013) deduced the wave celerity and periodicity with fast Fourier transfer. With the combination of periodicity and wave celerity one can derive the length of the wave. The only notable differences in the loop used by Matoušek and Talmon is the loop length, presence of vertical sections, and material used as sediment (ballotini B8 vs 200μm sand). Van Wijk

et al. (2022) showed that grain size affects peak concentration, and de Hoog et al. (2021a,2021b,2022) introduced the transient accumulation theory caused by vertical sections in a loop. The transient accumulation theory does not explain the measured 4 waves, there could be an additional effect not previously thought of like effects of grain size distribution.

Miedema (2003)

Miedema et al. (2003) wrote an article about the numerical simulation of density wave amplification. A 2-D mass exchange model is used for the calculation of the exchange between the bed and the suspended layer. What is surprising about figure 2.15 is that in front of the density wave the concentration is lower than behind the density wave. It is known that density wave amplification can only occur with a bed present, where it can take material to grow, thus leaving less concentration behind. This could possibly be a numerical mass balance error, however it is still interesting that the larger density peaks grow in concentration, while smaller peaks get attenuated.

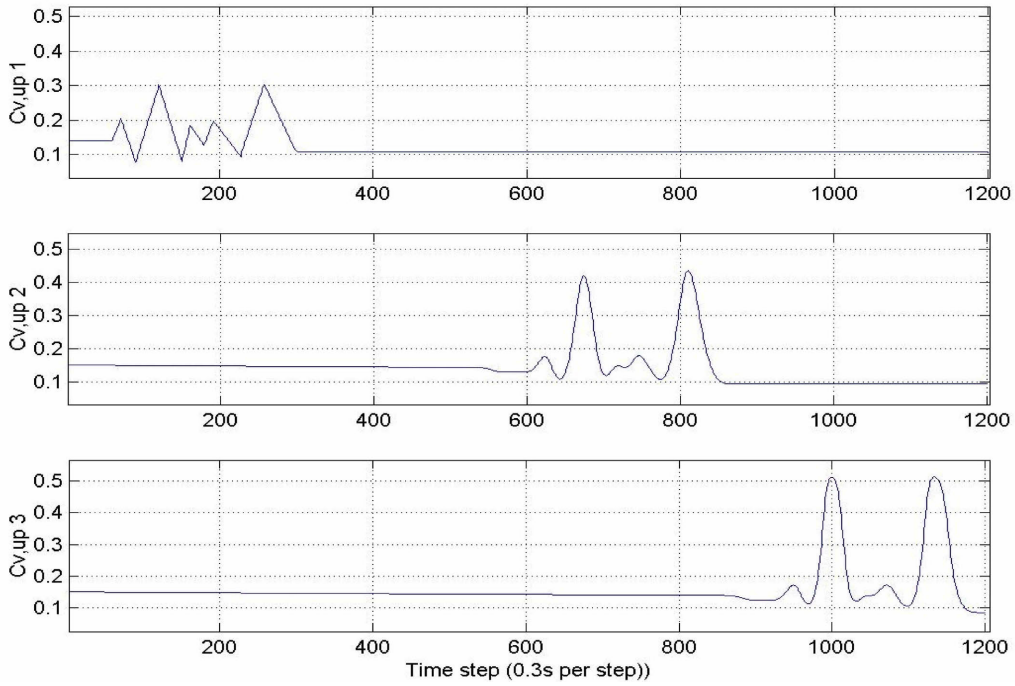

Figure 2.15: Deformation of density waves observed at the inlet, 500 meters behind the inlet and 800 meter behind the inlet (Miedema et al., 2003).

Outside Technical University of Delft & Prague institute of hydrodynamics

Outside the Technical University of Delft, there is not much attention given to this research topic. One notable article is from Samson and Biello (2017). Here longitudinal instability of slurry pipeline flow was investigated. There it is described that pipelines with a long range may exhibit surprising behaviour and that in certain situations concentration gradients may give rise to local plugs, containing anomalously high solids densities. And rather than dissolving with time as a result of turbulent mixing, such plugs self-amplify and become denser over time (Samson & Biello, 2017). This description from R. Samson and J.A. Biello describes the amplification of density waves. Also identified by Samson and Biello (2017) is that these 'plug formations' can be activated by accidental shutdowns causing massive demixing and sedimentation to settle. This also corresponds to the conclusions of Matoušek and Krupicka (2013), Talmon et al. (2007) and de Hoog et al. (2021a,2021b) that amplifying density waves only occur when a bed layer is present (for horizontal transport). Although the description of

the phenomena is accurate, their model could only provide a maximal increase in solids concentrations of a couple of volume per cent. Not sufficient enough to model a growing density wave. The article does however note that plug growth is dictated by the coarsest particles, and that accumulation time is shorter with coarser slurries. Which again hints to the importance of grain size distribution to density wave amplification.

2.4 Measuring principles

For a flow loop different parameters can be measured: flow rate, density, pressure, concentration distribution, pump power and pump revolutions are parameters that could be interesting to measure. Different measuring techniques can be used to determine certain parameters, density measurements are especially challenging.

2.4.1 Pressure measurements

Pressure sensors are relatively inexpensive, easy to install and have an error of ±0.5%. There are absolute and differential pressure sensors available. Differential pressure sensors can be used to derive the density of a mixture (see Figure 2.16). The inlet and outlet pressure of the pump can be measured by absolute pressure sensors, additionally a differential pressure sensor can be placed at the pump to more accurately measure relative changes in pressure.

2.4.2 Concentration measurements

Accurate measurements of the mixture concentration or density are essential to understanding slurry transport. Different concentration or density measurement techniques are available with all having their own advantages and disadvantages. This section aims for the understanding of the basic principles of these measuring techniques, and to have a complete overview of the available options when considering concentration/density measurement techniques.

Delivered concentration measurement with U-loop

With an U-loop the $\overline{C_{vi}}$ (average in situ volumetric solids concentration) can be calculated (see Equation 2.19), note that this is not C_{vd} (the delivered volumetric solids concentration). Although $\overline{C_{vi}}$ is usually very close to C_{vd}, they are not identical (Wilson et al., 2006). The magnitude of the fractional difference between $\overline{C_{vi}}$ and C_{vd} is generally less than $(\frac{v_t'}{v_m})^2$. A reasonable assumption made by Equation 2.19 is: $\tau_a = \tau_b = \tau$ (Clift & Clift, 1981). This assumption should be carefully considered when encountering density waves in the U-loop, due to the transient nature of the flow. The disadvantage of the U-loop is that it measures spatially averaged concentrations, not local concentrations. Also it contains vertical sections, which could influence the amplification of density waves.

$$\overline{C_{vi}} = \frac{C_{v,A} + C_{v,B}}{2} = \frac{1}{2} * \frac{1}{\rho_s - \rho_f} * \left[\frac{(p_1 - p_2) + (p_4 - p_3)}{gz} - 2 * \rho_f \right] \tag{2.19}$$

Where $p_1 - p_2$ is the pressure drop of the riser, $p_4 - p_3$ the pressure drop of the downgoer and z the length between the measured pressure drop.

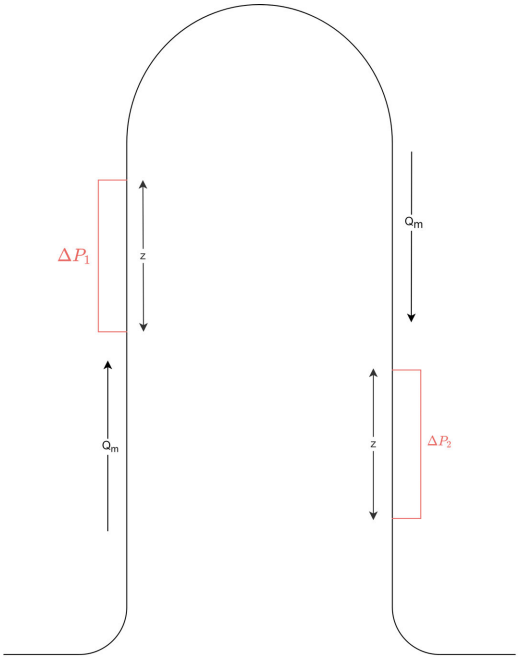

Figure 2.16: Profile of U-loop (schematic); ascending pipe: A; descending pipe: B.

Conductivity Concentration Meter - CCM

The electrical conductivity of a fluid containing suspended particles depends on the conductivity of the fluid and the volume fraction of the suspended particles (van Wijk & Blok, 2015). It is possible to measure the electrical conductance or resistance of a mixture and deduce volume fractions. The conductivity concentration meter, short for CCM, can measure local concentrations, is known for its quick response time and are flexible to integrate into different test setups (van Wijk et al., 2022). Conductivity electrodes made of inert materials like platinum are used, where multiple electrodes are oriented face-to-face in a pipe section. CCM's are highly dependent on temperature and salinity. With a closed loop test setup difficulties may arise when considering temperature, during a closed loop long duration test the temperature of the mixture will steadily rise and affect the output of the CCM. Salts present in the sediment are also highly undesirable, these salts can dissolve over time and affect measuring data. Washing sediments before use could be done to prevent salts from affecting measuring results. Although CCM's can measure concentrations locally and quickly, they need to be calibrated extensively and changing the water after each test is highly recommended by van Wijk et al. (2022). Van Wijk et al. (2022) wrote an extensive guide on how to calibrate the CCM for experimental flow loop purposes.

ERT systems (electrical resistivity tomography) are based on the same principles as CCM's, although ERT's are used to map 2D cross-sections of the concentration. Errors are expected to be between 0-25% . It is typical that an increase in concentration leads to an increase in error (van Wijk et al., 2022).

3. Methodology

This section gives an overview of the research methodology used for the experimentation. During the literature study a flow loop design has been made, which is visible in Figure 3.1 on page 34, With this flow loop experimentations will be carried out. A method for accurate and reliable determination of sensor data is important, to ensure acceptable results. These so called pre-tests are summarised in Section 3.3. Furthermore, before experimentation a stepwise plan is made to ensure the tests are performed in the same repeatable manner (Section 3.2). During experimentation a logbook with notations about the experiment like conditions, conspicuity, duration and goals are noted.

3.1 Experimental setup

At first, explorative studies were done in order to validate the experimental plan and setup. Based on literature research on how to design the best experimental setup for density wave amplification (Literature research question 2a), a diagram of the experiment has been made as shown in Figure 3.1. The bypass can be used to introduce high-density disturbances to the system by using valves 1 and 2 if there is need for it. The large radius bend of 1.5 meters limits bend disturbances that could influence density wave amplification. Along the straight sections the pressure drop is measured. Density measurement by the u-loops are located at a 180-degree and 90-degree bend location, to keep disturbances at a minimum over the whole flow-loop system. Additionally, an electrical resistivity tomography meter (ERT) will be used at a straight section before the U-loop, to measure the concentration distribution. The diameter of the ERT measuring section has a different inner diameter (40 mm instead of 46 mm). Adapters have been installed between the main loop and ERT measuring section to gradually adapt to the different diameters, limiting the influence of turbulence. Factory characteristics of the pump and flow loop are summarised in Table 3.1.

Table 3.1: Pump & pipeline characteristics.

	Name	Rated power	RPM	Max head	Max flow rate
Pump	SAER IR80-160C	15 [kW]	2900 [RPM]	30.5 [m]	195 [m^3/h]
	Material	Characteristics	Outer dia	Inner dia	Max pressure
Pipe	Polyvinyl chloride	Transparent	50 [mm]	46 [mm]	10 [Bar]

3.1.1 Diagram of the experimental setup

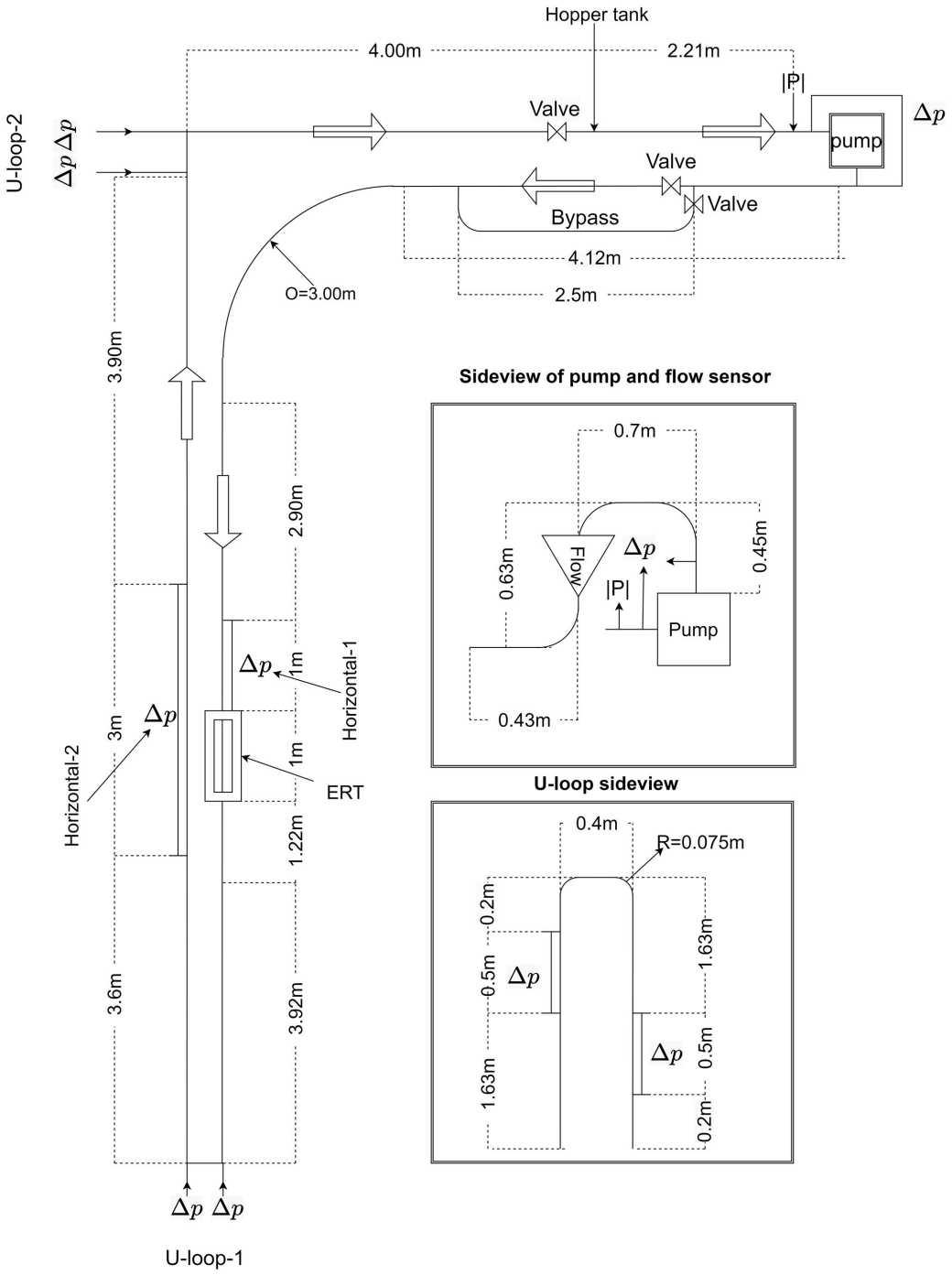

Figure 3.1: Top view diagram visualisation of the test loop used. Total lengths is 46 meters.

3.1.2 Data collection

Data will be collected using dewesoft hardware and software `https://dewesoft.com/`. Pressure sensors used are from General Electric. All sensors are calibrated before use. Calibration data can be found in Appendix part A.

Table 3.2: Sensors used.

Name	Purpose	Amount	Range	Accuracy
Dewesoft STG-M+	DAQ system	2	8 Channel	-
GE PTX 5032-TB-A3-CA-HO-PA	Pressure sensor	2	[0 35] kPa	<0.2%
GE PTX 5032-TB-A3-CA-HO-PA	Pressure sensor	2	[0 50] kPa	<0.2%
GE PTX 5032-TB-A3-CA-HO-PA	Pressure sensor	2	[-30 30] kPa	<0.2%
GE PTX 5032-TB-A3-CA-HO-PA	Pressure sensor	2	[-100 200] kPa	<0.2%
GE PTX 5032-TB-A3-CA-HO-PA	Pressure sensor	2	[0 1500] kPa	<0.2%
KROHNE optiflux 2100	Flow-rate sensor	1	[-12 12] m/s	±0.3%
Banner QS18VP6LPQ8	Rpm sensor	1	-	-
ITS z8000	ERT	1	-	-

In Figure 3.1 the top view diagram of the flow loop is visualised, at the corners two U-loops are installed to measure the concentration of the mixture. The method of determining the concentration of a mixture by means of an U-loop is explained in the literature review, in chapter 2.4.2.

Data will be processed using Python and the Dewesoft hardware and software. The data are collected in Dewesoft's environment and can be analysed and exported using JSON (JavaScript Object Notation) for analysis within Python. All signals are digitally filtered using a Butterworth filter. The output of these filter coefficients is processed using a zero-phasing filter (a so called "filtfilt"). This eliminates the phase shift that is common with hardware or causal filters. Typical cutoff frequencies depending on the test are set between [1-10] Hz to eliminate electrical noise, mechanical noise due to vibrations and noise due to turbulence.

3.1.3 Physical modelling

To get an idea of how the system responds to a given rounds per minute (RPM) a model has been made. Originally this model was to be used for the PID controller. However, the combination of very long wave periods and small mixture velocity variations led to this idea being dismissed. The modelling of density wave amplification is outside the scope of this thesis. Rather, this model gives a representation of the behaviour of the system and an estimate of the mixture velocities for a given mixture (see figure 3.2).

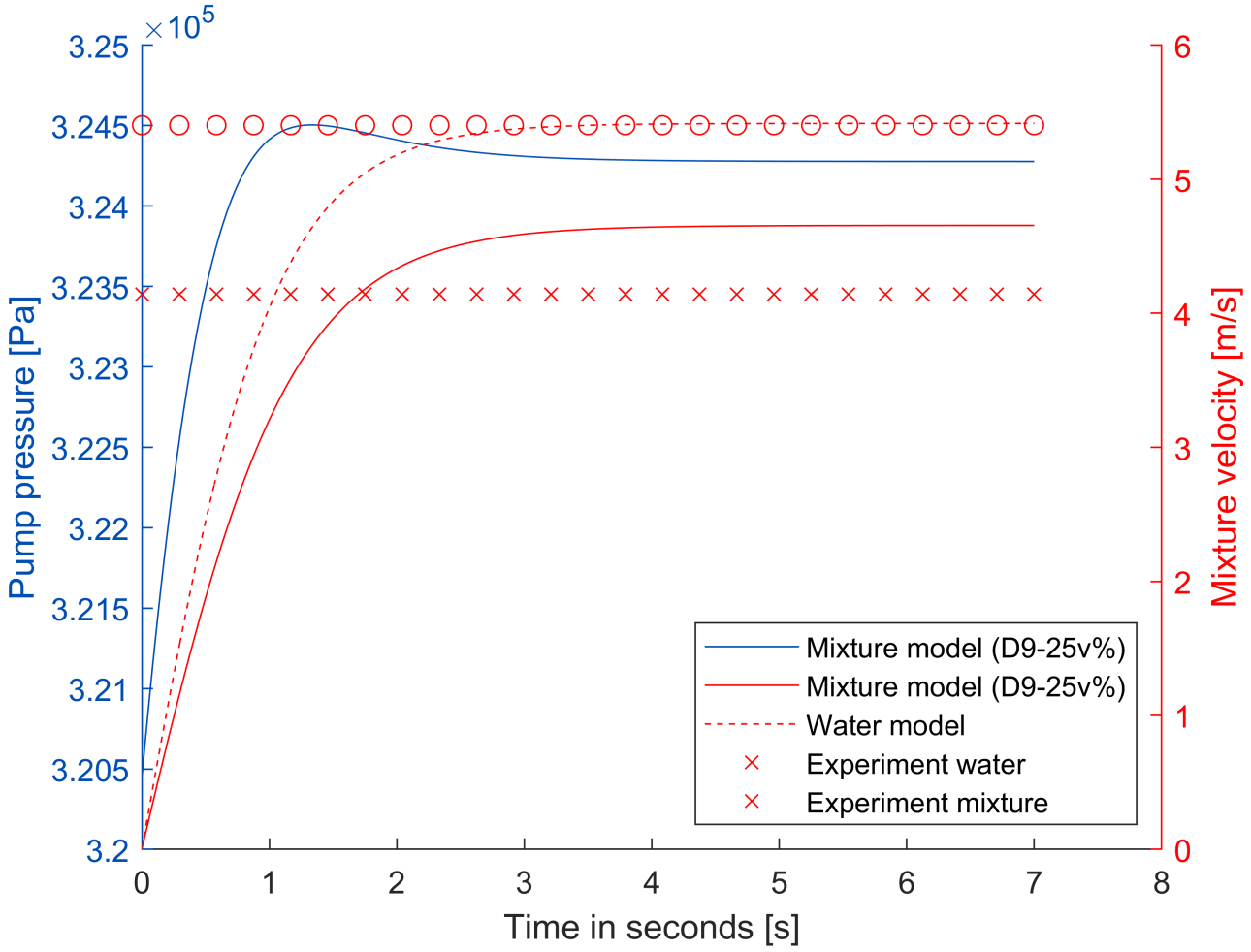

Figure 3.2: Water and mixture constant rpm model.

The model is based on Newton's second law:

$$F = m * a \tag{3.1}$$

Which in numerical analysis can be derived to:

$$(F_{pump} - F_{loss}) = m * \frac{V_{new}^{n+1}}{V^n} \frac{1}{\Delta t} \tag{3.2}$$

Where F_{pump} is the force added by the pump, F_{loss} the losses due to friction and solids effect, m the mass of the mixture and t represents time.

$$V_{new}^{n+1} = v^n * \frac{\Delta t}{m} * (F_{pump} - F_{loss}) \tag{3.3}$$

F_{loss} can be calculated with the following interpolation formula (Colebrook et al. (1939)):

$$\frac{1}{f^{1/2}} = -2 * log(\frac{\epsilon/d}{3.7} + \frac{2.51}{Re_d * f^{1/2}}) \tag{3.4}$$

Where f is the friction coefficient, ϵ/d the relative roughness and Re_d the Reynolds number. The friction coefficient can be used for:

$$F_{loss} = \frac{V^2}{8} * \rho_m * \pi * D * L * f \tag{3.5}$$

Where D is the inner diameter of the pipe. F_{loss} can be calculated through the Q-H curve of the pump. When velocity is known, pressure can be derived, and thus the force. With all the variables given the new velocity (V_{new}) can be calculated.

Constant power model

A pump can be operated with a constant rpm control but also with constant power. This can be actively done by lowering the available power for the motor, or due to a sudden mixture increase by which the extra power is not available.

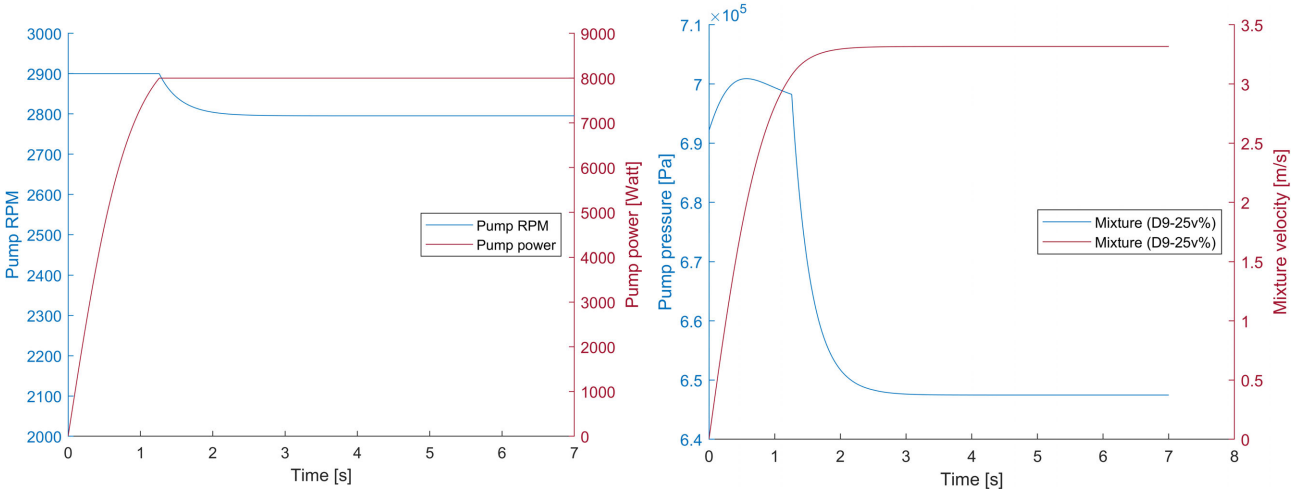

(a) **(b)**

Figure 3.3: (a): Modelled constant power curve set to 8kW, left side of the axis is rpm, the right axis is power. (b): Modelled constant power curve, left axis is pump pressure, and the right axis is mixture velocity.

When there is enough power available the model follows the Q-H curve of the pump (Figure 3.4, blue line). When the limit is reached, for this case 8kW, the pressure calculation is determined by the following formula (see Figure 3.4, red line):

$$H = \frac{P_{max}}{Q_m \rho_m g} * \eta_m \tag{3.6}$$

Where P_{max} is the maximum power of the pump and η_m the efficiency of the pump considering a mixture.

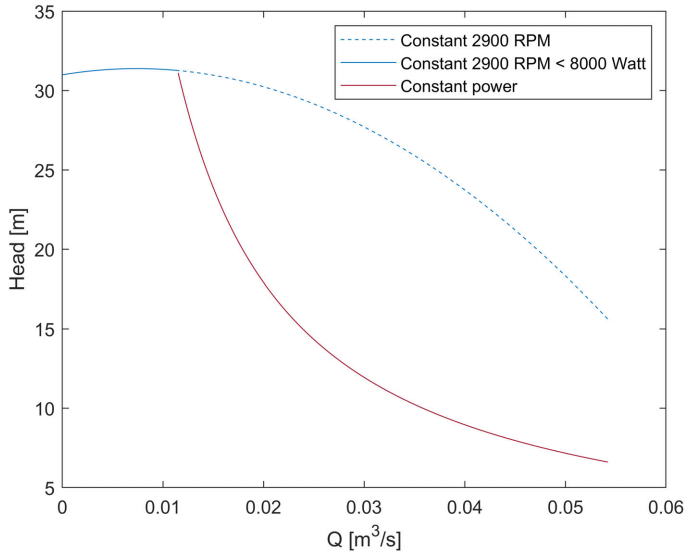

Figure 3.4: pump Q-H curve, where the constant RPM curve leads to a constant power curve set at 8kW.

3.2 Experimental plan

The goal of this research is to generate amplifying density waves. This, however, may be difficult due to the fact that this topic is not widely researched. Research has consensus that for long horizontal transport, density wave amplification to be possible, a bed has to be present somewhere in the pipeline. It is known that concentration has a significant influence on density wave amplification; low concentrations tend to cause attenuation of density waves (de Hoog et al., 2022). With larger sized particles the critical velocity is reached sooner compared to smaller sized particles. Will density wave amplification be more extreme and easier to generate with larger particles? What about a broader distribution of particle size (combination of Dorsilit 7 & 9)? Do the U-loops cause attenuation or amplification of density waves? What effects do the U-loops have on the pump? A combination of tests has to be performed to determine when density wave amplification occurs, and what the effects are on the system. The variation of rpm, concentration, particle size and particle distribution have to be tested systematically. The limited lifespan of the flow loop due to the abrasion caused by the sand may lead to carefully choosing which of the parameters are varied to which extent.

3.2.1 Measuring plan

The main research goal is to test the influence of grain size and concentration on density wave amplification. Firstly density waves have to be generated in a controlled and systematic way, literature's general consensus is that density waves can amplificate when the pipeline length is large, and the mixture velocity near the deposition limit velocity (for long horizontal transport). The particle size distribution aimed for during experimentation is a d_{50}= 200 μm to d_{50}= 1000 μm. First tests are performed with only water. This way the head loss can be measured and the test setup can be validated. When the experimental setup has been validated, the density wave experiment can start. First, any variation in concentration has to be damped by running the rpm far above the deposition limit velocity. After all concentration variations have been damped, rpm can be adjusted to a flow rate near the deposition limit velocity and density waves are allowed to amplify. Differences in amplification regarding concentration and PSD are investigated.

Water tests

When the loop is filled with water, pressure drop over a designated pipe length can be measured. Determining the Q-H pump curves can be done by increasing resistance within the pipeline by slowly closing a valve. Head will increase while flow rate will decrease. All the while the pump is kept at a constant rpm. Maximum allowable pressures (10 bar) have to be taken into account.

The accuracy of the U-loops can be checked using water. When differential pressure is measured at both the riser and downgoer the resulting calculation should conclude a concentration of one. This can be checked using different flow rates, if results are not within acceptable limits it may be due to insufficient entrance lengths.

Solids tests

At first, it has to be investigated at which concentration, particle size distribution and flow speed density wave amplification occurs the most (if any) using a constant rpm control (see Table 3.3). Variables like flow speed, pressure variations, concentration and power variations are logged to see the effects of these variables on the density waves. If there are any notable effects on the pump power, pressure or flow rate due to the density waves different control strategies like constant power, constant pressure or constant flow rate control can be considered. Furthermore, the effects of the U-loops are considered

by bypassing them and performing the same test to see the effects.

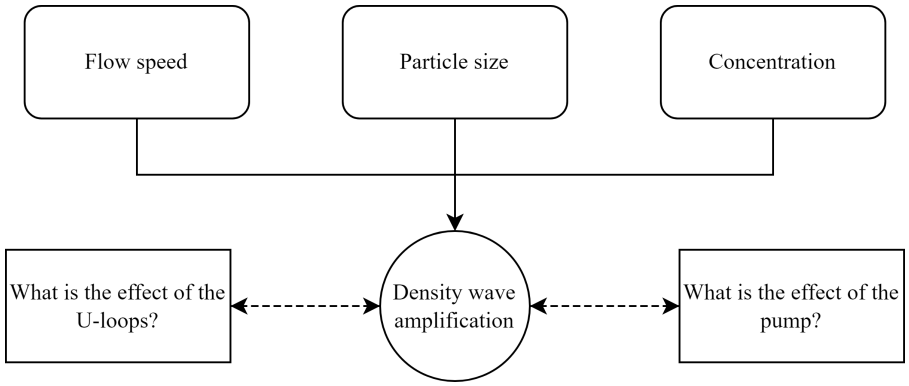

Figure 3.5: Variables to be adjusted when trying to commencement density wave amplification.

Table 3.3: Tests to be executed.

	Dorsilit 7	Dorsilit 8	Dorsilit 9	Dorsilit 7-8-9	Zilverzand
10 v%	Test 1	Test 4	Test 7	Test 10	test 13
20 v%	Test 2	Test 5	Test 8	Test 11	test 14
30 v%	Test 3	Test 6	Test 9	Test 12	test 15

The efficiency of the pump due to the solids effect can also be estimated. Efficiency reduction due to a change in slurry density is important to quantify, especially because smaller centrifugal pumps are more affected by a change in density than larger pumps (Wilson et al., 2006). This 'pump deration' as it is called can be estimated by using literature and experimental results which can be used to improve the pump model. Additionally, deration effects can be used to improve density measurements through the pump. Thus effects of the sediment type on the pump can be estimated, for this, the PSD of different particles have to be measured and calculated. In the next section, the sediment properties are elaborated on.

3.2.2 Sediment properties

The sediments used in the experiment are Dorsilit 7, 8, 9 & Zilverzand which are manufactured by Sibelco. For each sediment type the PSD has been determined two times from a different batch; see the graphical representation in Figure 3.6. All soil tests have been carried out in the MTI Holland laboratory in Kinderdijk. Before use, all sediments are extensively washed to eliminate the presence of salts and very fine particles.

Table 3.4: Characteristics of the sediments used.

Sand type	d_{10} [mm]	d_{20} [mm]	d_{30} [mm]	d_{40} [mm]	d_{50} [mm]	d_{60} [mm]	d_{70} [mm]	d_{80} [mm]	d_{90} [mm]
Dorsilit 7 (1)	0.774	0.860	0.946	1.023	1.086	1.149	1.212	1.275	1.338
Dorsilit 7 (2)	0.738	0.802	0.866	0.930	0.994	1.074	1.156	1.237	1.319
Dorsilit 8 (1)	0.441	0.515	0.549	0.583	0.617	0.651	0.684	0.744	0.882
Dorsilit 8 (2)	0.448	0.519	0.553	0.586	0.620	0.654	0.688	0.752	0.876
Dorsilit 9 (1)	0.193	0.230	0.261	0.285	0.308	0.332	0.357	0.405	0.454
Dorsilit 9 (2)	0.211	0.255	0.278	0.300	0.323	0.346	0.379	0.420	0.461
Zilverzand (1)	0.184	0.198	0.213	0.227	0.242	0.261	0.286	0.311	0.336
Zilverzand (2)	0.183	0.197	0.210	0.224	0.238	0.252	0.280	0.307	0.335

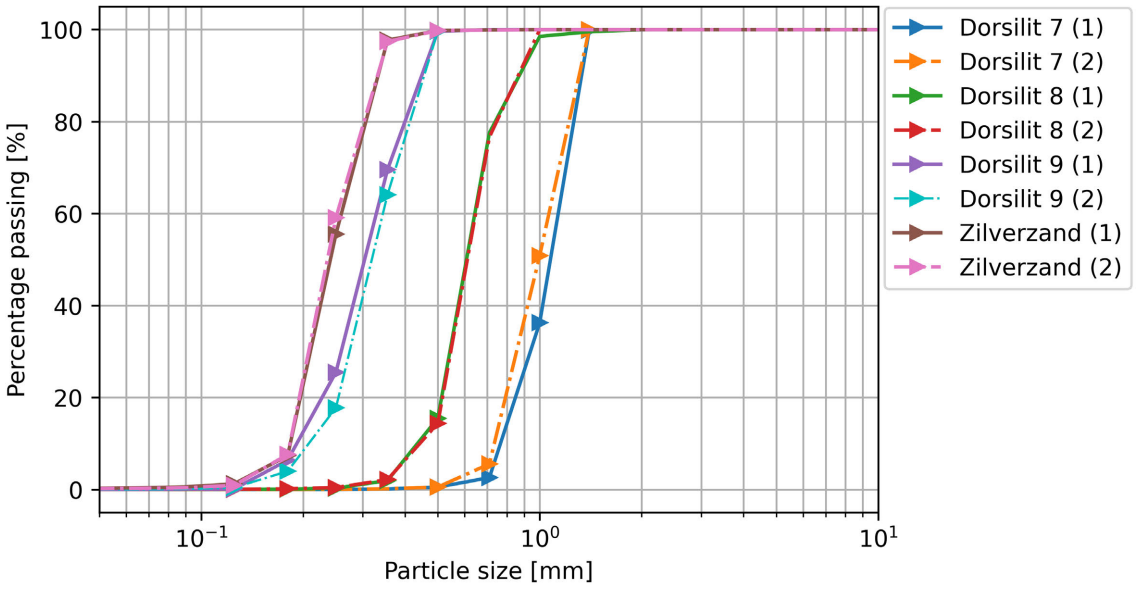

Figure 3.6: Particle-size distribution of the different sediments used (Dorsilit 7, 8, 9 & Zilverzand).

3.3 Validation of the setup

To test the limits of the loop tests have been performed to asses the limitations of the sensors due to turbulence, system vibrations and sensor limitations.

3.3.1 Maximum rpm test

For this test, the pump rpm was set at 50 hertz and the flow control valve was fully opened. The flow was reduced every minute by adjusting the flow control valve until it was fully closed. When fully closed, the system reached maximum pressure. See Figure 3.7 for a visualisation of the flow rate and pump pressure. Note that all pressures graphed have reduced noise because of the use of a digital Butterworth low-pass filter. .

Figure 3.8 visualises pressure drop per meter, dp-horizontal-1 and dp-U-2-up are notably higher than the other sensors. When looking at the raw data in Figure 3.7 it can be seen that three sensors

experience noise cutoff due to the sensor not being able to measure significant negative pressures (dp-U-2-up, dp-horizontal-1 and dp-horizontal-2). Note that in Figure 3.7 the y-axes are shifted so that all the pressures can be visualised. When the valve is closed, the system builds up pressure and mechanical vibrations increase. This increase in vibrations causes a sensor noise increase which is why part of the noise is cut off from the three sensors. This situation, however, is a stress test and during normal testing operation such vibrations are not common.

3.3.2 Variable rpm test

To validate that these vibrations are not common under normal testing conditions a second test was performed, where instead of adjusting the flow rate valve the rpm was lowered, resulting in a lower flow velocity. In Figure 3.10 it can be seen that during expected operation the sensor data are not cut off. Furthermore in the figure it is visible that turbulent noise is reduced when the flow rate is decreased. During mixture tests the pressure drop is going to be more significant compared with water, and so sensor cut off will be even less likely of an occurrence.

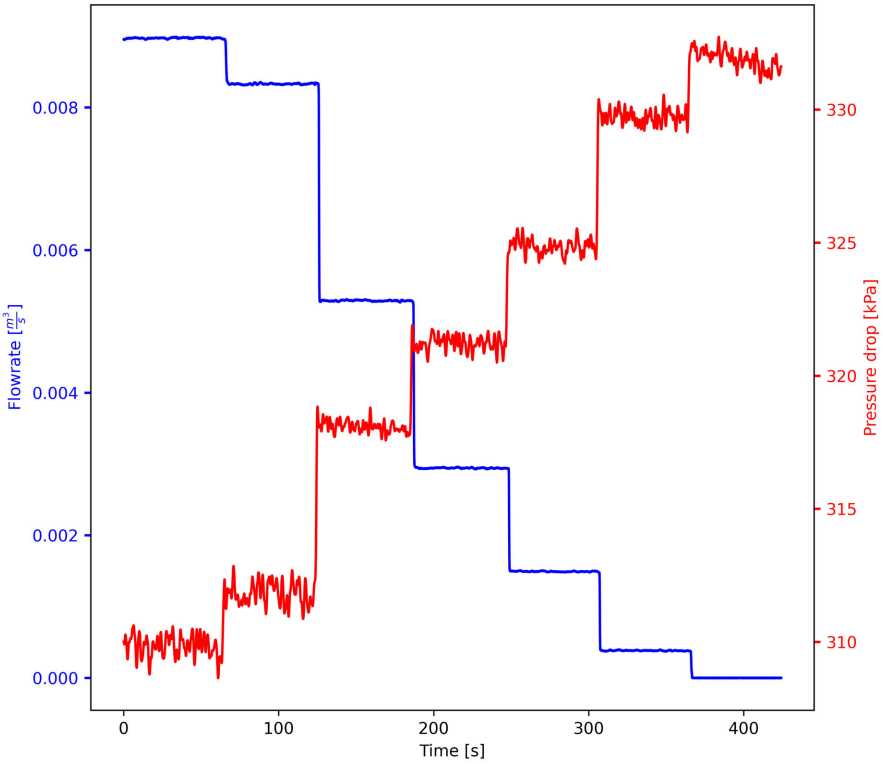

Figure 3.7: Maximum rpm test; flowrate & pressure over time.

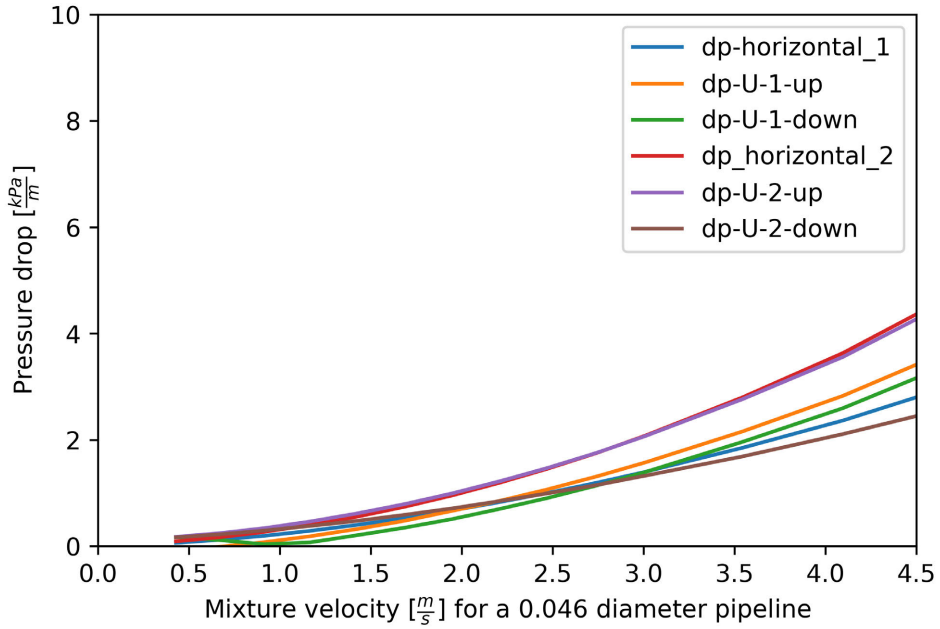

Figure 3.8: Water test run with maximum rpm; pressure drop per meter over flow rate.

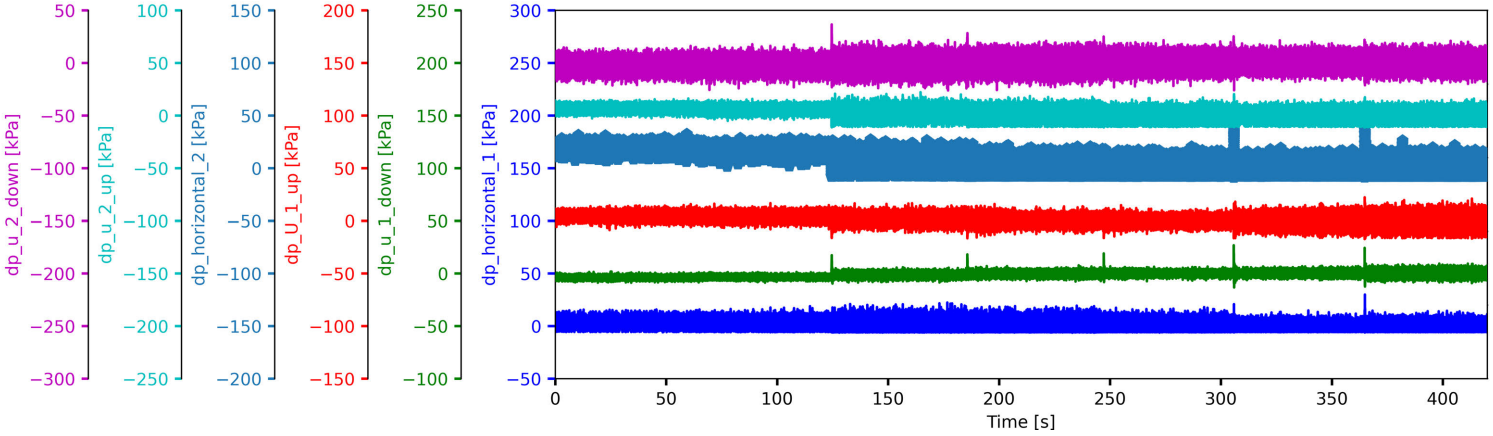

Figure 3.9: Water test run with maximum rpm; pressure drop over time.

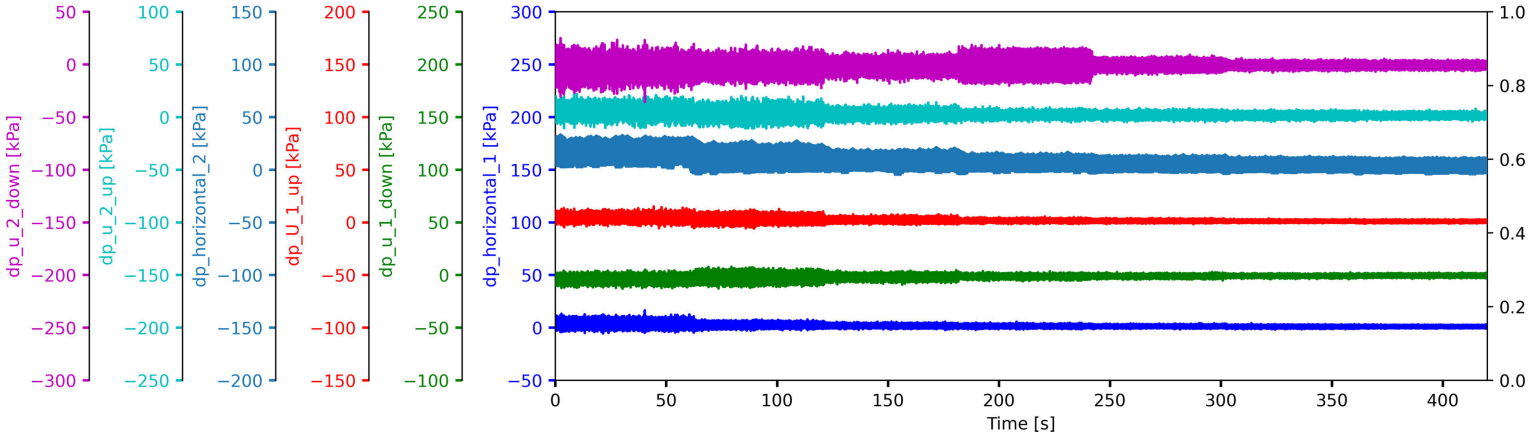

Figure 3.10: Water test run with variable rpm; pressure drop over time.

3.3.3 U-loop validation

The U-loops were tested using a Dorsilit 8 mixture of 15 percent volumetric concentration. Figure 3.11b shows the concentration distribution over time using Clifts & Clifts method explained in Section 2.4, where again every minute the rpm is lowered. As can be seen in Figure 3.11b a density wave is present and is decreasing in amplitude over time. When the pump frequency is adjusted after one minute, the density wave decreases further in amplitude and period due to the decreased flow velocity. Also, the overall average concentration decreases further with the pump frequency, suggesting that a bed is forming resulting in less concentration present in the U-loops. Figure 3.11a shows the pressures of U-loop 1 & 2 of the riser and downgoer. The differential pressure sensors are oriented such that the hydrostatic pressure causes a positive pressure drop. In the riser the hydrystatic pressure drop, and frictional pressure drop are both positive. In the downgoer the pressure drop is positive and the frictional perssure drop is negative. It can be seen that for the downgoer the pressure drop due to friction is dominant, and at 60 seconds when the pump frequency significantly lowered (thus also the mixture velocity), the pressure increases, making the hydrostatic pressure drop dominant. The difference in concentration between the two U-loops can be compensated by correcting the initial error when only water is present in the U-loop (and thus the concentration should be zero).

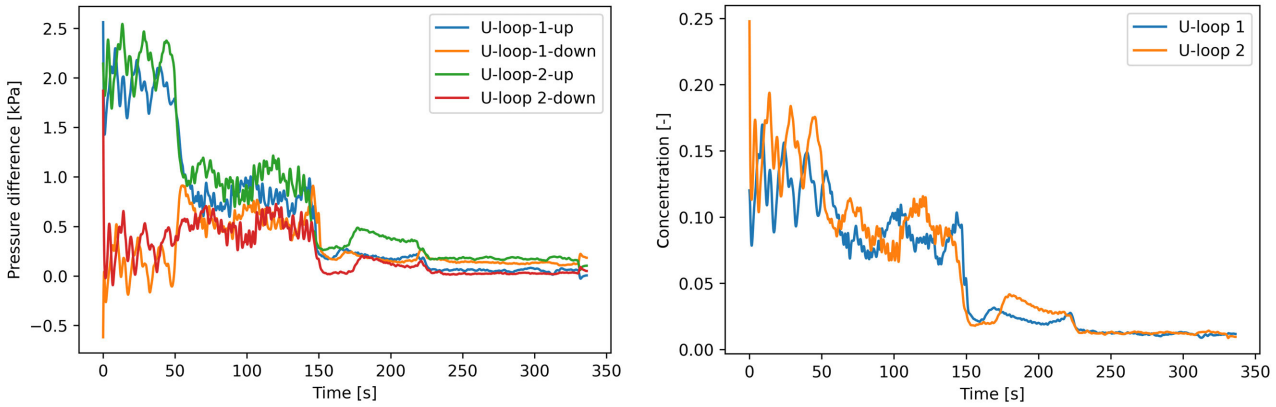

(a) **(b)**

Figure 3.11: (a): Pressure variations in the riser and downgoer of the U-loop , (b): Concentration fluctuations of both U-loops with 15% volumetric concentration calculated using Clifts & Clifts method.

A way to validate the horizontal sensors is to derive the roughness through the measured pressures. As seen in Figure 3.8, horizontal sensors dp-horizontal-1 and dp-horizontal-2 have some differences. These differences can be led back to an initial zero-value error. When correcting for this offset, and calculating the roughness through the Colebrook interpolation formula both sensors overlap (see Figure 3.12). At low flow rates, the measured pressures are very low and prone to sensor errors. At higher flow rates, the pressure differences get bigger and sensor errors are less of an issue. The roughness converges towards 0.03 millimeters.

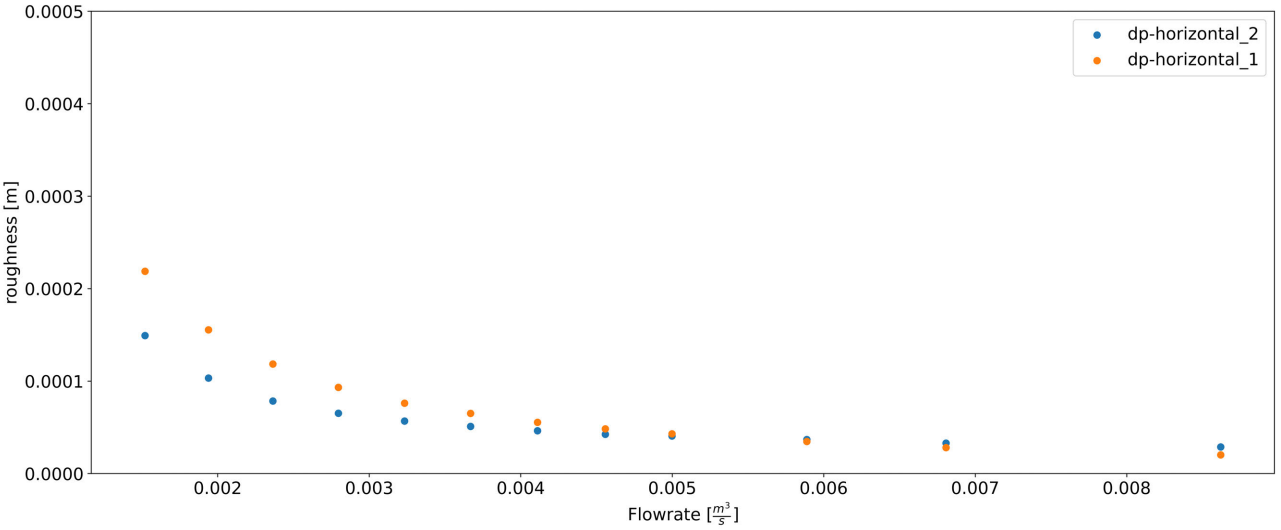

Figure 3.12: Validating the calibrated sensors. Water test run with variable rpm. Roughness over flow rate.

3.3.4 Generating amplifying density waves

There is a significant amount of research on the deposition-limit velocity, and model predictions when this velocity is reached. Known models of the deposition-limit velocity and hydraulic gradient are Durands model, Führböter model, Jufin - Lopatin model, Wilson - GIW model, MTI Holland model and the Demi-McDonald model. Most of these models are based on empirical data. The Demi-McDonald model is based upon a two-layer model. These models are shown in Figure 3.13 with the exception of Wilson - GIW and MTI Holland's model. The MTI Holland model is recommended for pipelines larger than 200mm, and the Wilson - GIW model is not suited for narrow-graded solids. Because the critical velocity of Demi-McDonald and Jufin-Lopatin are particle-dependent, they have an estimate of Dorsilit 7 and Zilverzand. Experimental data from Dorsilit 7, 8, 9 and Zilverzand are included in the I-V curve. An estimated range of the deposition-limit velocity for the experiment according to the models are [1.09-2.27] m/s. It can be seen in Figure 3.13 that the experimental data have a relatively low hydraulic gradient at high velocities when compared to the models. This can be due to the fact that most models are based on empirical data tested with large-diameter pipelines. Because the experimental results are from a 0.046 millimeter in diameter pipe, pressure drop can be different when compared to the larger diameter pipelines which the empirical models are deduced from. Also at a high rpm, the mixture velocity varies significantly, which could give inaccuracies regarding experimental data. This is not a problem due to the experiments being done around the deposit limit velocity.

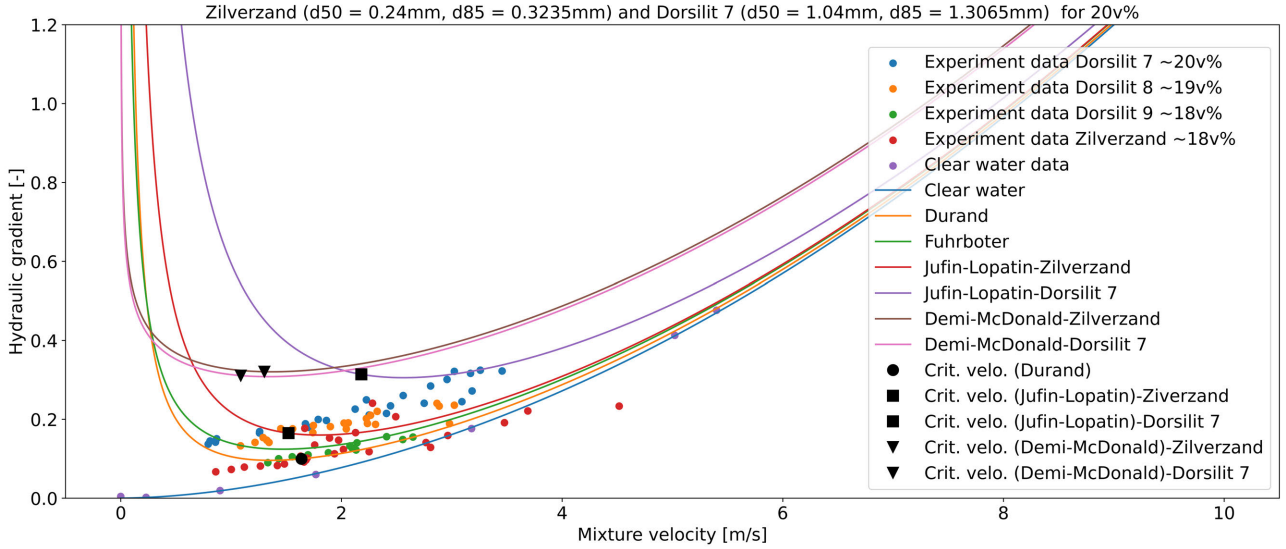

Figure 3.13: Hydraulic gradient ($\frac{\Delta P}{\rho_f g L}$) with deposition limit velocity estimations according to different models: Durand (1953), Führböter (1961), Jufin and Lopatin (1966), Wilson (1992).

4. Results

In this chapter, an overview of the results from the experiments are given. The data from the Dewesoft data acquisition system and ERT (ITS z8000) are post-processed using Python. All the data will be visualised in Appendix B, the most important findings are elaborated on in this chapter.

In multiple experiments, the density wave amplification was successfully measured. With various sediments, concentrations and mixture velocities, different behaviour of density wave amplification was measured. Various wave parameters are determined to characterise the found differences in the density waves: amplification rate, wavelength, wave period, and wave celerity. From the literature review in section 2.2, the mixture velocity and concentration have been found to have significant impact on the development of density wave amplification. The latter is confirmed by this study. As described before in subsection 2.2.1, the sedimentation erosion imbalance is the central theory of density wave amplification for long horizontal slurry transport. However, the effect of grain sizes on density wave amplification has not yet been validated by means of an experiment. This study is the first to show that there is a significant impact of the grain size on density wave amplification.

Table 4.1: Characteristics of the sediments used.

Tests	Max concentration [-]	Mean concentration of the wave [-]	Wave Period [s]	[Mix. velocity, min, max] [m/s]	Wave celerity [m/s]	Wave length [m]
Dorsilit 7 test 1	0.1149	0.0374	60.9818*	[0.8492, 0.67, 1.05]	0.7707	<Loop
Dorsilit 7 test 2	0.2047	0.0751	55.4881*	[0.7097, 0.25, 0.98]	0.8470	<Loop
Dorsilit 7 test 3	0.2442	0.1068	54.0352*	[0.6031, 0.44, 0.80]	0.8698	<Loop
Dorsilit 8 test 1	0.1194	0.0522	44.0322*	[1.0557, 0.76, 1.38]	1.0674	<Loop
Dorsilit 8 test 2	0.1904	0.0455	59.9725*	[0.6785, 0.60, 0.82]	0.7837	<Loop
Dorsilit 8 test 3	0.2559	0.1205	59.6719*	[0.6203, 0.35, 0.88]	0.7876	<Loop
Dorsilit 9 test 1	0.1103	0.0651	54.4440	[1.1778, 0.98, 1.42]	0.8921	48.57
Dorsilit 9 test 2	0.1802	0.0352	127.9510	[0.6428, 0.62, 0.68]	0.3867	49.48
Dorsilit 9 test 3	0.2157	No waves	-	-	-	-
Zilverzand test 1	0.0991	0.0545	62.6080	[1.1176, 1.06, 1.17]	0.7887	49.38
Zilverzand test 2	0.1518	0.0868	58.9755	[1.1244, 0.94, 1.35]	0.8145	48.03
Zilverzand test 3	0.1808	0.0648	82.7005	[0.9763, 0.61, 1.53]	0.5922	48.98

* Wave period is calculated through the wave celerity and length of the loop.

4.1 Amplification

Amplification of density waves is most pronounced with relatively smaller grain sizes; Zilverzand and Dorsilit 9. Smaller grain sizes result in longer wavelengths and significantly slower amplification of density waves. This makes the amplification itself more visible due to the growing wave passing the two U-loops multiple times (see Figure 4.1). With the coarser particles (Dorsilit 7 & 8) the rate of amplification is not as apparent. This is due to the wavelengths being shorter and amplification stronger, compared to the finer particles (Zilverzand and Dorsilit 9). Due to these differences, a single loop around the flow circuit can already fully amplificate the density wave of the coarser particles, and thus make it harder to visualise (see Figure 4.3). The mixture velocity and Hertz of the centrifugal

pump are visualised in figure 4.2 and 4.4 for both Zilverzand and Dorsilit 8. To differentiate between these two different types of density waves, the fine sediment waves are identified as suspended-driven density waves, and the coarse sediment density waves are identified as bed-driven density waves.

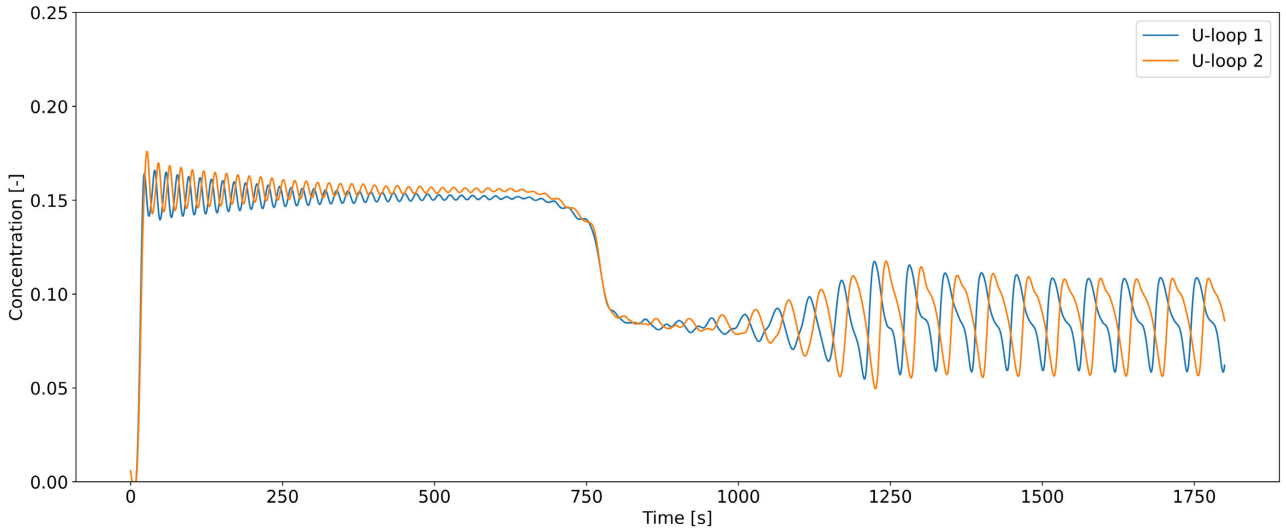

Figure 4.1: Density wave amplification with Zilverzand, a single wave with the same wavelength as the length of the flow loop. Concentration over time.

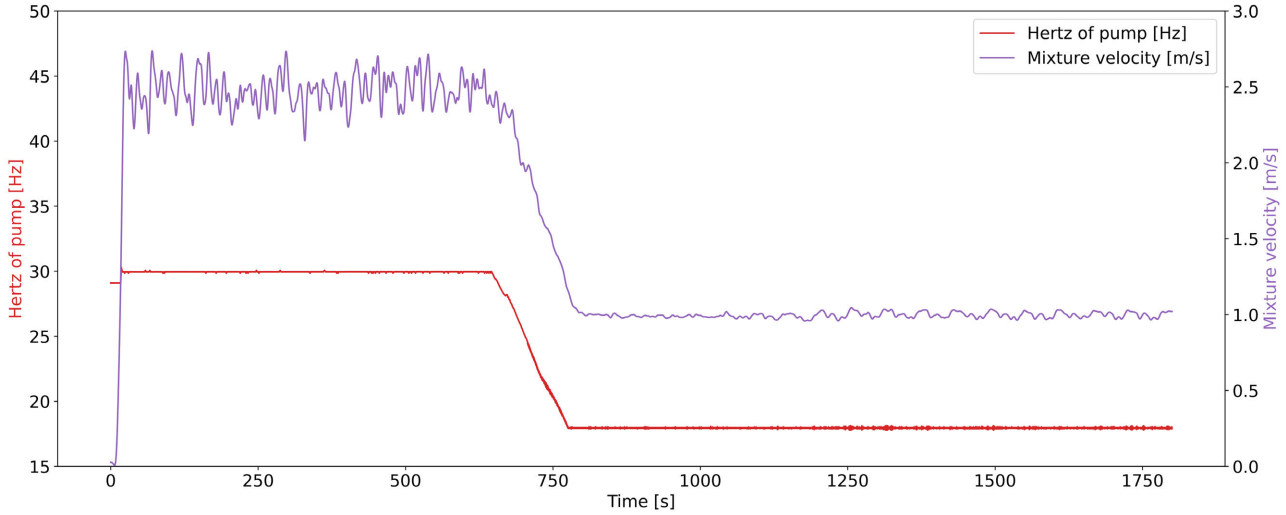

Figure 4.2: Density wave amplification with Zilverzand, a single wave with the same wavelength as the length of the flow loop. Mixture velocity and Hertz over time.

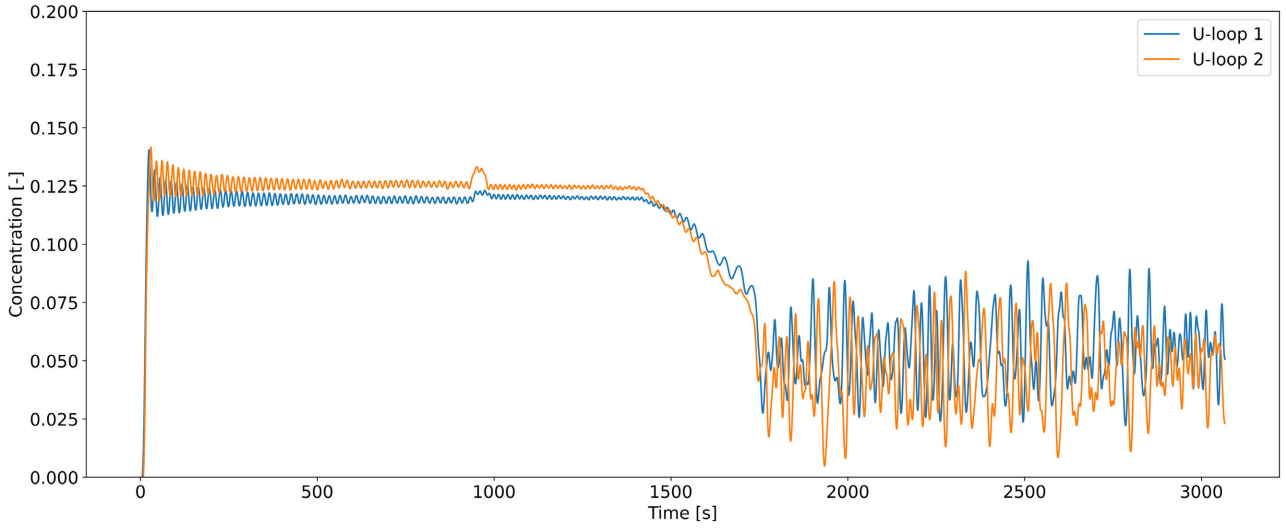

Figure 4.3: Density wave amplification with Dorsilit 8, multiple density waves with diverse wavelengths. Concentration over time.

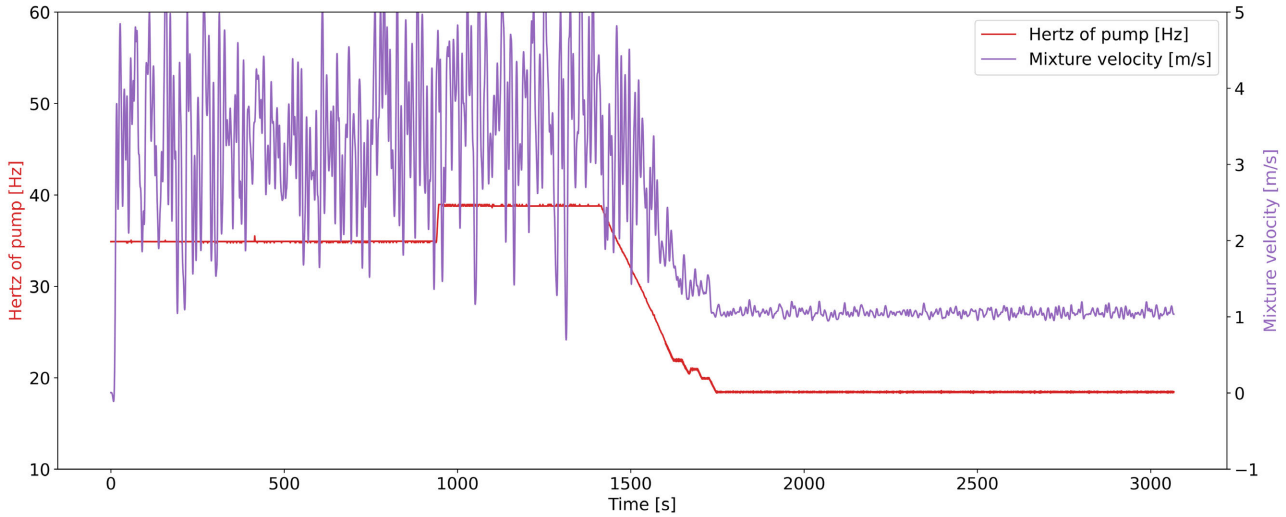

Figure 4.4: Density wave amplification with Dorsilit 8, multiple density waves with diverse wavelengths. Mixture velocity and Hertz over time.

With fine sediments, a first-order fit can be made to quantify the growth. Amplification can be described by means of an amplifying coefficient, this factor can be used for the following formula:

$$y = A * e^{\lambda t} * cos(\omega t - \phi) \tag{4.1}$$

Where A is the initial amplitude, λ the amplification rate, ω the angular frequency and ϕ the phase angle. This first-order fit with the aforementioned "suspended-driven" density wave amplification is visualised in Figure 4.5. Besides the growth rate for Zilverzand (18v%), the density wave is also shown.

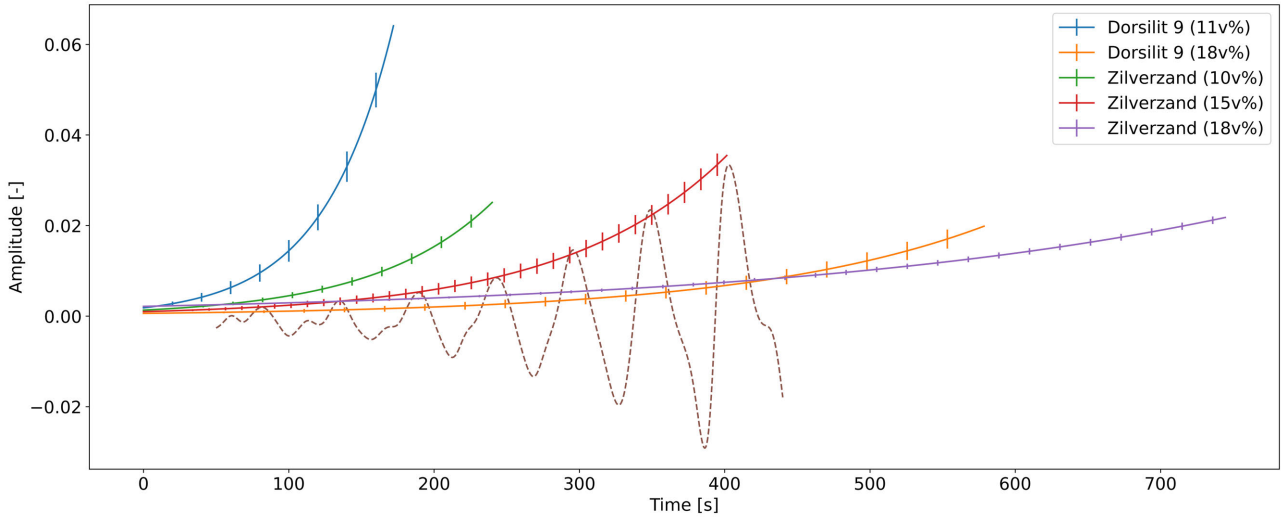

Figure 4.5: First-order polynomial fit to quantify the observed amplification of density waves.

The resulting amplification factors and initial amplitudes are summarised in Table 4.2. Concentration, mixture velocity and grain size have a significant impact on the amplification of density waves. The third test with Dorsilit 9, which corresponds with test 9 in Table 3.3, is not described as no amplification was found. Meanwhile, the coarser particles, Dorsilit 7 and 8, showed amplification for all tested concentrations. These results suggests that the tests with finer particles, Zilverzand and Dorsilit 9 appertain under a different phenomenon.

Table 4.2: Suspended-driven density waves with a summary of the concentration, initial amplitude, amplification rate, period and amplification time.

Tests	max concentration [-]	Mean concentration of wave [-]	Initial Amplitude [-]	Amplification rate [-/s]	Period [s]	Amplification time [s]
Dorsilit 9	0.1103	0.0654	0.0018	0.0207	52.48	189
Dorsilit 9	0.1802	0.0739	0.0006	0.0061	79.40	600
Zilverzand	0.0991	0.0527	0.0013	0.0123	56.68	263
Zilverzand	0.1518	0.0839	0.0010	0.0089	53.47	453
Zilverzand	0.1808	0.1311	0.0021	0.0031	42.77	840

4.2 Wavelength

The number of density waves present in the flow loop, and the wavelength are dependent on the grain size, concentration and mixture velocity. With smaller grain sizes, Zilverzand and Dorsilit 9, the wavelength is as long as the flow loop. With coarser grain sizes, Dorsilit 7 and 8, there are multiple density waves present within the loop. Having multiple density waves within one flow loop results in smaller wavelengths. These multiple density waves interact, as they have different wave celerities. Higher concentrations have a higher average particle velocity compared to lower concentrations, due to the material being in suspension and thus experiencing less friction (de Hoog et al., 2021b). Larger waves merge with smaller waves making it harder to analyse the wave characteristics.

4.3 Concentration gaps

Dorsilit 7

When comparing two different concentrations with the same coarse sediment, multiple density waves develop (see Figure 4.6 and 4.7). The waves do not have the form of a smooth wave and have large gaps where the concentration can fall as far as to zero. These concentration gaps increase in size if less volumetric concentration is put in the flow loop overall. In Figure 4.6 and 4.7 the difference in concentration gaps and the number of density waves present in the loop is shown. Furthermore, the sediments are in a state of stationary bed regime with limited suspended flow. At 11 percent volumetric concentration there are sliding bed conditions when a density wave flows by. At 25 percent volumetric concentration the bed is stationary even when a density wave passes, the wave has not enough force to overcome the shear stress of the bed.

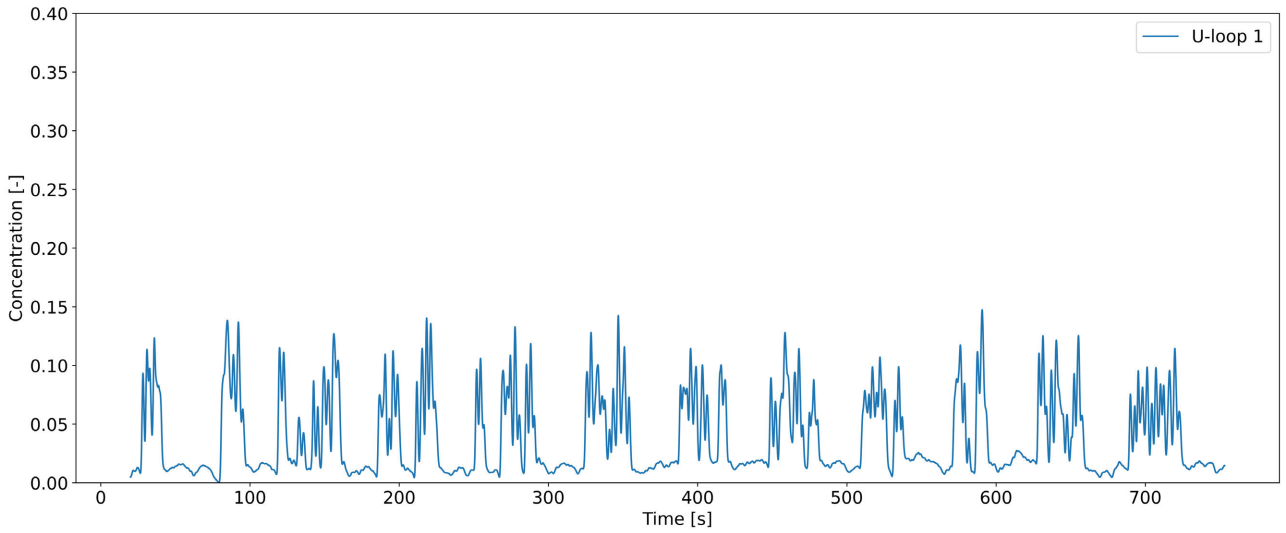

Figure 4.6: Dorsilit 7 11v%, concentration over time, with multiple density waves and significant concentration gaps.

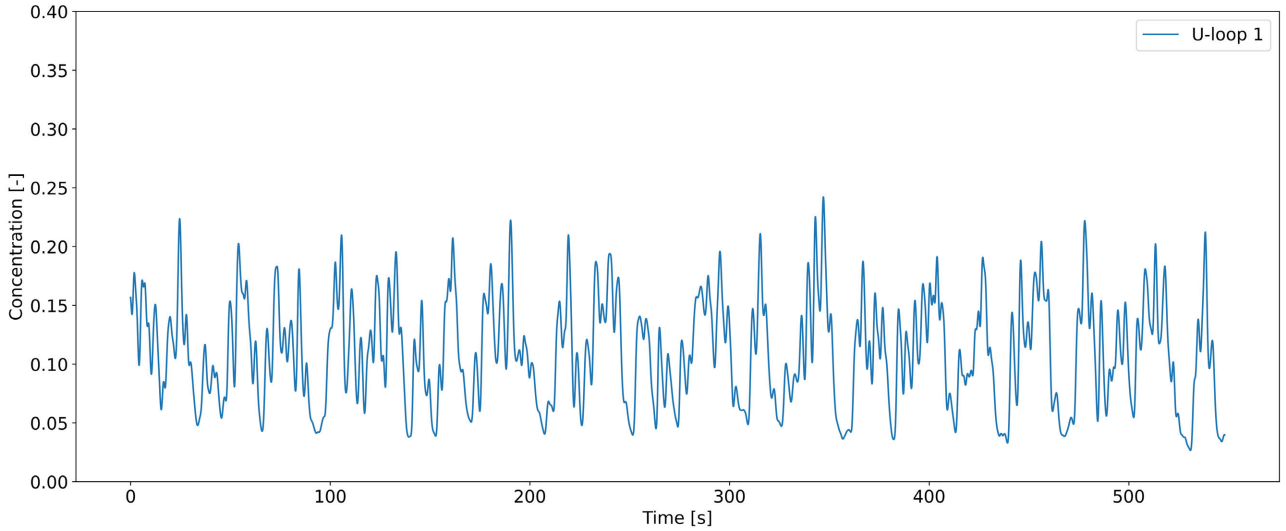

Figure 4.7: Dorsilit 7 25v%, concentration over time, with multiple density waves.

Dorsilit 8

Compared to Dorsilit 7, more material is in suspension in the Dorsilit 8 test. Another difference with the Dorsilit 7 tests, are the large concentration gaps, which are present in all tests. For all tests, the flow conditions are in a stationary bed regime, more material is in suspension than with the Dorsilit 7 tests. When a density wave passes a combination of a sliding bed and a heterogeneous flow regime is caused: the density waves have enough force to cause movements in the bed, which results in larger concentration gaps. This phenomenon is clearly visible in the Dorsilit 8 tests with high concentrations, where heavy sudden amplification resulted in parts of the pipe left with only water (see Figure B.7.4 in Appendix B). This behaviour is entirely different from the "caterpillar-like" waves that initiate when the density waves are not yet fully developed.

Zilverzand and Dorsilit 9

With the Dorsilit 9 and Zilverzand tests, the behaviour of density waves was significantly different, as no concentration gaps arised. The vast majority of the sediments are in suspension. The fine sediment tests all have sinusoidal-like density waves.

4.4 Wave celerity

The wave celerity ratio, the wave celerity divided by the mixture velocity, is given in Table 4.3. Remarkable is that for most coarser particle tests the ratio is above 1. This indicates that the wave celerity is higher than the mixture velocity. Coarser sediments experience more slip and thus this results in a lower transport factor (Matoušek, 1997). However, as the results show, this is not the case with the ratio between the wave celerity and mixture velocity. This is due to the mixture velocity being measured in a vertical orientation, while the wave celerity is calculated through a horizontal orientation. Horizontal parts have a sediment bed, and thus the true flow volume of the mixture is reduced. The wave celerity ratio can be corrected using the true volume of the pipe, which can be calculated with the average bed height, see Equation 4.2. The measurements of the bed height are estimated through close-up video footage of the pipe, which could not be determined for the finer grains due to visibility issues. The corrected celerity ratio can be calculated by dividing the corrected wave celerity with the mixture velocity, and can be found in Table 4.3. The correlation between the corrected wave celerity ratio and concentration be seen in Figure 4.8. Here, results suggest that the sediment type has no great influence on wave celerity ratio, considering suspended-driven density waves.

$$A_{ratio} = \frac{\frac{\pi}{4} * (D-h)^2}{\frac{\pi}{4} * D^2} = \frac{(D-h)^2}{D^2} \tag{4.2}$$

$$C_{w,corrected} = c_w * A_{ratio} \tag{4.3}$$

Where D is the inner diameter of the pipe and h is the height of the bed. The corrected wave celerity ratio visible in Table 4.3 and can be calculated by $C_{w,corrected}/V_m$.

Table 4.3: Characteristics of the sediments used.

Tests	In-situ concentration [-]	[Mix. velocity, min, max] [m/s]	Wave celerity [m/s]	Celerity ratio	Corrected celerity ratio [-]	Average bed height [m]
Dorsilit 7 test 1	0.1149	[0.8492, 0.67, 1.05]	0.7707	0.9076	0.7067	0.0054
Dorsilit 7 test 2	0.2047	[0.7097, 0.25, 0.98]	0.8470	1.1935	0.5185	0.0157
Dorsilit 7 test 3	0.1068	[0.6031, 0.44, 0.80]	0.8698	1.4422	0.4022	0.0217
Dorsilit 8 test 1	0.0522	[1.0557, 0.76, 1.38]	1.0674	1.0110	0.7274	0.0070
Dorsilit 8 test 2	0.0455	[0.6785, 0.60, 0.82]	0.7837	1.1550	0.5421	0.0145
Dorsilit 8 test 3	0.1205	[0.6203, 0.35, 0.88]	0.7876	1.2698	0.4448	0.0188
Dorsilit 9 test 1	0.0651	[1.1778, 0.98, 1.42]	0.8921	0.7574	0.7574	-
Dorsilit 9 test 2	0.0352	[0.6428, 0.62, 0.68]	0.3867	0.6016	0.6016	-
Dorsilit 9 test 3	No waves	-	-	-	-	-
Zilverzand test 1	0.0545	[1.1176, 1.06, 1.17]	0.7887	0.7057	0.7057	-
Zilverzand test 2	0.0868	[1.1244, 0.94, 1.35]	0.8145	0.7244	0.7244	-
Zilverzand test 3	0.0648	[0.9763, 0.61, 1.53]	0.5922	0.6066	0.6066	-

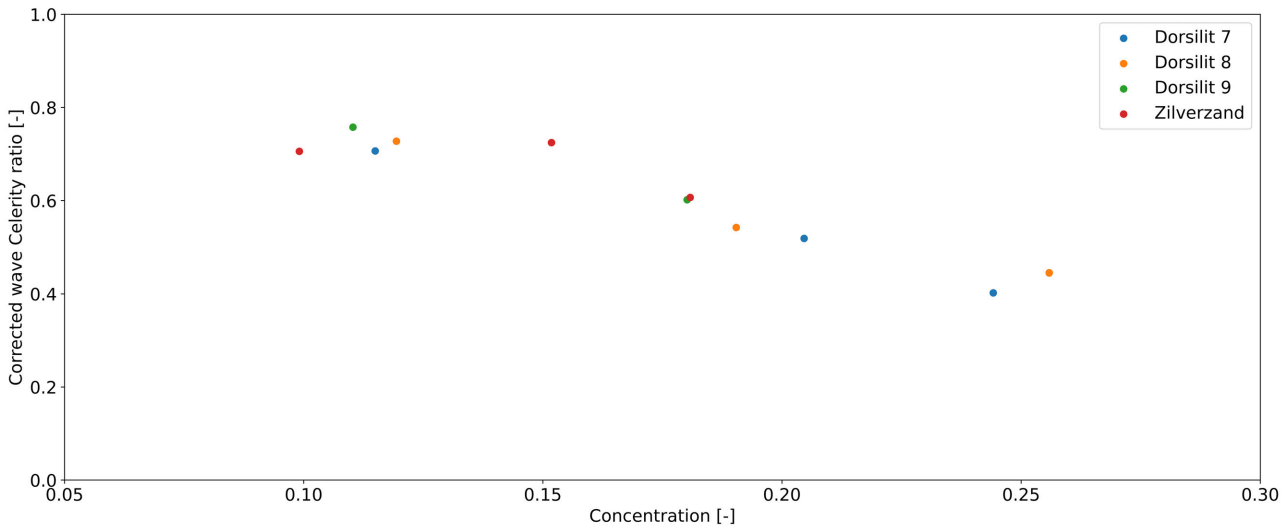

Figure 4.8: Correlation between the dimensionless wave celerity (corrected) and concentration.

4.5 Effect of the pump and U-loop on density waves

As previously described, there are two main theories of density wave amplification. One for long horizontal slurry transport and one for a combination of horizontal and vertical slurry transport. To measure the concentration in the flow loop, two U-loops were installed. With these U-loops the wave characteristics can be determined. A disadvantage of the U-loop is that it introduces a vertical element in the flow loop. To rule out the effect of the transient accumulation the U-loops are bypassed once so that there are no vertical elements in the flow loop. The sensor results are compared, with and without the U-loops, while other parameters like concentration, sediment type and flow velocity are kept the same. Without these concentration measurements, it is still possible to observe the density wave. The transient accumulation is caused by local particle velocity differences in combination with variation of flow rate, as a function of the pipe orientation (de Hoog et al., 2022). Coarser sediments have more

slip, and thus are more prone to cause an effect of transient accumulation in the loop. It is observed by de Hoog et al. (2022) that the rate of amplification may be dependent on particle size, which this study confirms. To test the effect of the transient accumulation and see if it is negligible compared to the erosion sedimentation imbalance, the coarsest material must be compared. The comparison, with or without U-loops, can be observed in Figure 4.9 and 4.10. It is clear that for both tests the behaviour of density waves is comparable. However, it takes longer to reach a steady-state with the U-loops included. Besides, there is more variation of the mixture velocity with the U-loops included, this is caused by the density wave travelling through the U-loop and resulting in extra points of acceleration and deceleration.

Removing the U-loops also results in a shorter loop. It is now known that the finer sediments have the same wavelength as the length of the loop. The loop length has an influence on the density wavelength with coarser particles. Without the U-loops the wavelength is [21.5 - 22.5] m. With the U-loops installed the wavelength is [28.5 - 30.5] m.

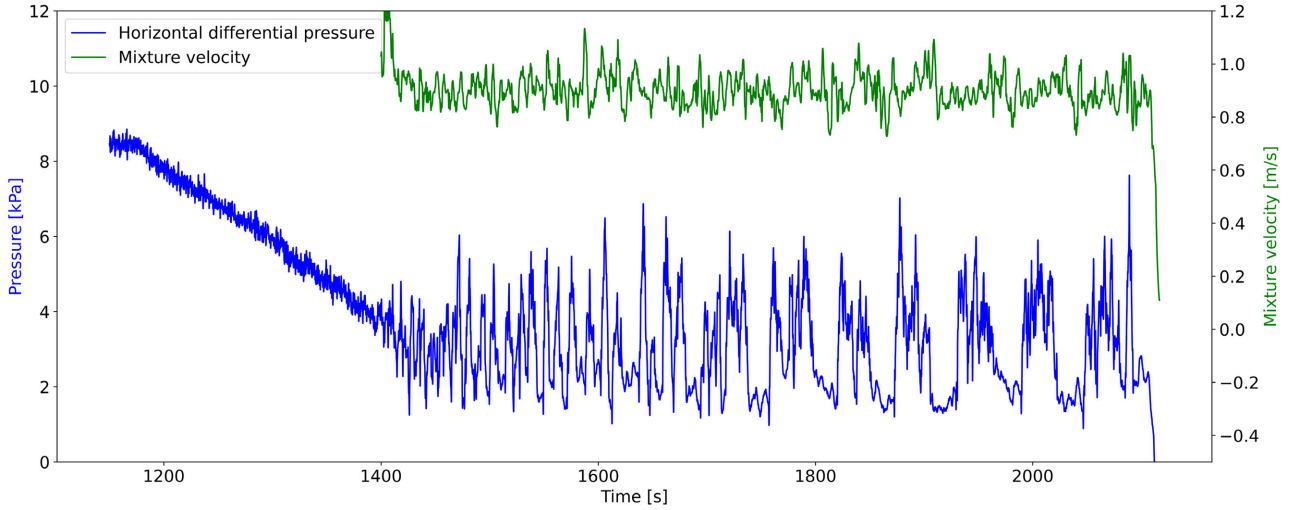

Figure 4.9: Dorsilit 7 11v%, pressure (horizontal dp-sensor) over time, with U-loops installed.

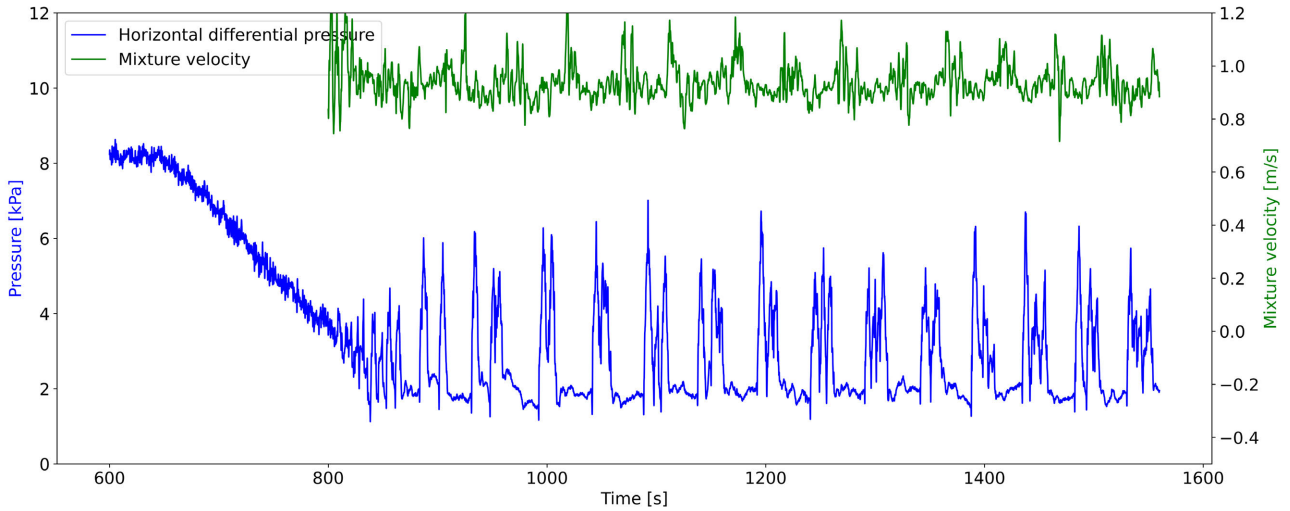

Figure 4.10: Dorsilit 7 11v%, pressure (horizontal dp-sensor) over time, without U-loops installed.

In Figure 4.10 two peaks can be identified. First the peak in horizontal differential pressure due to the density waves. Second, a peak can be identified related to the mixture velocity, which is caused

by the density wave passing through the centrifugal pump. This effect can be modelled by Stepanoff's formula (see Section 2.3).

$$f_c = 1 - C_{vd} * (0.8 + 0.6 * log(d_{50}) = \frac{P_{man,m}}{P_{man,f}} * \frac{\rho_f}{\rho_m} \tag{4.4}$$

To compare the sensor data with the Stepanoff factor, the equation can be rewritten..

$$f_{c1} = \frac{P_{wave}}{P_{fluid}} * \frac{\rho_{fluid}}{\rho_{wave}} \tag{4.5}$$

$$f_{c2} = \frac{P_{mix}}{P_{fluid}} * \frac{\rho_{fluid}}{\rho_{mix}} \tag{4.6}$$

Where P_{wave} is the pressure increase by the pump of a density wave, P_{fluid} the pressure increase by the pump of only water and P_{mix} the pressure increased by average mixture concentration.
Combining Equation 4.4, 4.5 and 4.6 results in:

$$\frac{P_{wave}}{P_{mix}} * \frac{\rho_{mix}}{\rho_{wave}} = \frac{f_{c1}}{f_{c2}} = f_{wave-mix} = \frac{1 - C_{wave} * (0.8 + 0.6 * log(d_{50}))}{1 - C_{mix} * (0.8 + 0.6 * log(d_{50}))} \tag{4.7}$$

The right- and left hand sides of Equation 4.7 can be compared resulting in Table 4.4. The data necessary to compute ρ_{wave} and ρ_{mix} is extracted from the ERT see Figures 4.11a-4.12. Although the ERT does not give the delivered concentration, the ERT data is still used, considering that when a density wave passes the whole bed slides. Using U-loop data would not be sufficient because there is a "smearing" effect caused by the length of the U-loop over which the concentration is calculated.

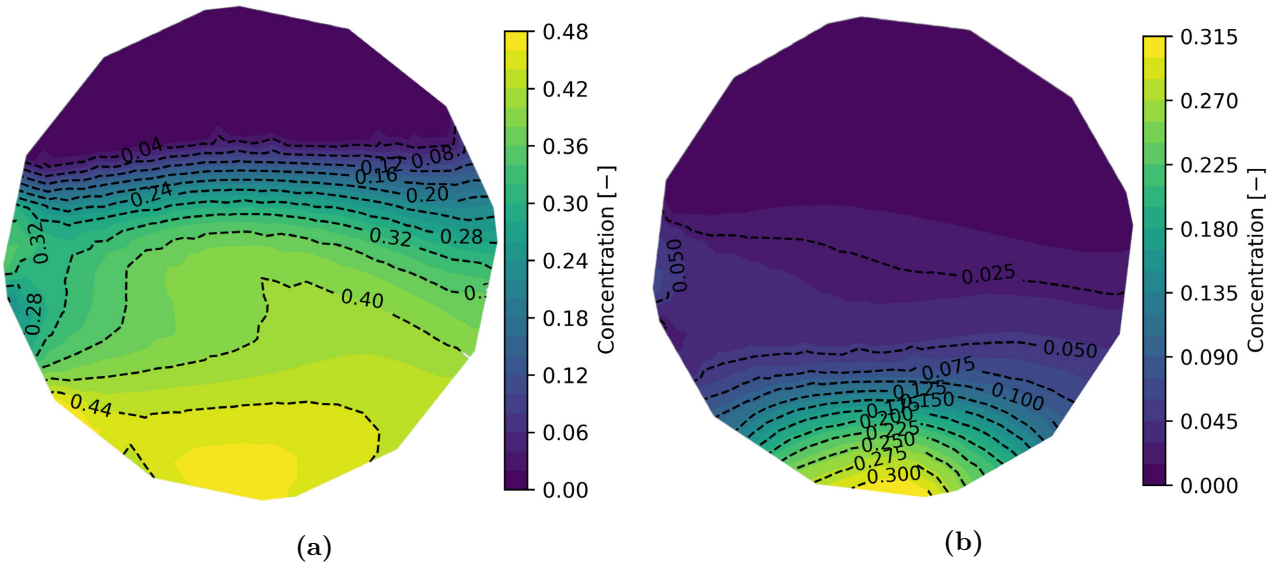

(a) **(b)**

Figure 4.11: (a): Concentration tomogram with a density wave, $C_{vd} = 0.206$ [−], (b): Mean concentration tomogram, $C_{vd} = 0.05$ [−]. Dorsilit 7 test without U-loop 15v%

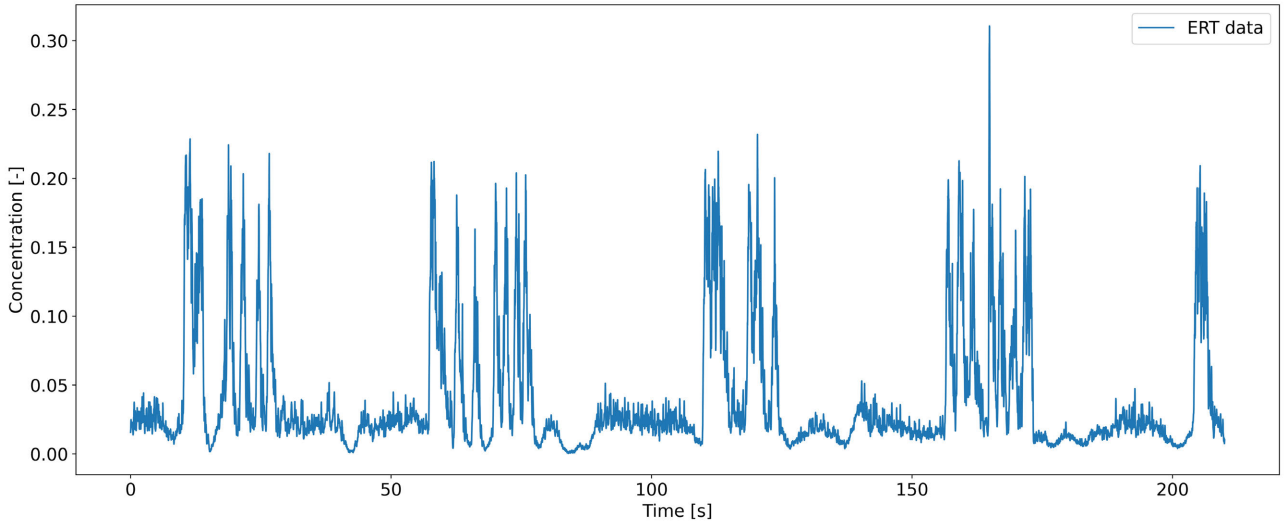

Figure 4.12: Dorsilit 7, ERT data without U-loops 15v%.

The difference in pressure is thus due to the density wave flowing through the pump, which corresponds with the estimated and calculated factors given in Table 4.4.

Table 4.4: A comparison between the calculated Stepanoff factor and experimentally derived factor.

	Wave 1	Wave 2	Wave 3	Wave 4	Wave 5
Stepanoff's factor	0.874866	0.872068	0.87704	0.871667	0.827687
Factor from experiment	0.925542	0.932924	0.90158	0.905111	0.906555

4.6 Density wave and centrifugal pump

As previously mentioned in Section 2.3, density waves can either accelerate or decelerate the mixture velocity temporarily. In the experiments as performed in this research, the centrifugal pump accelerates the mixture velocity (see Figure 4.13) due to having enough power for the extra load. The sudden acceleration caused by the pump has an effect on the whole loop. Dependent on the shear stress of the bed, this can result in a temporarily sliding bed, which is shown in Figure 4.13. Locally, the density wave accelerates, causing an increase in erosion, which in turn increases the concentration of the density wave.

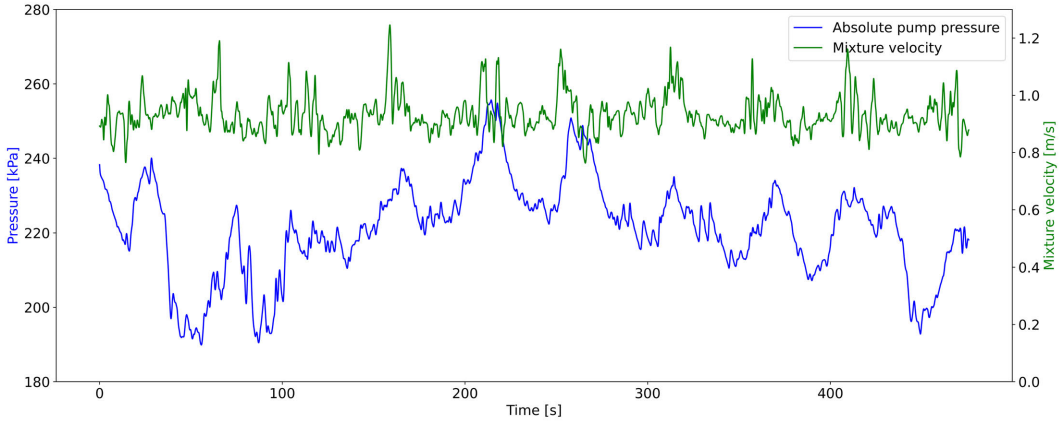

Figure 4.13: Dorsilit 7 11v%, absolute pump pressure and mixture velocity over time, without U-loops installed.

5. Discussion and conclusion

The research questions of this thesis are:

1. What is the effect of concentration, grain size and mixture velocity on density wave amplification?

   Sub-questions thesis:

   (a) What system dynamics play a role in amplifying density waves?
   (b) What is the influence of the centrifugal pumps on density wave amplification?

The main findings are outlined below:

5.1 Main findings

- The main findings of this study is that density wave mechanisms are heavily affected by the grain size:

  1. Suspended-driven density waves; fine sediments (Dorsilit 9 and Zilverzand; d_{50} of 316 μm and 240 μm respectively) where a single smooth density wave is present.
  2. Bed-driven density waves; Coarse sediments (Dorsilit 7 and Dorsilit 8; d_{50} of 1040 μm and 619 μm respectively) where multiple density waves are present.

Conclusions regarding both suspended-driven and bed-driven amplification

- Density wave amplification occurred at all but one test (test range of 10-25v%).
- Suspended-driven density waves have larger wavelengths than bed-driven density waves; the grain size influences the wavelength.
- The extent of amplification is dependent on the mixture velocity, concentration and grain size.
- Higher volumetric concentrations lead to a higher wave celerity, and lower corrected wave celerity compared to lower concentrations.
- Bed-driven density waves have a faster amplification than suspended-driven density waves.
- The length of the loop influences the length of the density wave; a shorter loop results in shorter wavelengths.
- There is no amplification of density waves when there is no bed present.

Conclusions regarding suspended-driven amplification

- There is one density wave, and it has the same length as the length of the loop.
- It takes multiple loop lengths to reach the full amplification.
- High concentrations ($C \geq 21.5v\%$) with Dorsilit 9 did not cause amplification of the density waves; high concentrations can cause damping of density waves.

Conclusions regarding bed-driven amplification

- There are multiple density waves within the loop for bed-driven density waves.
- Bed-driven density waves reaches full amplification within approximately one loop length.
- Higher concentrations lead to more density waves being present.

Conclusions regarding U-loops on density wave amplification

- The U-loops have no significant impact on the density waves.
- The U-loops cause more damping within the loop.
- The U-loops cause more mixture velocity variations.

Conclusions regarding the centrifugal pump on density wave amplification

- Density waves are accelerated within the centrifugal pump, which results in acceleration of the mixture within the entire loop.
- Coarser sediments cause more mixture velocity variations.
- The acceleration of the density waves causes more suspended sediments in the loop.
- In some cases with coarse particles, when a density wave flows through the centrifugal pump, the whole bed starts sliding temporarily.

5.2 Discussion

Two theories and two main findings

How can it be possible that density wave amplification is so vastly different when considering different grain sizes? Talmon et al. (2007) hypothesised that density wave amplification was a consequence of the imbalance between hindered settling and hindered erosion (see Figure 5.1a). This relation was made by the following formula:

$$Flux = C * \omega_0 * (1 - C)^4 \tag{5.1}$$

$$Flux/\omega_0 = C * (1 - C)^4 \tag{5.2}$$

To possibly extend on the influence of grain size on density waves the formula for hindered settling can be expanded by including the settling velocity of a single particle and make the exponent particle dependent (Rowe, 1987):

$$Flux = C * \omega_0 * (1 - C)^n \tag{5.3}$$

$$n = \frac{4.7 + 0.41 Re_p^{0.75}}{1 + 0.175 Re_p^{0.75}} \tag{5.4}$$

Figure 5.1b shows the result of the influence on the grain size with respect to hindered settlement. With increasing grain size, the maximum flux shifts to higher concentrations and a higher overall flux. However, the imbalance between erosion and sedimentation does not explain the bed-driven density waves, which are among the test results. These bed-driven density waves result in density waves with

a stationary bed, shaking bed or fully sliding bed. The erosion and sedimentation imbalance does not explain extreme cases like the Dorsilit 8 tests with high concentrations. Here, amplification happened suddenly and extreme concentration variations were measured (see Figure 5.2). A concentration peak likely caused extreme density wave growth. This case was so extreme that the density wave could be considered a plug, because it took every sediment in its passing, and left only water behind. This behaviour could be explained with the theory of Matoušek and Krupicka (2013), and that amplification could be due to the unstable slip point of the bed. With high concentrations, the hydraulic gradient is high, which can result in a sliding bed regime, or shaking bed. This sliding bed regime can develop in a plug that is observed in the Dorsilit 8 tests. This also explains why the amplification of these bed-driven waves cannot be identified; the bed regime changes from stationary bed to sliding bed. This increases the measured concentration almost instantly (concentration was measured in vertical orientation). The transition from density waves to no density waves and visa versa is fastest with the bed-driven density waves. When there was not enough suspended particle transport to move the bed, no bed-driven density waves can grow.

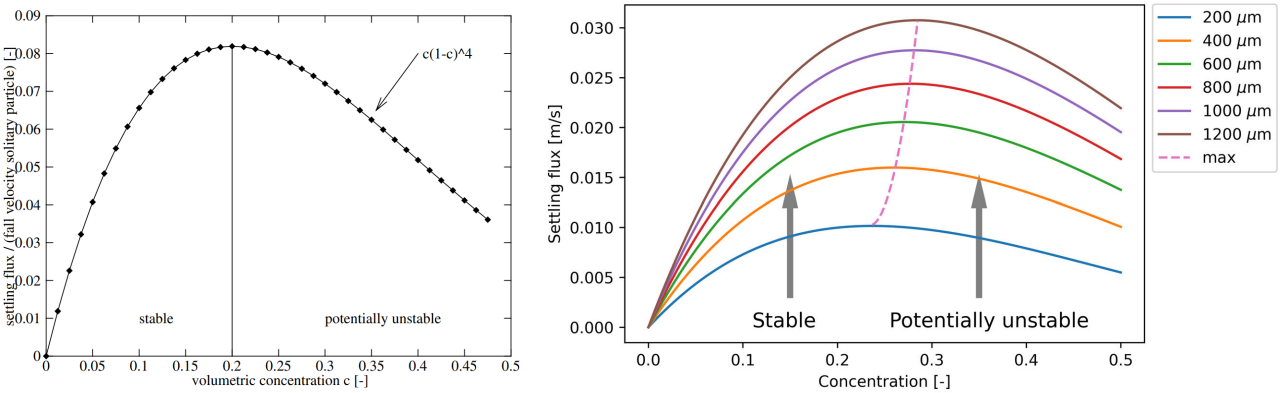

(a) (b)

Figure 5.1: (a): Settling flux/fall velocity of a single particle over concentration (Talmon et al., 2007), (b): Settling flux over concentration.

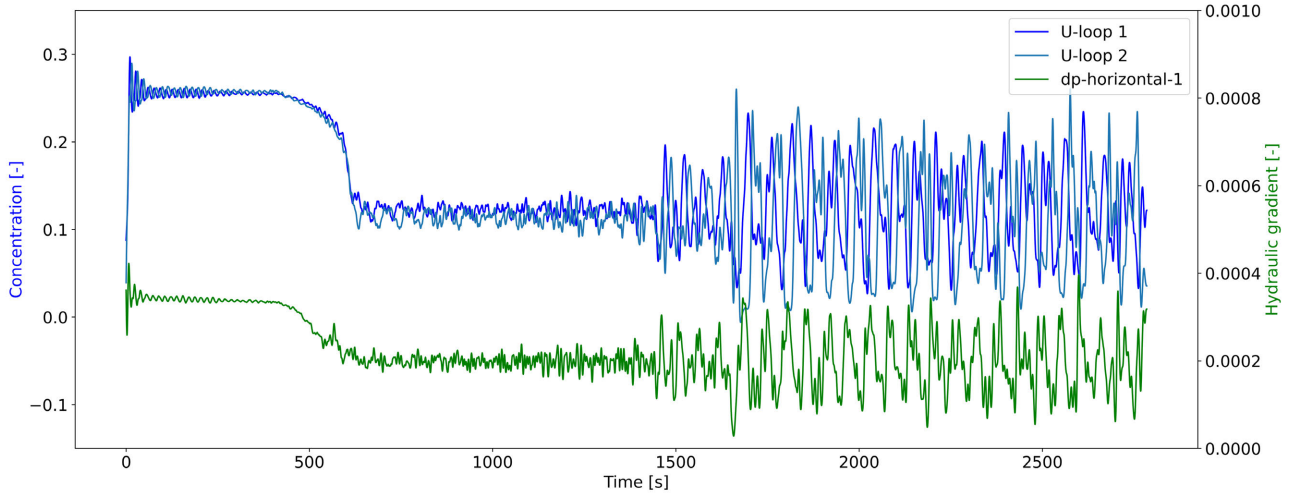

Figure 5.2: Extreme density amplification with Dorsilit 8 tests where at 2700 seconds a moving plug formed (pump RPM was kept constant).

Bed-driven density waves are similar to the data from Prins-Clausplein

This behaviour of concentrations gaps is very comparable to the results from the Prins Clausplein pipeline. With the Prins Clausplein pipeline there were multiple waves grouped together followed by large sections of extremely low concentration, see Figure 5.3a. The density waves observed in the coarse sediment tests also showed similar behaviour of multiple grouped waves and concentration gaps, see Figure 5.3b. This suggests that the density waves which occurred in the Prins Clausplein pipeline were the same as the bed-driven density waves observed in the coarse sediment tests of these experiments.

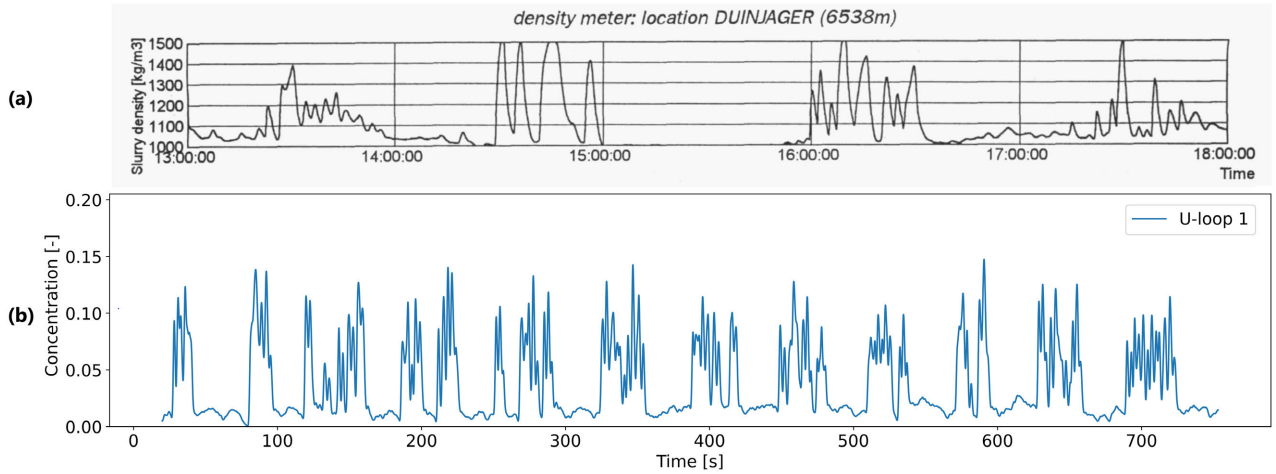

Figure 5.3: (a): Density waves measured along DN650 Prins Clausplein pipeline (11/02/81), slurry density over time (Matoušek, 1996). (b): Dorsilit 7 test at 11v%, concentration over time.

Density waves do not always occur

There has to be enough sediment in suspension to enable density wave amplification. The other way around goes for concentration, if there is a bed, density wave amplification is possible. When the concentration is very high, suspended transport can be reduced to a level where there is not enough suspended concentration to enable density wave amplification, which happened in the tests of Dorsilit 9 (21.5v%). No density waves were observed. With bed-driven density waves, there were still density waves occurring above 25 percent volumetric concentration, mixture velocity variations were bigger compared to the finer grain size tests. These large mixture variations are caused by high densities flowing through the centrifugal pump, causing temporarily bed shaking and sliding.

Loop length affects the density wave length

It can be concluded that the flow loop has a large effect on the wavelength of the density wave. Removing the U-loops resulted in shorter wavelengths even if there were multiple waves. It is observed that for the finer sediments, the wavelength was the same as the loop, even when the U-loops were removed, which made the loop shorter. It would be interesting to know what the wavelength would be if the loop had a much larger size. Turbulence causes damping and has a greater effect on finer sediments. This damping could dampen density waves and thus make the wavelength longer. Having longer wavelengths not only means a more spread-out concentration distribution along the axis of the pipe, but also less acceleration and deceleration of the mixture velocity due to sudden concentration variations in the centrifugal pump. However, this may be different for the bed-driven or suspended-driven density waves, because the bed-driven density waves seem to always have a sharp concentration gradient regardless of the wavelength.

The centrifugal pump has an effect on the density wave: two possible mechanisms

The mixture velocity can accelerate or decelerate depending on the available power of the centrifugal pump. The data do not support any conclusions on the mechanisms of pump and wave other than the density wave acceleration when flowing through the pump. However, one can speculate about possible mechanisms.
The first mechanism is: when there is a very small bed, and the density wave increases the mixture velocity, the bed can fully erode, resulting in no amplification, because there is no bed to grow from. When the bed is larger, and the acceleration does not cause a fully eroded bed, the increased mixture velocity can aid density wave growth. This is because the combination of the density wave and velocity increase can change the bed regime from stationary to sliding. Hindered settling effects could prevent damping of the density wave right after the mixture velocity decreases again, resulting in a net growth of the wave when considering the situation before and after the centrifugal pump. This all depends on the mixture velocity, concentration, shear stress of the bed and particle size.
The second mechanism is: when considering deceleration due to a sudden increase in concentration, there will be fewer sediments in suspension in the case there is a bed. When there is no bed, the decrease in the mixture velocity could create a bed depending on how close the mixture velocity is to the deposition limit velocity. The second mechanism can be expanded further. The bed could facilitate density wave growth and have a positive feedback, as the same wave re-enters the centrifugal- or booster pump and have an even greater concentration gradient, and thus deceleration de Hoog et al. (2021b).

Finer grains have slower amplification

Suspended-driven density waves have a slower amplification than bed-driven density waves. Within a single loop length, a bed-driven density wave can already fully been amplified. With suspended-driven density waves it takes multiple loop lengths to fully amplify. The theory of Matoušek and Krupicka (2013); "the unstable slip point of the bed" was tested with B8-ballotini sediment (d_{50} = 0.53 mm). Which comes closest to the Dorsilit 8 (d_{50} = 0.619 mm) which was tested in this studies experiment. Matoušek concluded multiple density waves within the loop which is comparable with our results of the Dorsilit 7 and Dorsilit 8 tests. The theory of Talmon et al. (2007) stating that the imbalance between hindered erosion and hindered settling was tested with much finer sand: d_{50} = 200 μm, d_{85}/d_{50} = 1.9 comparable with the Zilverzand (d_{50} = 240 μ) tests of this experiment. Also, amplification time is in the same order of magnitude. The results of Matoušek and Krupicka (2013), Talmon et al. (2007), and the overarching results of this study show that both theories are right; grain size determines the predominant effect.

Bed-driven density waves dominate with a wide particle size distribution

When an equal mixture of Dorsilit 7, 8 and 9 is used, bed-driven density waves are the predominant waves. With all tested concentrations, suspended-driven density waves of low periods did not occur. In the natural dredging process, a wide particle size distribution is common, and thus for long horizontal transport bed-driven density waves can be expected if the mixture velocity falls near the deposition limit velocity. In the rare occurrence that fine particles with a narrow PSD are transported near the deposit limit velocity, suspended-driven density waves can be expected. These density waves do not oppose such a threat as the bed-driven density waves, due to their predictability. The concentration variations will gradually vary, which is only a problem if a booster pump does not have sufficient power for high concentrations.

Small density waves are attenuated

With suspended driven density waves it is observed that some small peaks, especially at the beginning of the test, were attenuated these small waves get redistributed towards the larger density waves. Figure B.1.1 is a good example of such behaviour. This behaviour of the redistribution of density waves is mentioned in the literature section of the thesis, see Figure 2.15 on page 30). Although it is discussed that it does not make sense that the concentration before the wave is lower than after the density wave, the behaviour of attenuation of small density waves and amplification of larger waves is correct and observed in the experiment.

The transition between the two wave mechanisms is pipe diameter dependable

The transition of suspended-driven density waves to bed-driven density waves could depend on the diameter of the pipeline. The deposit limit velocity increases with increasing pipe diameter, which means that deposits form at a higher mixture velocity. With the particles tested in these experiments, a larger diameter pipeline may lead to different results considering the particle diameter where suspended-driven- and bed-driven density waves occur. It is likely, with a larger diameter pipeline, that suspended-driven density waves occur at coarser particles then what is observed in these experiments.

5.3 Conclusion

The main conclusion is that there are two density wave mechanisms dominated by grain size: bed-driven density waves and suspended-driven density waves. Bed-driven density waves, occurring with a particle size of $d_{50} \geq 619\ \mu m$ have multiple sharp waves in the flow loop, that can fully amplificate within one loop length. Amplification of these bed-driven density waves is dependent on the movement of the bed layer. If the bed layer shakes, only small density waves are observed. When there is enough concentration in suspension to fully overcome the Coulomb friction of the bed with respect to the pipe wall, sliding bed conditions can cause extreme amplification where plug formation is observed, which leaves no bed layer behind.

The suspended driven density waves have the same wavelength as the length of the loop and take multiple loop lengths to fully amplificate, which occurs with a particle size of $d_{50} \leq 317\ \mu m$. The rate of density wave growth is dependent on the mixture velocity, sediment bed height, sediment properties and concentration. For the suspended-driven density waves; larger mixture velocities causes faster amplification to a certain extend (if there is enough sediment bed height to facilitate the growth). For suspended-driven density waves, the high concentrations cause damping which do not result in density waves.

A mixture of equally divided sediment (Dorsilit 7,8,9 and Zilverzand) causes bed-driven density waves. Thus, given the natural dredging process where a broad PSD is most common, it would be expected that bed-driven density waves would most often occur.

Density waves have an impact on the centrifugal pump. When a wave flows through the centrifugal pump, the absolute pressure rises, causing an increase in mixture velocity. With the bed-driven density waves, in some cases the sediment bed starts to slide in the loop when a density wave flows through the centrifugal pump. There is no density wave growth if there is no sediment bed present.

6. Recommendations

6.1 Modelling

- While research is found on hindered settling, little is known about hindered erosion. An increase in prediction accuracy on the imbalance between hindered erosion and hindered settling could give insight into the dominance of suspended-driven density waves or bed-driven density waves for different grain sizes.

- Bed-driven density waves were overall less predictable and not as smooth as suspended-driven density waves. Suspended-driven density waves were more uniform. This is in accordance with the current theory by Talmon et al. (2007), who states that this is caused by the effect between settling and erosion. This effect could be enough to physically model suspended-driven density waves.

- Physically modelling bed-driven density waves is not recommended with a hindered settling and erosion model, because results from these experiments and previous theory by Matoušek and Krupicka (2013) conclude that this is a different process, namely the unstable slip point of the bed. Reliably modelling these density waves could be difficult due to the irregularity of these density waves, the slip point of the bed is dependent on the pipe diameter, the pipe material and the type of sediment used.

6.2 Experiment

- Suspended-driven density waves were as large as the flow loop. If the loop length is extended, it is most probable that the density wavelength also increases. Regarding bed-driven density waves, Matoušek and Krupicka (2013) concluded that the number of waves did not change when the length of the loop doubled in size, meaning that the wavelength became larger. This might also be the case for suspended-driven density waves.

- Instead of a closed-loop design, an open-loop design can be used. With an open-loop design suspended-driven density waves are more difficult to fully develop. For example, the high-concentration Zilverzand test took 800 meters to fully develop. Low-concentration Zilverzand test took 230 meters which is still impractical. If open-loop tests are to be carried out, coarse particle sizes are recommended, as these took less than 20 meters, which can can be carried out on a laboratory scale.

- Larger diameter testing is recommended. A larger diameter results in less flow profile distortion at bends or other disturbances. Furthermore, smaller diameter pipeline may not fully facilitate full eddy development which results in less upward flux due to turbulence. Testing the diameter size, and thus also the effect of turbulence on density wave growth, would be interesting.

- Placing two U-loops in the flow loop made the wave analysis of density wave development more self-evident. The effects of the two U-loops were minimal when regarding dampening effects.

- The ERT is a useful tool to analyse wave to bed interaction. Because of the cross-sectional concentration data, the bed height over time can be estimated. This estimation of the bed height can be used to study wave to bed interaction regarding different sediments. With this data the transition between suspended-driven and bed-driven density waves could be determined with more accuracy.
- The fact that the ERT is temperature sensitive to its measurements is a downside when compared to the U-loop. However, the benefit to using an ERT is that the measurement area is relatively small compared to the U-loop. A small measurement area is more beneficial due to the space needed for implementation to the setup and measurement of dynamic behaviour. For this reason an ERT is recommended when analysing dynamic slurry behaviour.
- GE PTX 5032-TB-A3-CA-HO-PA pressure sensors gave a raw pressure signal which could easily be post-processed using a low-pass filter design. During experiments, one sensor had to be replaced with another. This Rosemount pressure sensor had an additional hardware filter integrated which gave a more smooth signal. This feature however removes the possibility of fully analysing the signal including the noise. Having control with a digital filter to analyse raw data enables more capabilities for analysing the signal.

7. Acknowledgements

While I am extremely proud of the work I have delivered over the last year, I have some people to thank for their support and guidance along the way. It has not always been easy and fun. Research is accompanied by high peaks and long valleys of emotional gratification.

First of all I want to thank Arno and Cees, whom I had many interesting meetings with. Not the standard question-, answer- and critique-format, but with lively discussions. These discussions made me think critically about the work I have done and gave me more insight into this topic. Also inviting Cees and Arno to the location of Royal IHC and showing the progress I was making with my experiments gave me more energy towards the thesis.

Second all of the colleagues at IHC, for all the chats, coffees, lunches, and most of all help at the experimental phase of this study. For the latter, I especially want to thank Yarno, who repeatedly helped me build, adapt, rebuild, troubleshoot, and run the tests. I really liked this physical part of my thesis; to improve my welding, building and woodworking while being splashed with the water and sand mixture, every once in a while.

Furthermore, I am so glad about all the help from André, to actually write things down, in an organised way. Reviewing papers is your expertise and it helped me create a more organised and well-structured thesis.

Besides my dad I also want to thank Marjolein, Viktor, Menno, Suus en Mark, for the support throughout the project; most of all the trips we did: skiing, sailing, fishing and other activities which gave me new energy to work on my thesis.

My very pretty girlfriend: who I think is very cute and intelligent and helped review this document while also busy writing a thesis. The adventures we did together, like visiting Jordan, helped me vent out a lot of stress.

To Lucrees, for helping to print everything but this text.

For Turhan to help with both studying throughout this master's and critically think with me during this thesis.

But most of all I want to thank Edwin, who really was a 'daily' supervisor for me. At all times, he would be available, with ideas and help. To give feedback even over his holiday. The trust he put in me. Thinking back to all the fun moments of problem-solving, showing each other things we are enthusiastic about, like making sausages or archaeological digging of old stuff.

References

Clift, R., & Clift, D. H. M. (1981). Continuous measurement of the density of flowing slurries. *International Journal of Multiphase Flow*, *7*(5), 555–561.

Colebrook, C. F., Blench, T., Chatley, H., Essex, E., Finniecome, J., Lacey, G., ... Macdonald, G. (1939). Correspondence. turbulent flow in pipes, with particular reference to the transition region between the smooth and rough pipe laws.(includes plates). *Journal of the Institution of Civil engineers*, *12*(8), 393–422.

de Hoog, E., Talmon, A. M., & van Rhee, C. (2021a). *The relevance of time domain effects for the design and stability of hydraulic transport pipelines.* CEDA Dredging Days 2021, Virtual Conference-Proceedings.

de Hoog, E., Talmon, A. M., & van Rhee, C. (2021b). Unstable transients affecting flow assurance during hydraulic transportation of granular two-phase slurries. *Journal of Hydraulic Engineering*, *147*, 04021029. doi: 10.1061/(asce)hy.1943-7900.0001913

de Hoog, E., van Wijk, J. M., Talmon, A. M., & van Rhee, C. (2022). Predicting density wave amplification of settling slurries using a 1d driftux model. *Powder Technology*, *400*, 117252. Retrieved from `https://www.sciencedirect.com/science/article/pii/S0032591022001462` doi: https://doi.org/10.1016/j.powtec.2022.117252

Durand, R. (1953). Basic relationships of the trnsportation of solids in pipes-experimental research. *Intern. Assoc. Hydr. Res., 5th Congr. Minneapolis, 1953*.

Ferguson, R. I., & Church, M. (2004). A simple universal equation for grain settling velocity. *Journal of sedimentary Research*, *74*(6), 933–937.

Führböter, A. (1961). Uber die förderung von sand-\vasser-gemischen in rohrleitungen. *Mitteilungen des Franzius-Instituts fur Grund-und Wasserbau der TH Hannover*(19), 1–148.

Garside, J., & Al-Dibouni, M. R. (1977). Velocity-voidage relationships for fluidization and sedimentation in solid-liquid systems. *Industrial & engineering chemistry process design and development*, *16*(2), 206–214.

Jufin, A., & Lopatin, N. (1966). O projekte tuin na gidrotransport zernistych materialov po stalnym truboprovodam. *Gidrotechniceskoe Strojitelstvo*, *9*, 49–52.

Matoušek, V. (1995). Non-stationary solids flow in a long slurry pipeline with pumps in series-process of material aggregation. In *Proc., 8th int. conf. on transport and sedimentation of solid particles. wroclaw, poland: Wroclaw univ. of environmental and life sciences.*

Matoušek, V. (1996). Unsteady solids flow in a long slurry pipeline with pumps in series - process of material aggregation. *Journal of Hydrology and Hydromechanics*, *44*, 396-409.

Matoušek, V. (1997). *Flow mechanism of sand-water mixtures in pipelines.* [PhD-thesis]. Delft University of Technology.

Matoušek, V. (2001). *Solids transportation in a long pipeline connected with a dredge. an internal structure of slurry flow under a condition of fluctuating slurry density.* Delft University of Technology.

Matoušek, V., & Krupicka, J. (2013). *Different types of unsteady flow of solids generated in laboratory slurry pipe loop.* 16th International Conference on transport and sedimentation of solid particles.

Matoušek, V., & Talmon, A. M. (2021). *Dredge pumps and slurry transport* (No. OE44035). Delft University of Technology.

Miedema, S. A. (2019). *Slurry transport fundamentals, a historical overview & the delft head loss & limit deposit velocity framework 2nd edition* (R. C. Ramsdell, Ed.). Delft University of Technology. doi: 10.5074/T.2019.002

Miedema, S. A., Lu, Z., & Matoušek, V. (2003). Numerical simulation of a development of a density wave in a long slurry pipeline. In *23rd weda technical conference & 35th tamu dredging seminar,*

chicago, usa.

Richardson, J. F., & Zaki, W. N. (1954). Sedimentation and fluidisation: Part i. *Transactions of the institution of chemical engineers*, *32*, 35–53.

Rowe, P. (1987). A convenient empirical equation for estimation of the richardson-zaki exponent. *Chem. Eng. Sci.*, *42*, 2795–2796.

Samson, R., & Biello, J. A. (2017). Longitudinal instability of slurry pipeline flow. *International Journal of Multiphase Flow*, *90*, 57-63. doi: 10.1016/j.ijmultiphaseflow.2016.12.005

Sobota, J., & Kril, S. I. (1992). Liquid and solid velocity during mixture flow. In *Proc. 19th int. kolloquium massenguttransport durch rohrleitungen (1992).*

Talmon, A. M. (1992). Bed topography of river bends with suspended sediment transport. *Communications on hydraulic and geotechnical engineering (USA).*

Talmon, A. M. (1999). *Mathematical analysis of the amplification of density variations in long-distance sand transport pipelines.* Maastricht, Netherlands: 14th International Conference on Slurry Handling and Pipeline Transport.

Talmon, A. M. (2002). Solids transport instability in the sliding bed regime. In *11th international conference on transport and sedimentation of solid particles. ghent, belgium* (pp. 9–12).

Talmon, A. M., Aanen, L., & Bakker-Vos, R. (2007). Laboratory tests on self-excitation concentration fluctuations in slurry pipelines. *Journal of Hydraulic Research*, *45*, 653-660. doi: 10.1080/00221686.2007.9521801

Talmon, A. M., Feixin, W., de Ridder, J. K. D., & Guojun, H. (2019). Stationary waves measured in sand transport pipes. In *Proceedings 22nd world dredging congress* (pp. 281–290). Chinese Dredging Association (CHIDA).

van de Berg, C., & Stam, N. (2013). Ihc merwede handbook for centrifugal pumps and slurry transportation. MTI Holland B.V.

van Wijk, J. M., & Blok, B. W. (2015). The influence of grain size on the performance of conductivity concentration meters. *Flow Measurement and Instrumentation*, *45*, 384-390. doi: 10.1016/j.flowmeasinst.2015.08.005

van Wijk, J. M., de Hoog, E., Talmon, A. M., & van Rhee, C. (2022). Concentration and pressure measurements of dense sand and gravel multiphase flows under transient flow conditions in a vertically oriented closed conduit — assessment of system and sensor performance. *Flow Measurement and Instrumentation*, *84*. doi: 10.1016/j.flowmeasinst.2022.102126

van Wijk, J. M., van Grunsven, F., Talmon, A. M., & van Rhee, C. (2015). Simulation and experimental proof of plug formation and riser blockage during vertical hydraulic transport. *Ocean Engineering*, 58-66. doi: 10.1016/j.oceaneng.2015.04.015

van Wijk, J. M., van Rhee, C., & Talmon, A. M. (2014). Axial dispersion of suspended sediments in vertical upward pipe flow. *Ocean Engineering*, *92*, 20-30. doi: 10.1016/j.oceaneng.2014.09.041

Wilson, K. C. (1992). Influence of particle properties on solids effect. *Proceedings of the 10th International Kol. Massenguttransport Druch Rohrleitungen.*

Wilson, K. C., Addie, G. R., Sellgren, A., & Clift, R. (2006). *Slury transport using centrifugal pumps* (3rd ed.). New York, USA: Springer.

A. Supplement: Calibration

A.1 Differential pressure sensor 'dp-horizontal-1'

Table A.1: Voltages and pressures measured during calibration.

Pressure [kPa]	8.28	14.26	24.5	30.49	34.95
Voltage [Volt]	0.397	0.5329	0.7659	0.9022	1.0038

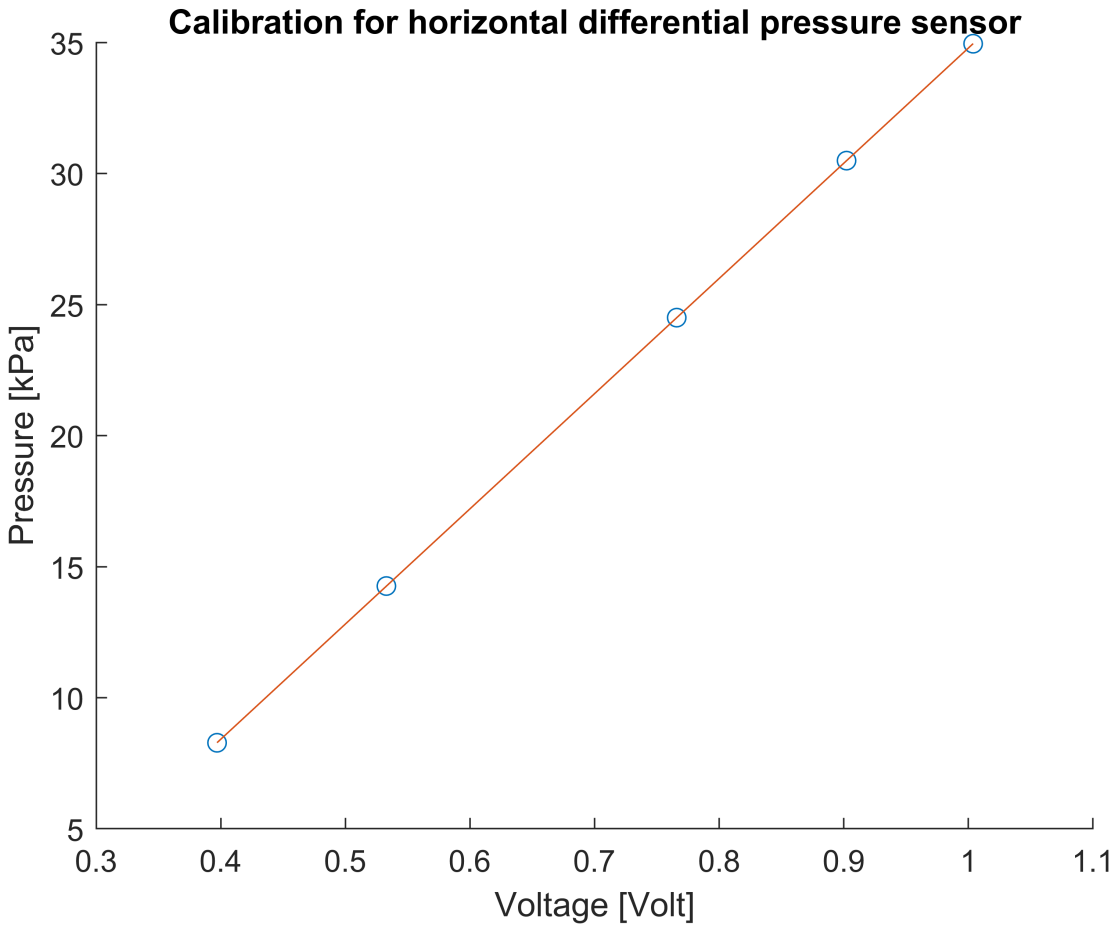

Figure A.1.1: Calibration curve for the differential pressure sensor in the horizontal oriented pipe (dp-horizontal-1).

$$\Delta P = -9.165122682167410 + 43.951805600210200 * volts \tag{A.1}$$

A.2 Differential pressure sensor in the riser for U-loop 1

Table A.2: Voltages and pressures measured during calibration.

Pressure [kPa]	0	8.14	31.31	32.85	49.15
Voltage [Volt]	0.2066	0.3368	0.5468	0.731	0.9907

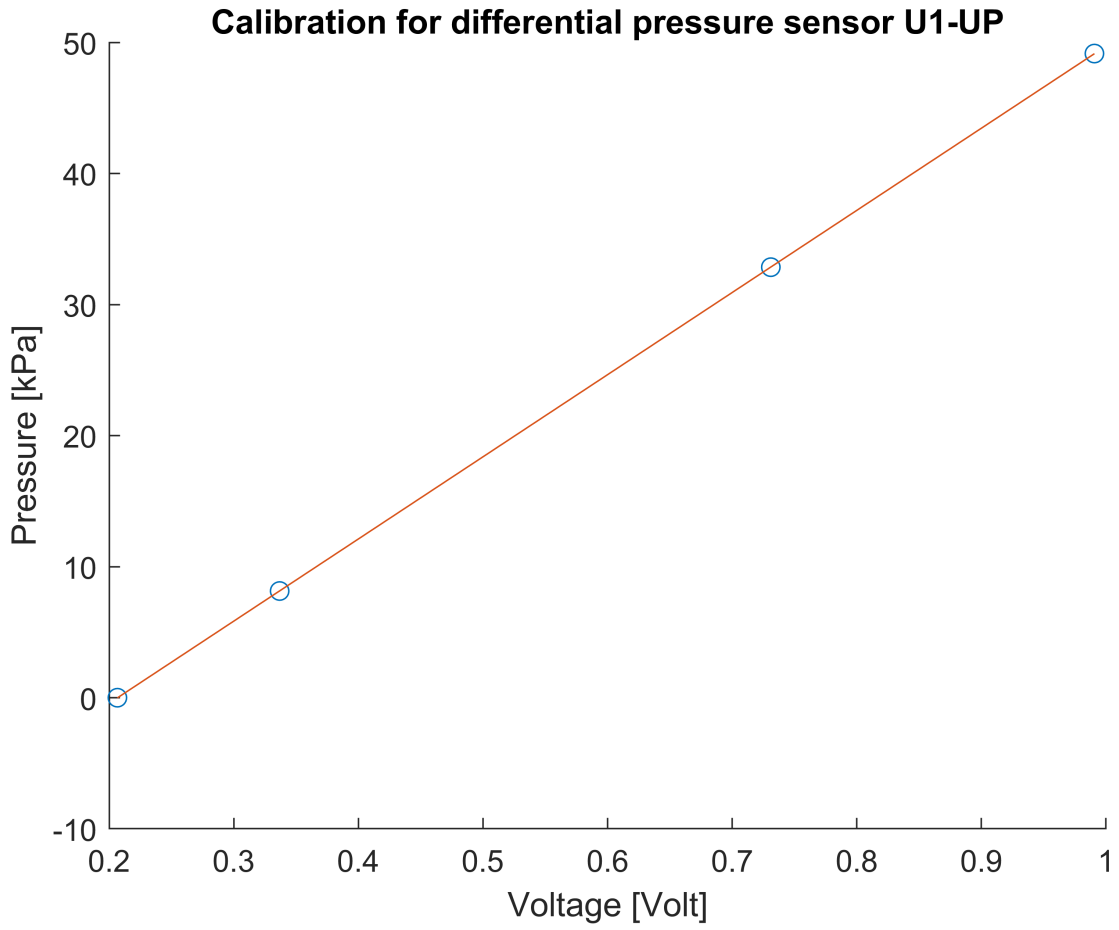

Figure A.2.1: Calibration curve for the differential pressure sensor in the riser of U-loop 1.

$$\Delta P = -12.963071424899500 + 62.686983223521300 * volts \tag{A.2}$$

A.3 Differential pressure sensor in the downgoer for U-loop 1

Table A.3: Voltages and pressures measured during calibration.

Pressure [kPa]	-28.09	-16.49	-9.66	0	8.62	15.33	23.06	29.41
Voltage [Volt]	0.2302	0.3849	0.4757	0.6045	0.7194	0.8083	0.9115	0.9955

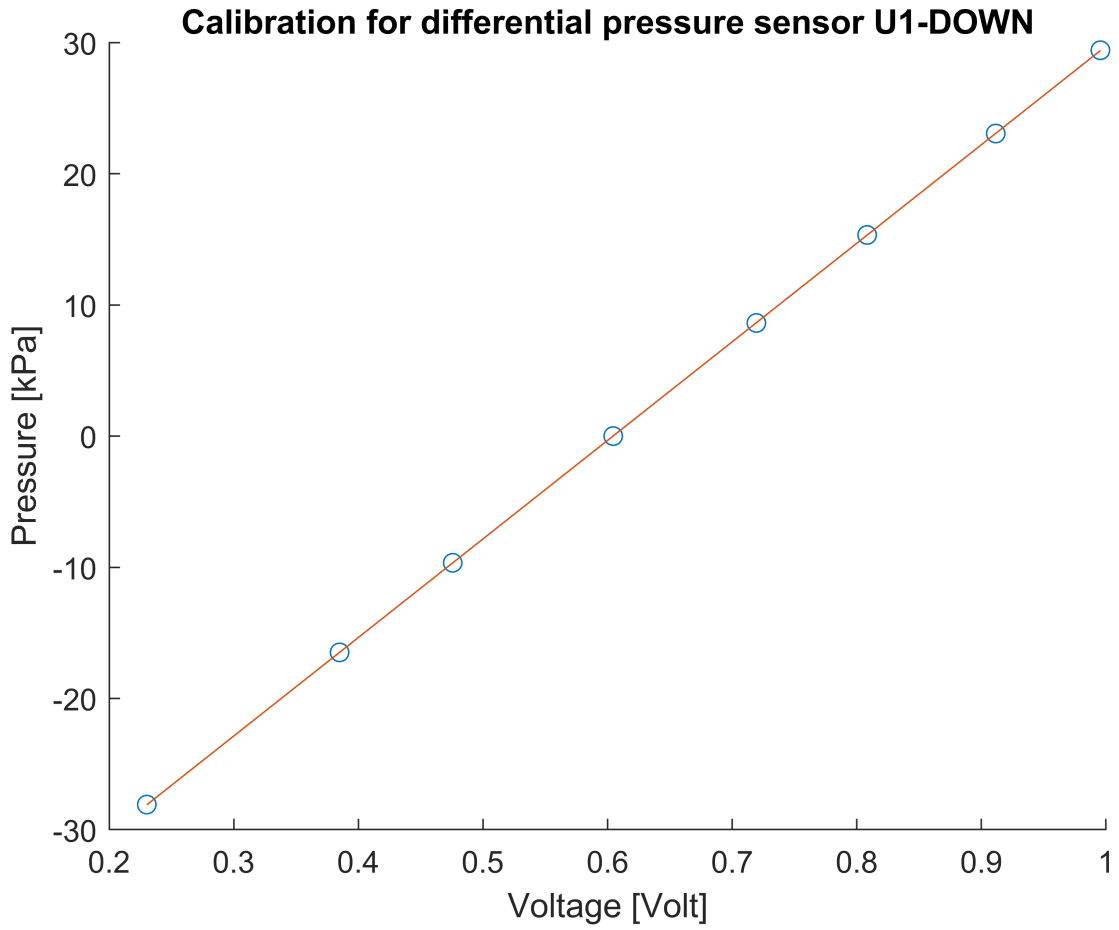

Figure A.3.1: Calibration curve for the differential pressure sensor in the downgoer of U-loop 1.

$$\Delta P = -45.398311028492400 + 75.120173143847800 * volts \tag{A.3}$$

A.4 Differential pressure sensor 'dp-horizontal-2'

Table A.4: Voltages and pressures measured during calibration.

Pressure [kPa]	14.92	24.29	37.13	41.18	49.89
Voltage [Volt]	0.444	0.5934	0.7981	0.8631	1.0019

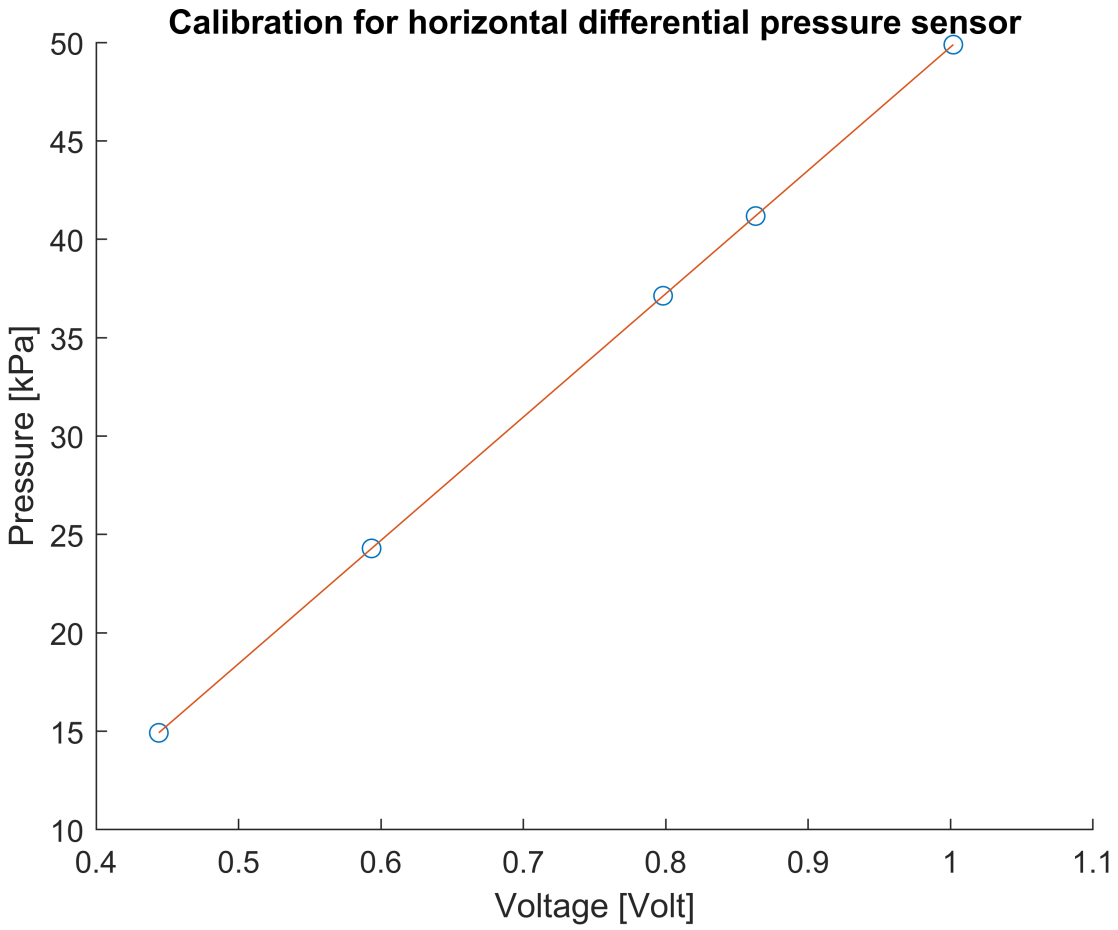

Figure A.4.1: Calibration curve for the differential pressure sensor in the horizontal oriented pipe (dp-horizontal-2).

$$\Delta P = -12.90420421851400 + 62.67559008041340 * volts \tag{A.4}$$

A.5 Differential pressure sensor in the riser for U-loop 2

Table A.5: Voltages and pressures measured during calibration.

Pressure [kPa]	0	8.78	15.65	23.42	29.76
Voltage [Volt]	0.2083	0.4076	0.5632	0.7406	0.8846

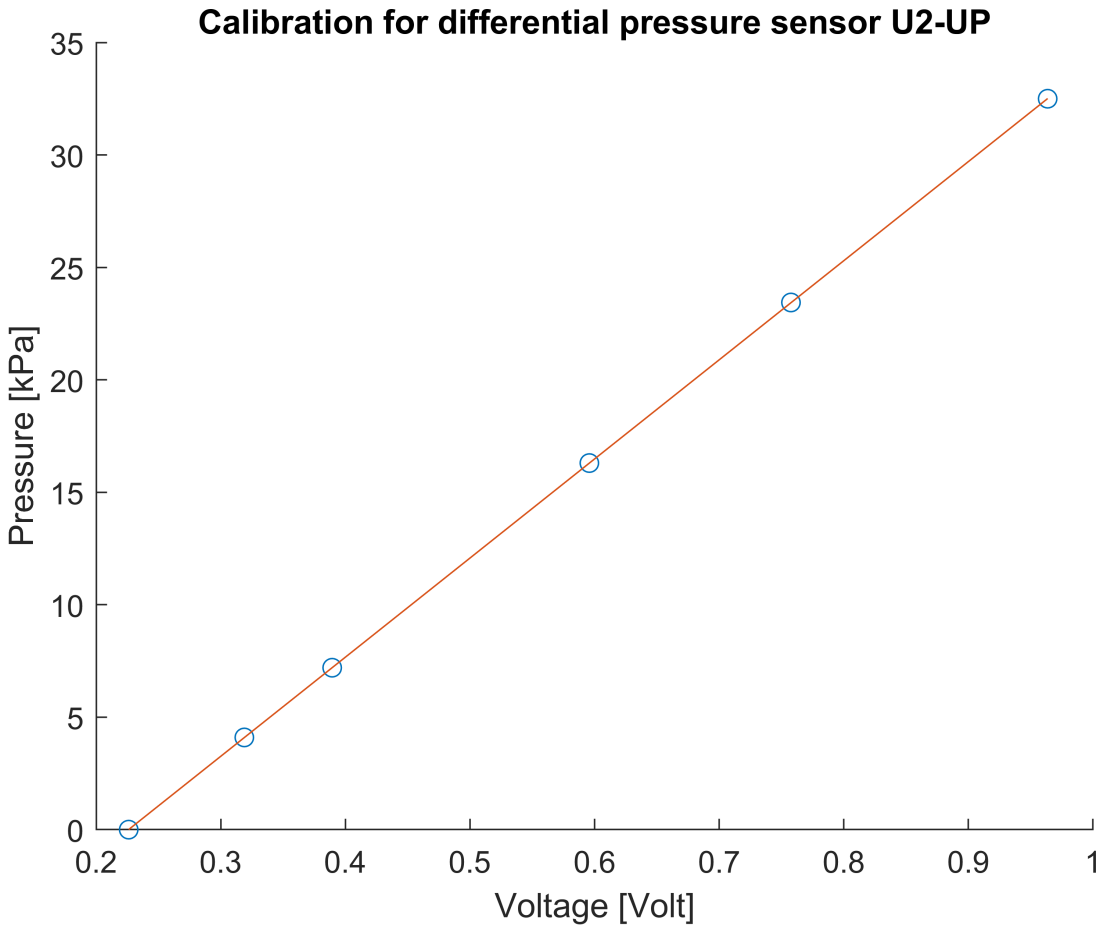

Figure A.5.1: Calibration curve for the differential pressure sensor in the riser of U-loop 2.

$$\Delta P = -9.154099922152770 + 43.996897482710100 * volts \tag{A.5}$$

A.6 Differential pressure sensor in the downgoer for U-loop 2

Table A.6: Voltages and pressures measured during calibration.

Pressure [kPa]	-27.14	-22.75	-13.68	-0.08	4.15	10.61	17.62	20.63	27.85
Voltage [Volt]	0.2476	0.3054	0.4261	0.6072	0.6618	0.747	0.8406	0.8805	0.9763

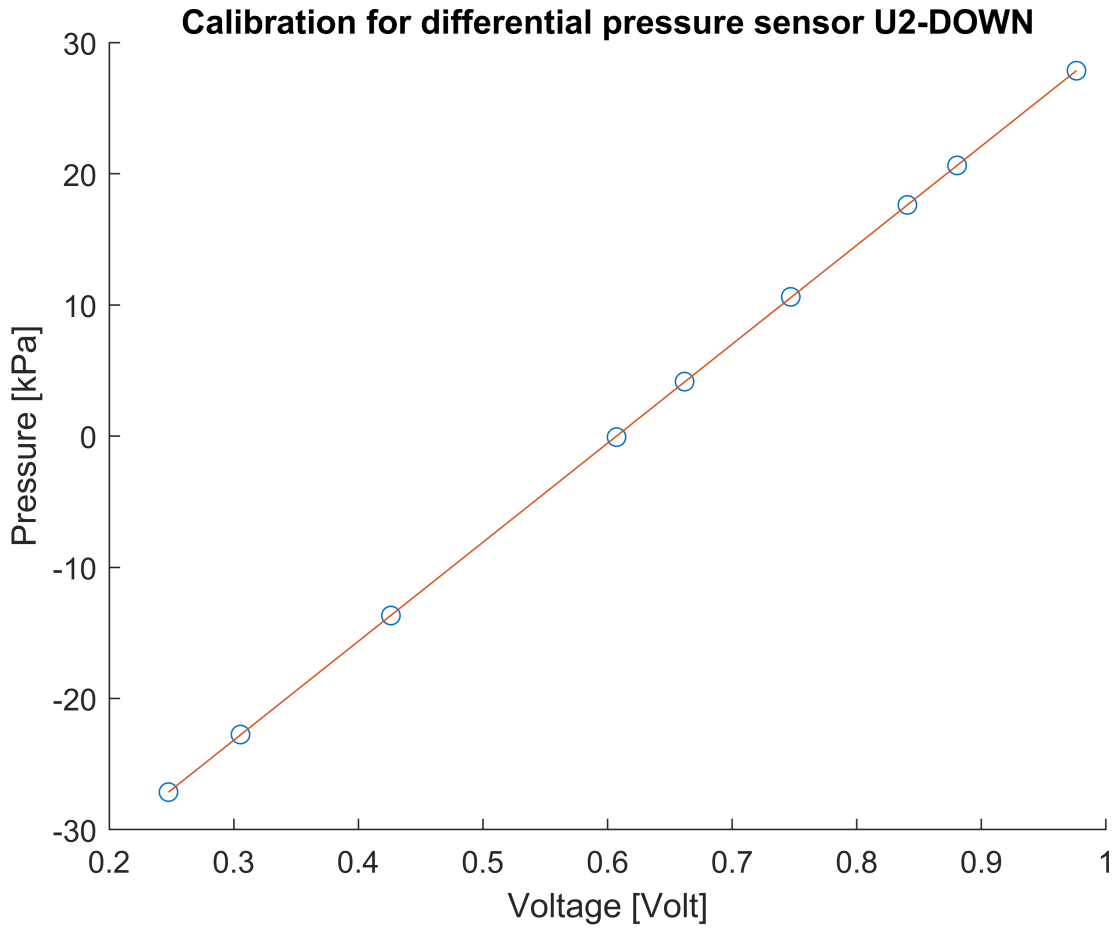

Figure A.6.1: Calibration curve for the differential pressure sensor in the downgoer of U-loop 2.

$$\Delta P = -45.8271370038436 + 75.4772477882464 * volts \tag{A.6}$$

A.7 Absolute pressure sensor for the pump

Table A.7: Voltages and pressures measured during calibration.

Pressure [kPa]	-81.98	-60.81	-40.23	-19.32	0	38.43	86.33	130.68	184.92
Voltage [Volt]	0.2501	0.3051	0.3594	0.4148	0.4658	0.5681	0.6953	0.8135	0.9583

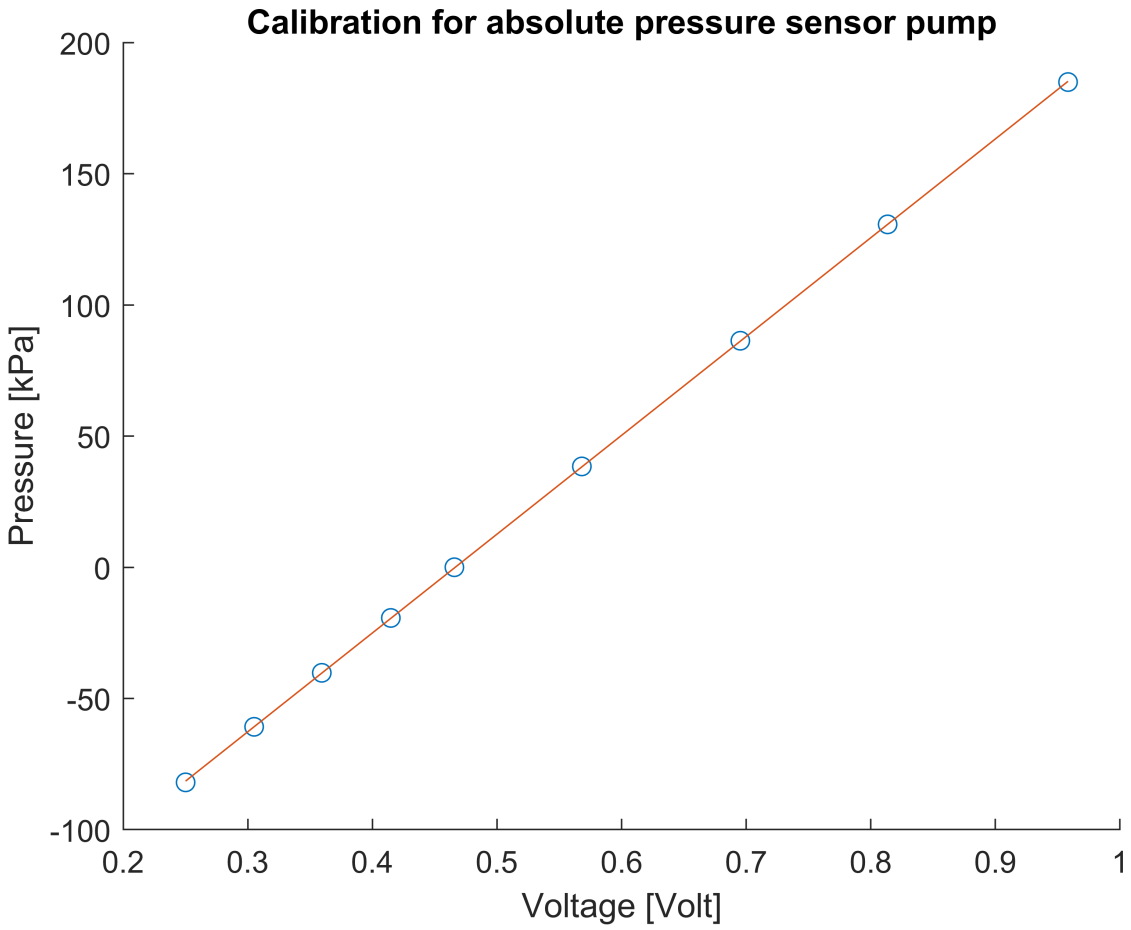

Figure A.7.1: Calibration curve for the absolute pressure sensor for the pump.

$$P = -175.675947758554000 + 376.594801636922000 * volts \tag{A.7}$$

A.8 Differential pressure sensor for the pump

Table A.8: Voltages and pressures measured during calibration.

Pressure [kPa]	0	55.49	96.06	137.95	181.52	202.72
Voltage [Volt]	0.2009	0.2894	0.3557	0.4209	0.4904	0.5241

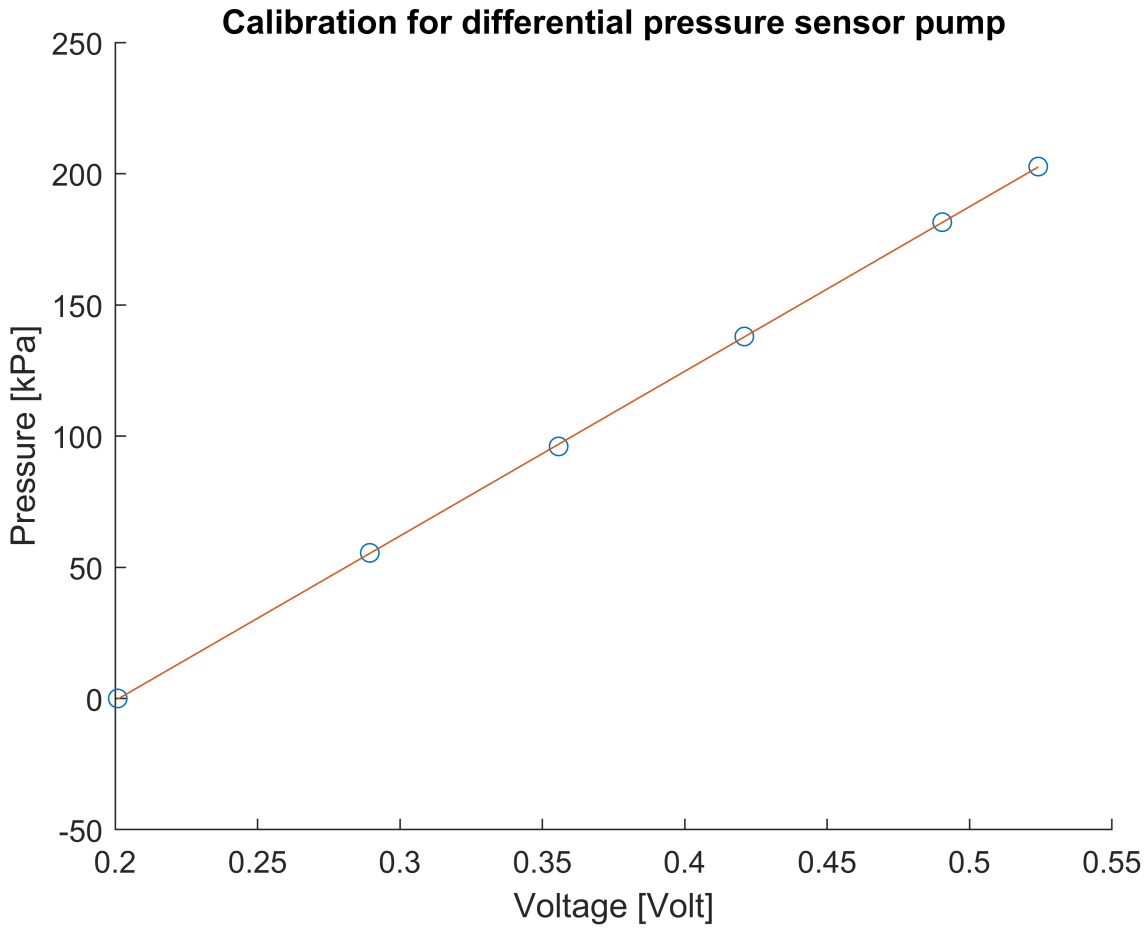

Figure A.8.1: Calibration curve for the differential pressure sensor for the pump.

$$\Delta P = -126.2968902414420 + 627.4749458440660 * volts \tag{A.8}$$

A.9 Flow meter

Table A.9: Voltages and pressures measured during calibration.

Pressure [kPa]	0	5	10
Voltage [Volt]	0.19954	0.5989	0.9982

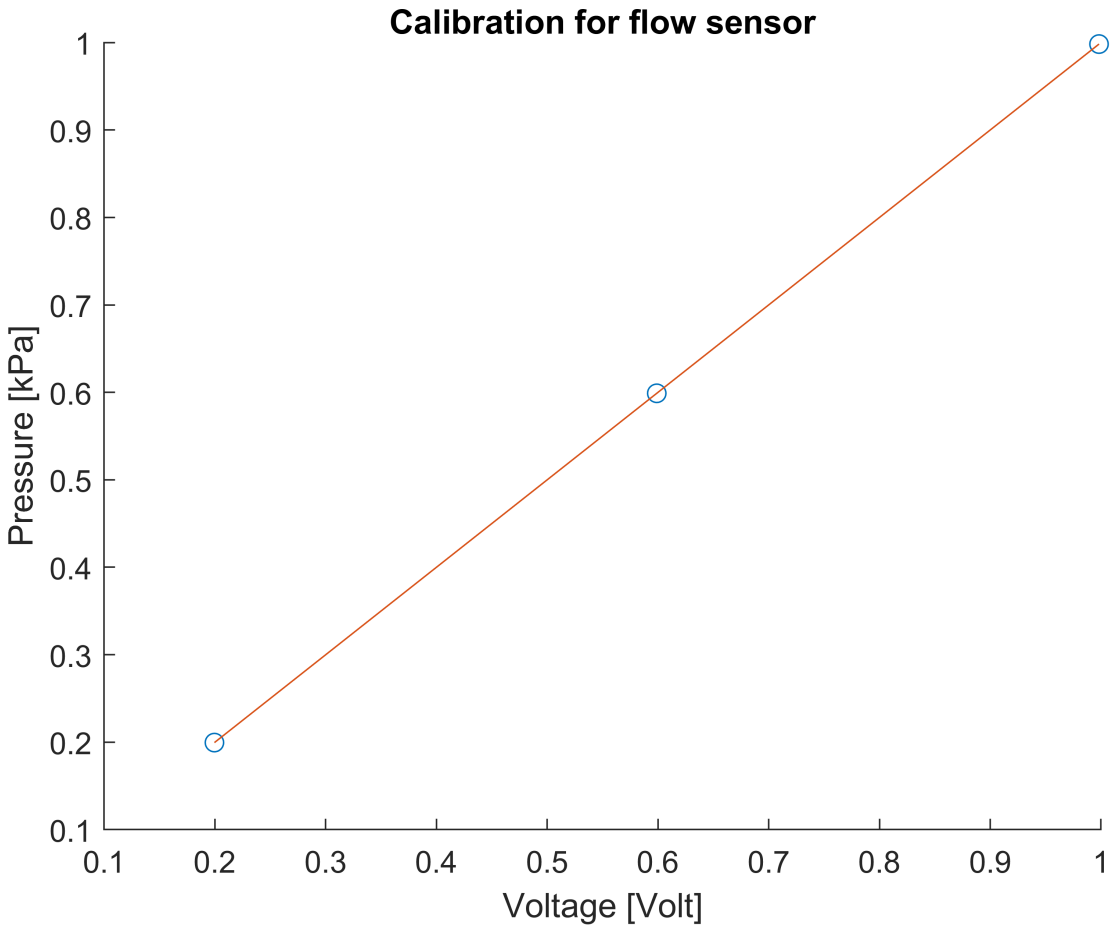

Figure A.9.1: Calibration curve for the flow meter.

$$Q_{flow} = -2.498560074040630 + 12.520972605598200 * volts \tag{A.9}$$

B. Supplement: Full tests

B.1 Zilverzand

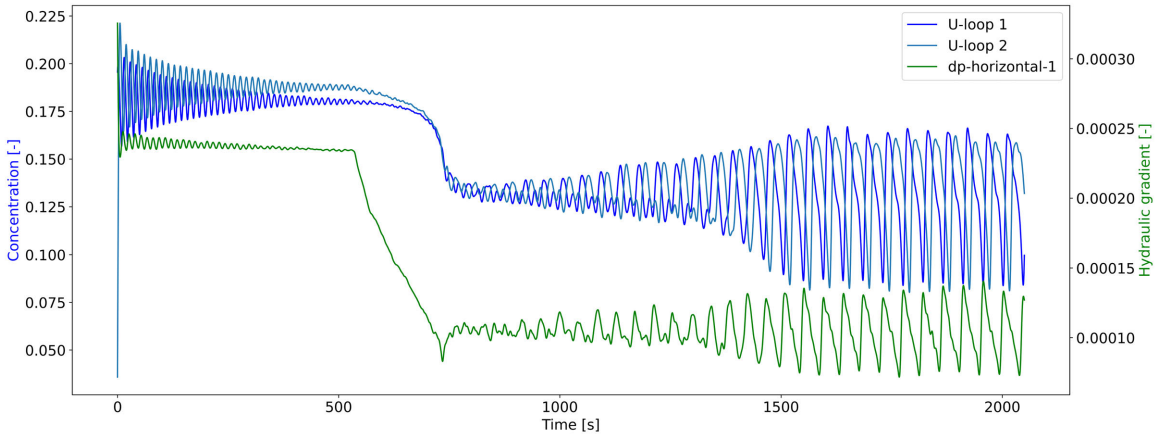

Figure B.1.1: Zilverzand 35v% test.

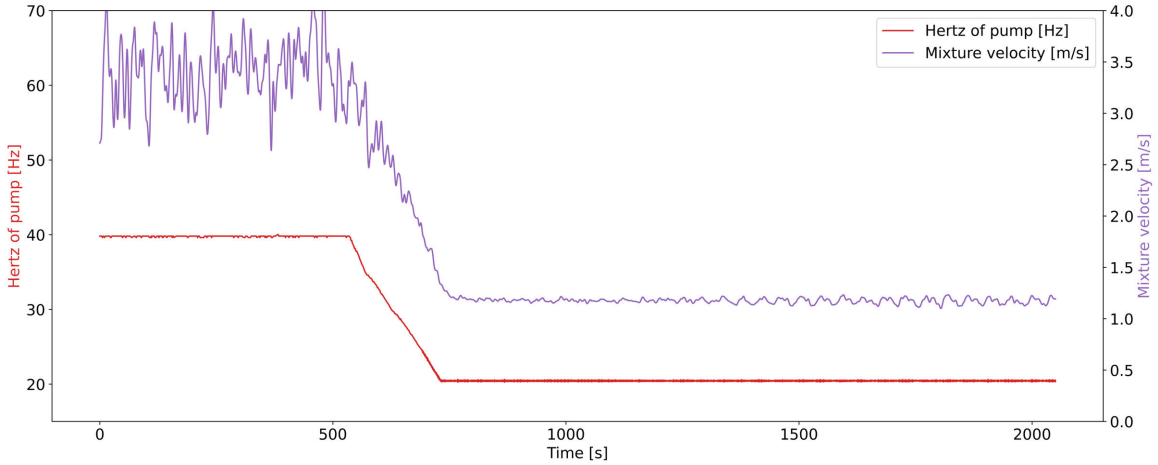

Figure B.1.2: Zilverzand 35v% test.

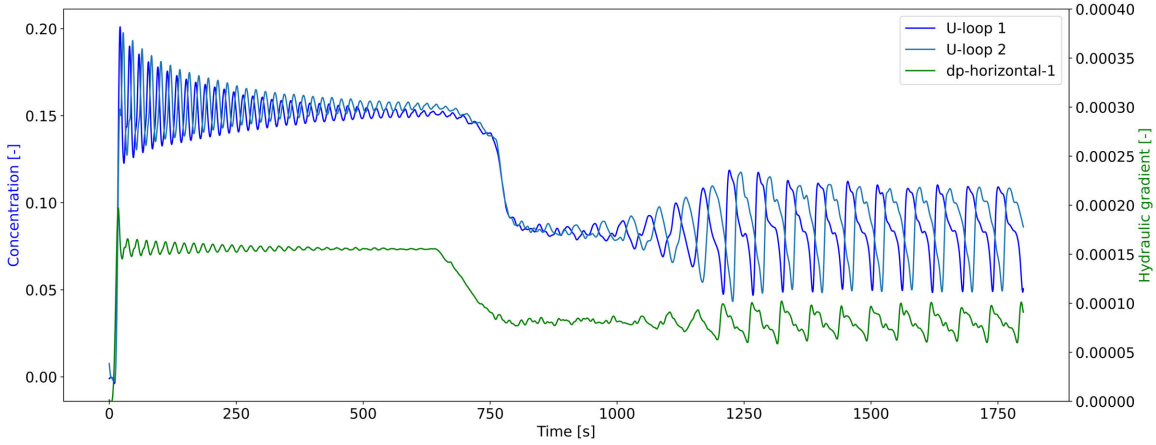

Figure B.1.3: Zilverzand 25 v% test.

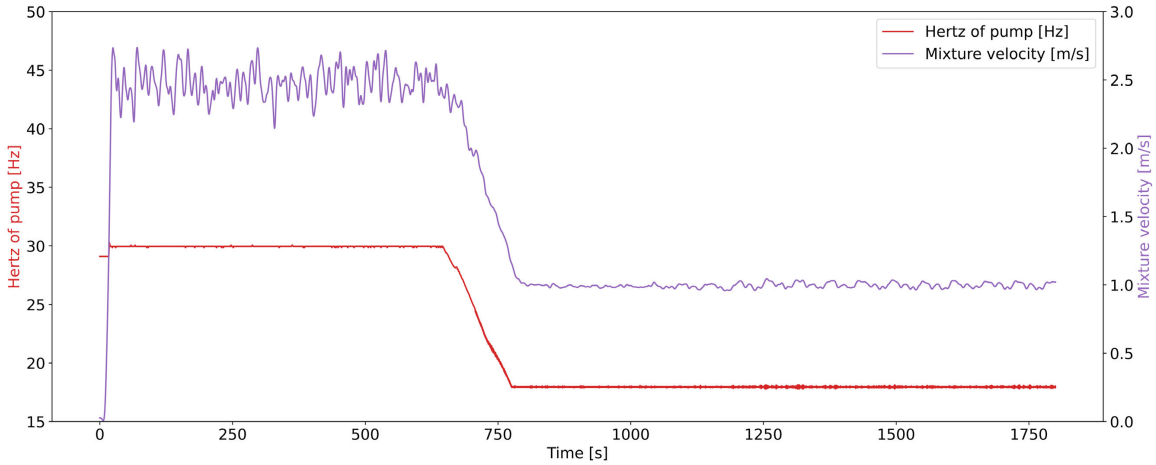

Figure B.1.4: Zilverzand 25v% test.

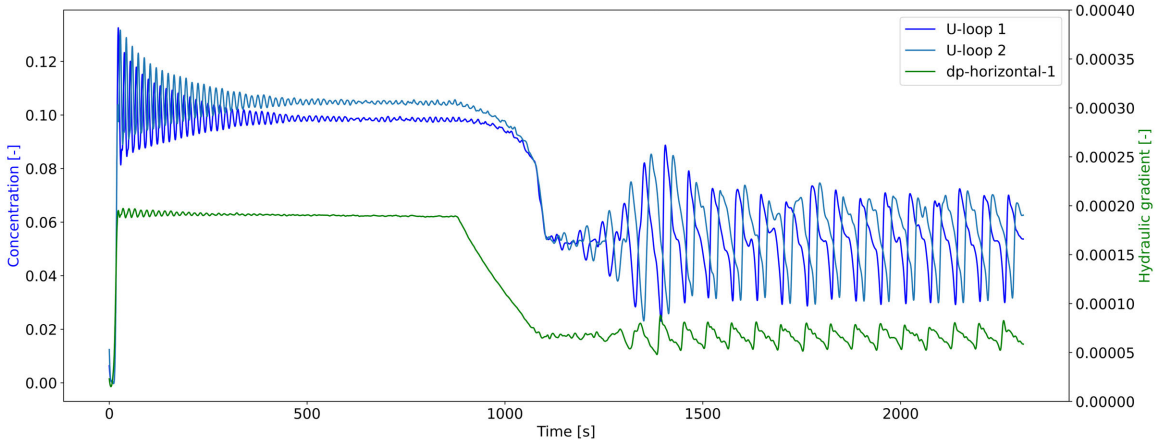

Figure B.1.5: Zilverzand 15v% test.

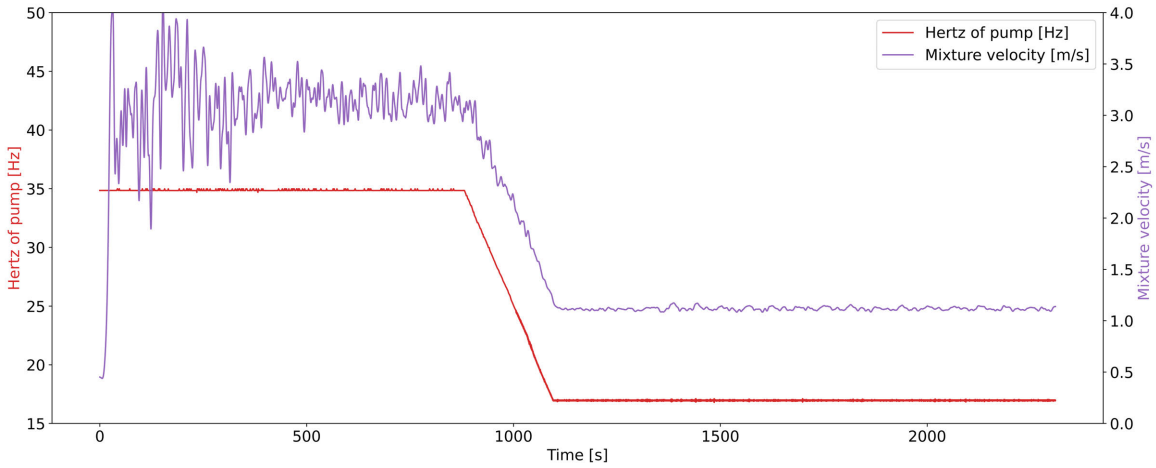

Figure B.1.6: Zilverzand 15v% test.

B.2 Dorsilit 9

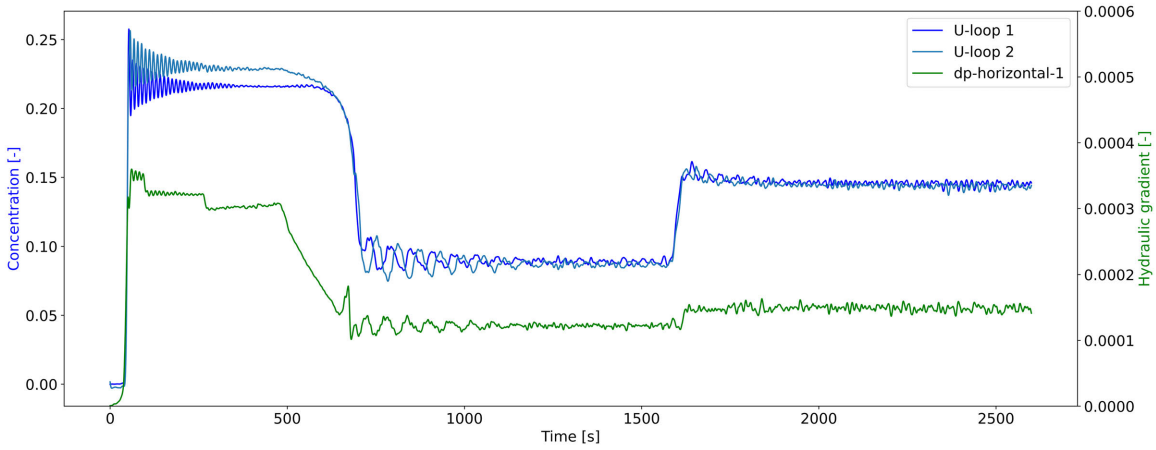

Figure B.2.1: Dorsilit 9 35v% test.

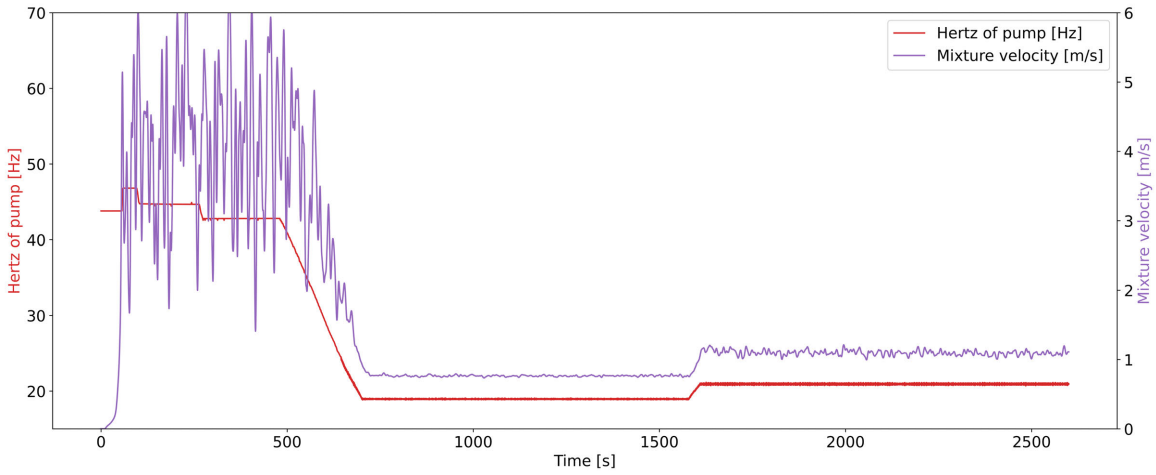

Figure B.2.2: Dorsilit 9 35v% test.

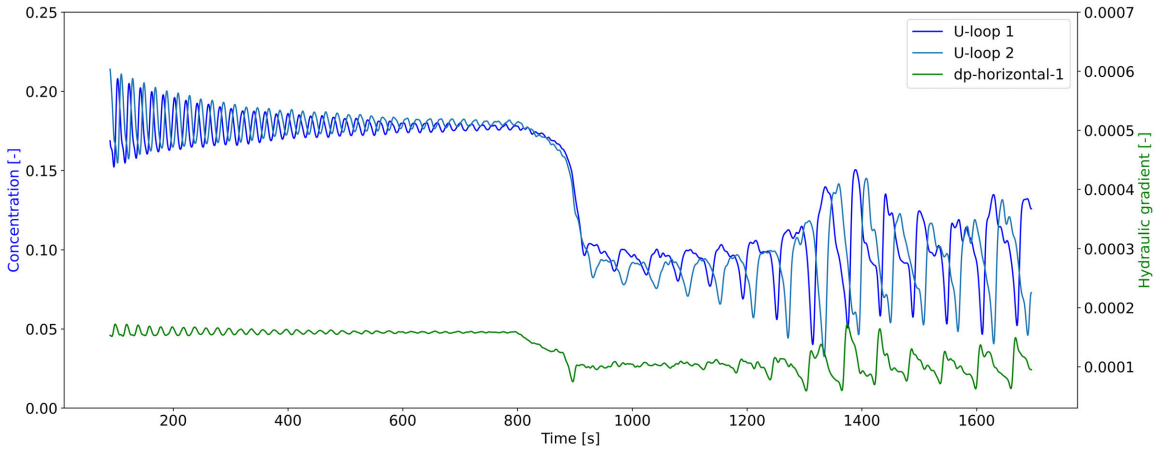

Figure B.2.3: Dorsilit 9 25v% test.

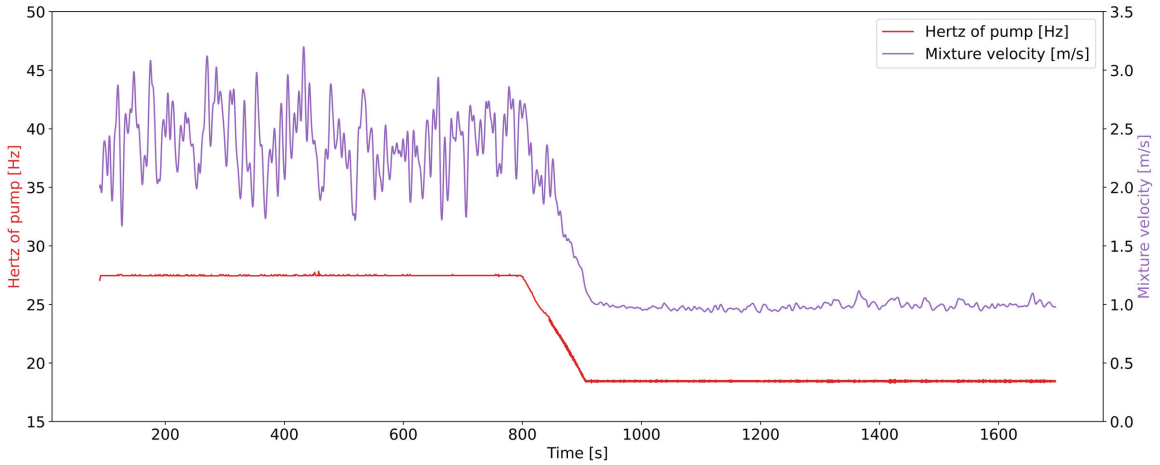

Figure B.2.4: Dorsilit 9 25v% test.

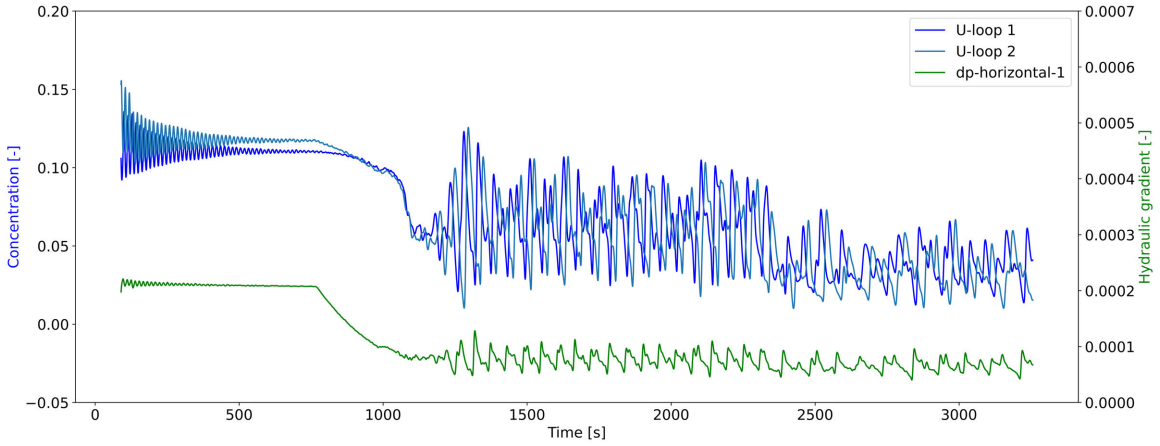

Figure B.2.5: Dorsilit 9 15v% test.

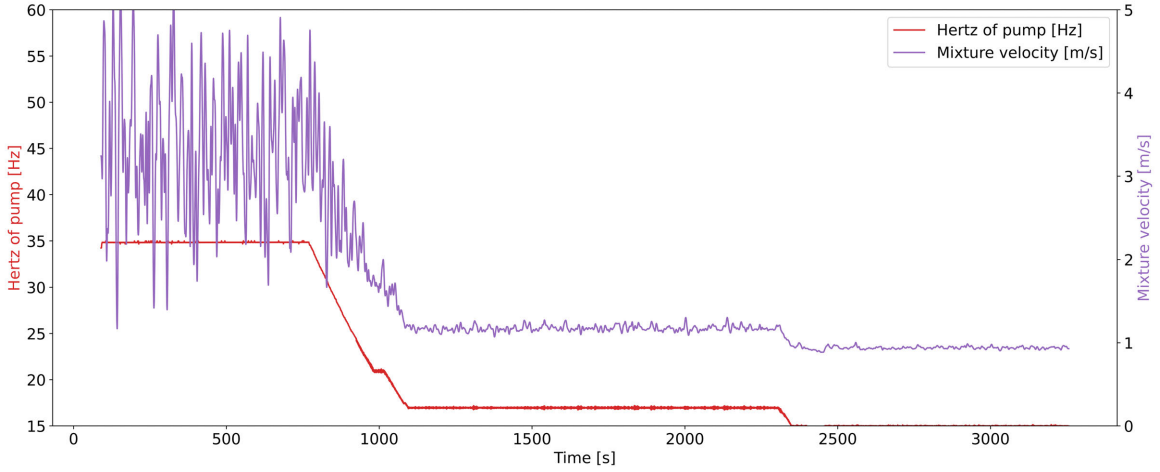

Figure B.2.6: Dorsilit 9 15v% test.

B.3 Dorsilit 8

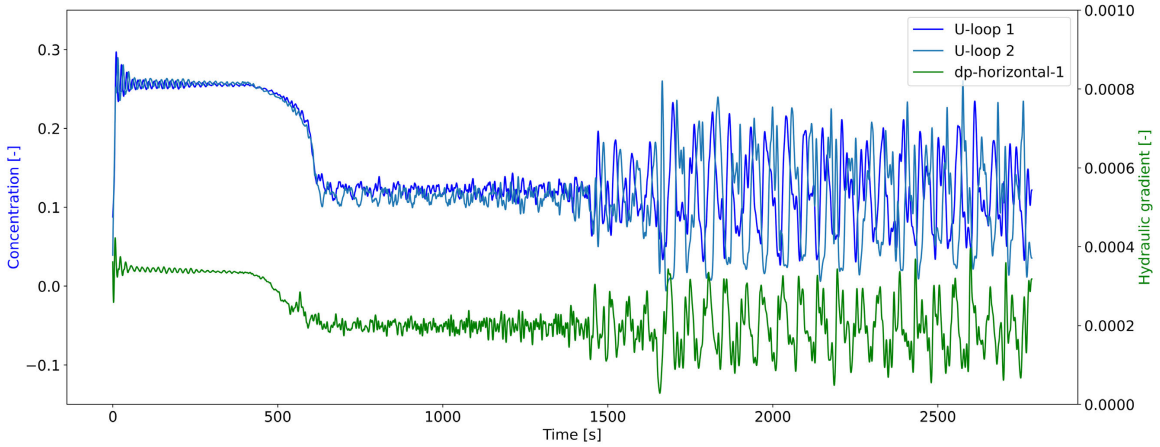

Figure B.3.1: Dorsilit 8 35v% test.

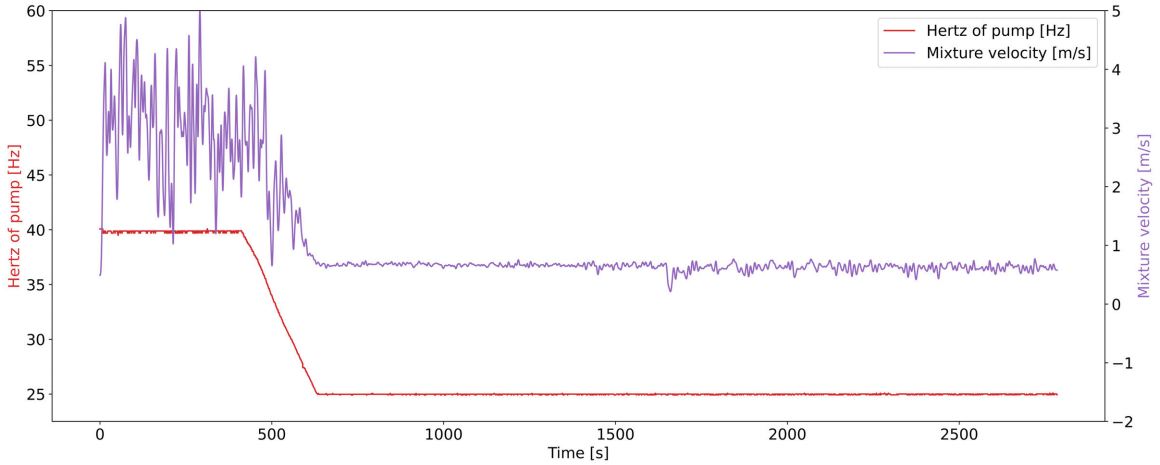

Figure B.3.2: Dorsilit 8 35v% test.

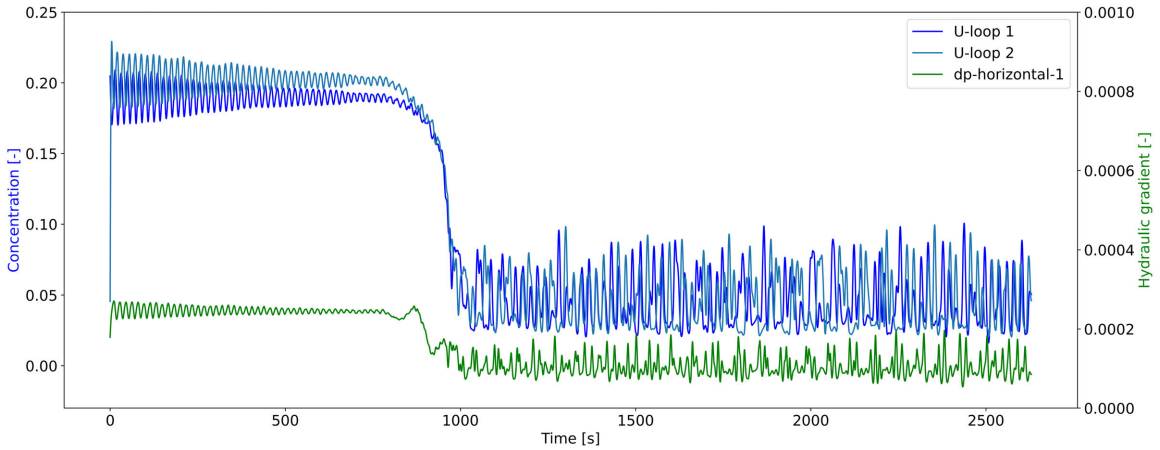

Figure B.3.3: Dorsilit 8 25v% test.

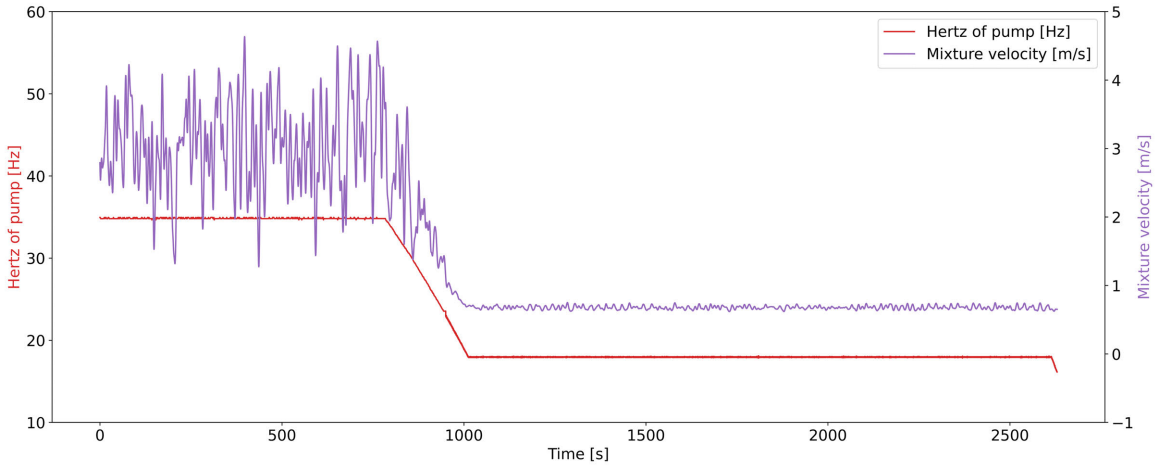

Figure B.3.4: Dorsilit 8 25v% test.

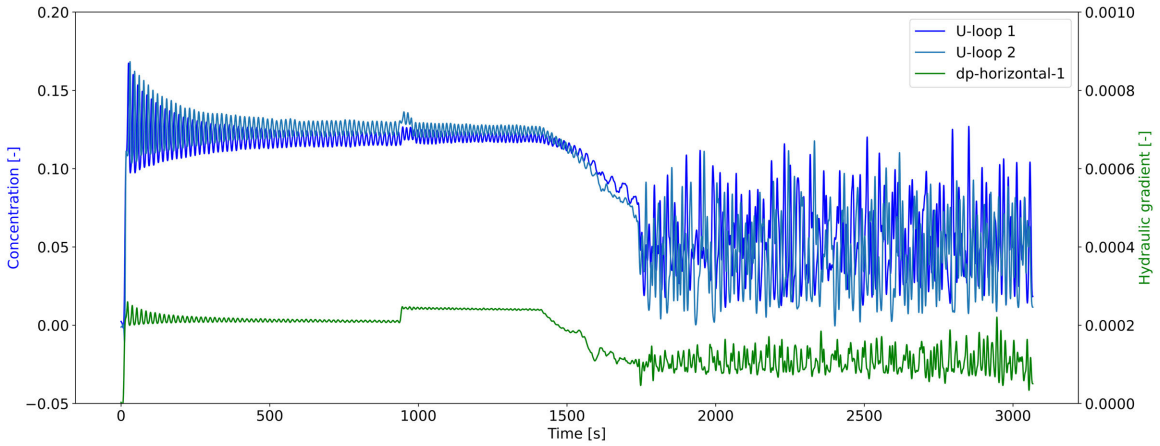

Figure B.3.5: Dorsilit 8 15v% test.

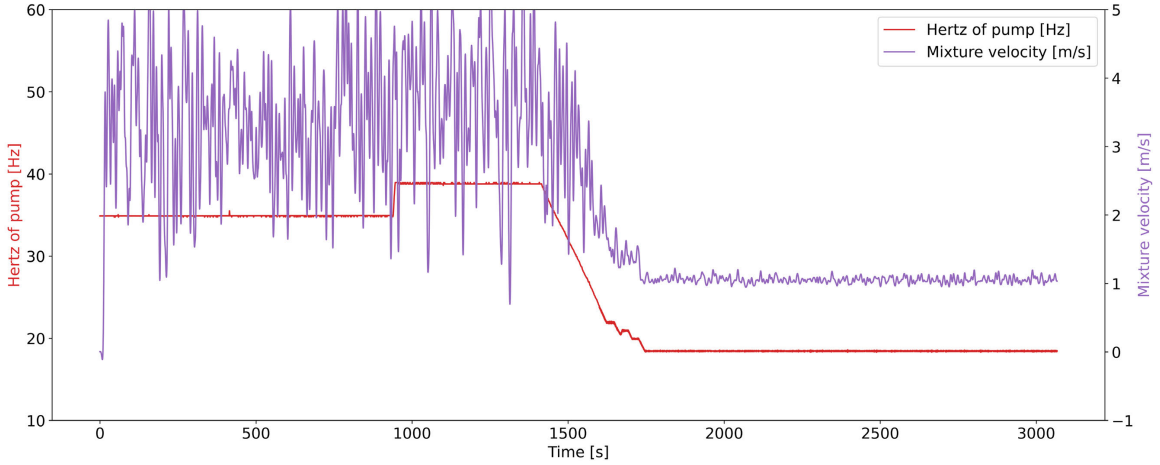

Figure B.3.6: Dorsilit 8 15v% test.

B.4 Dorsilit 7

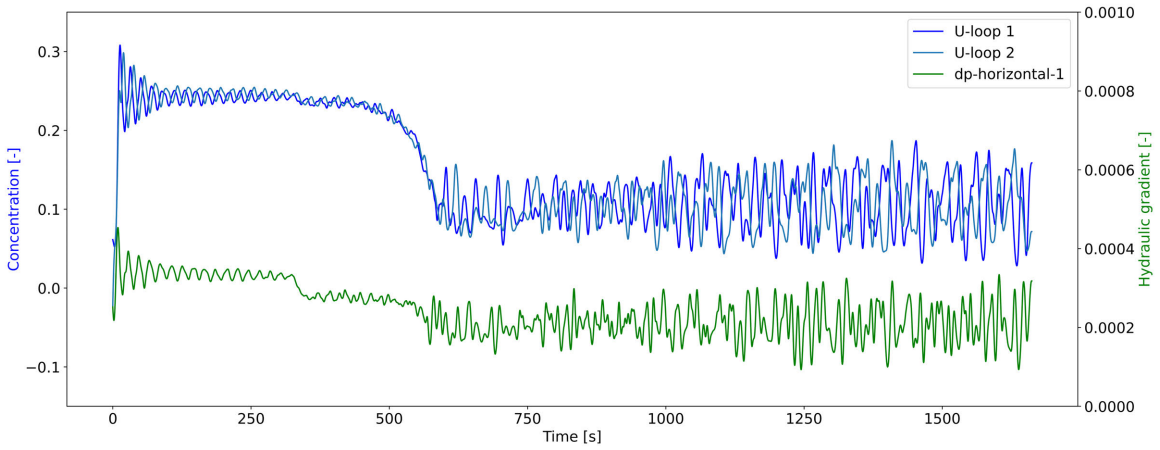

Figure B.4.1: Dorsilit 7 35v% test.

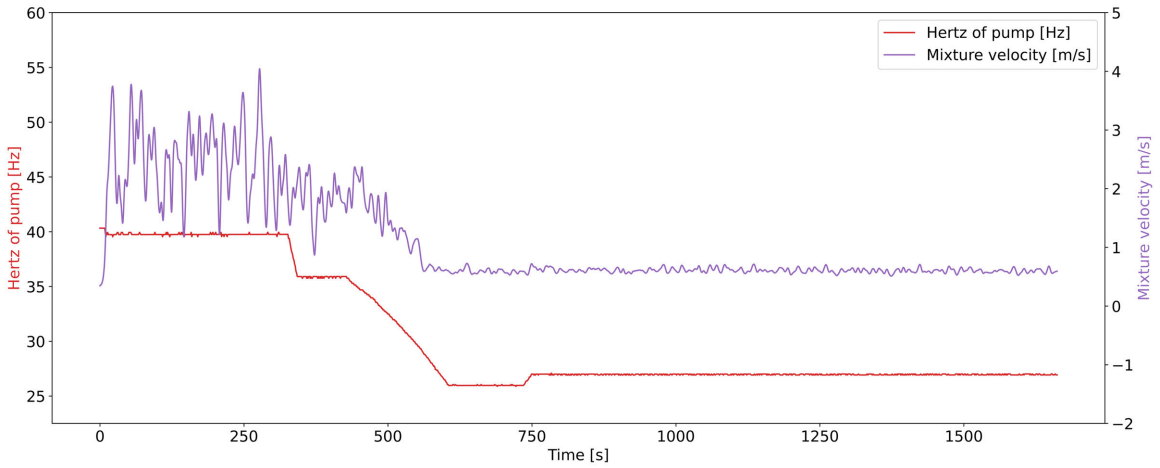

Figure B.4.2: Dorsilit 7 35v% test.

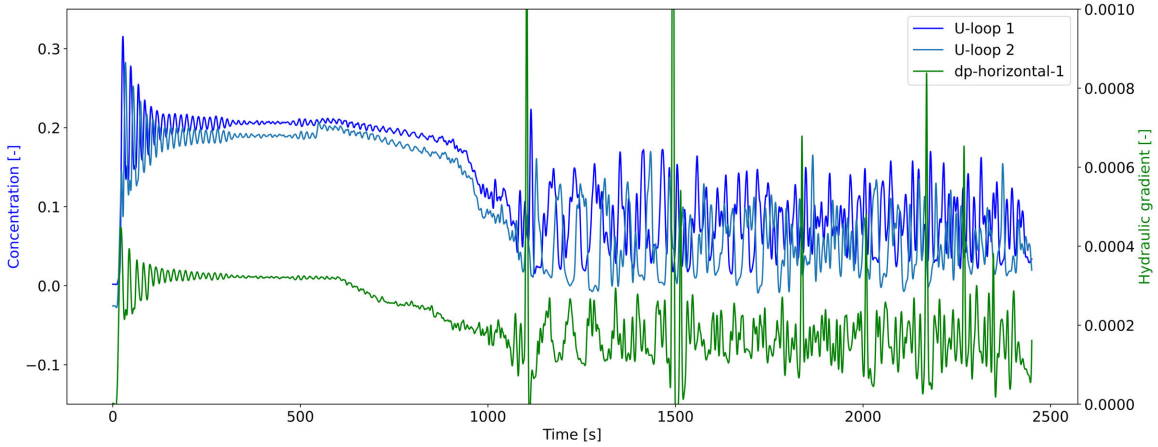

Figure B.4.3: Dorsilit 7 25v% test.

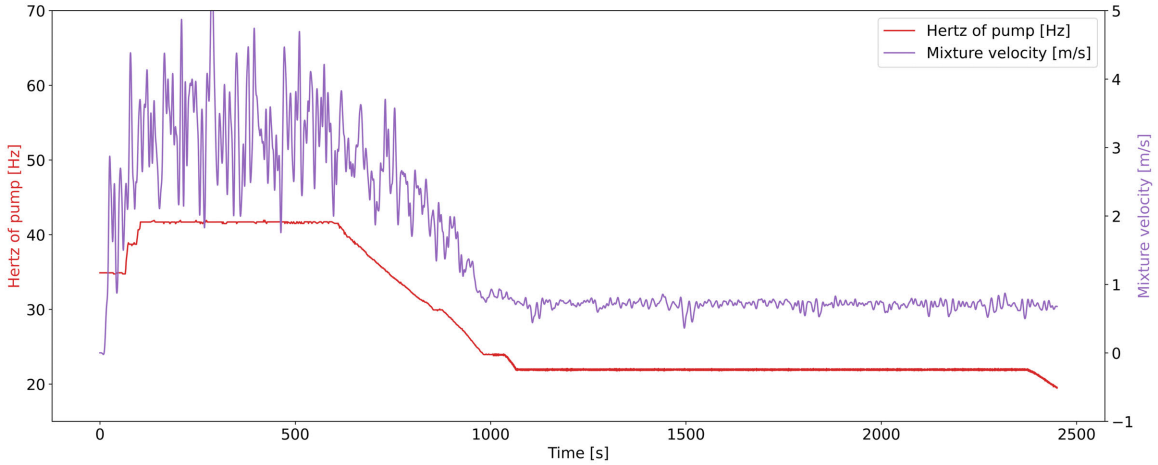

Figure B.4.4: Dorsilit 7 25v% test.

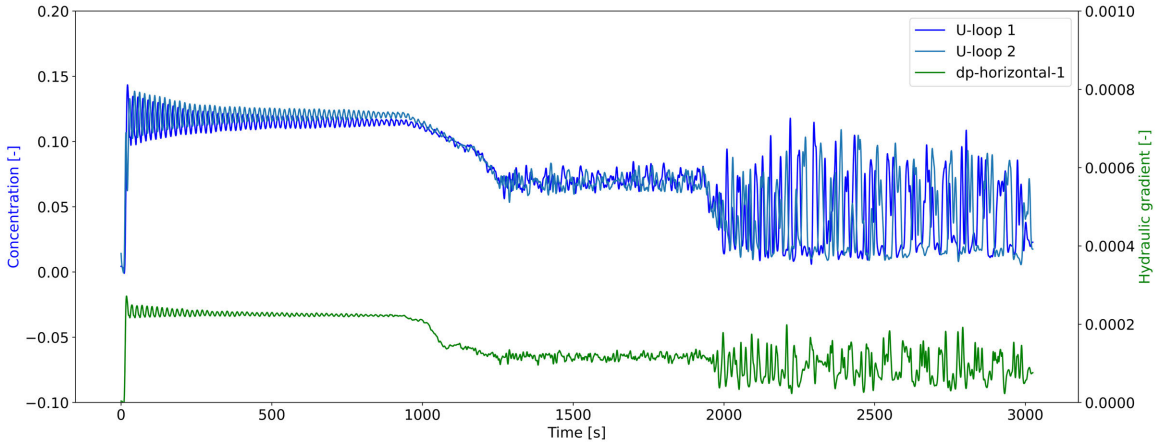

Figure B.4.5: Dorsilit 7 15v% test.

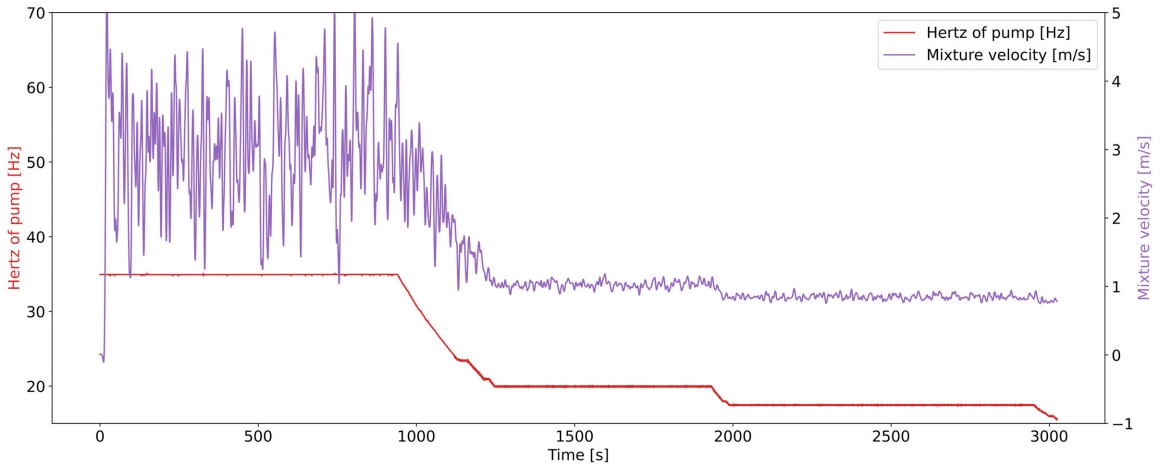

Figure B.4.6: Dorsilit 7 15v% test.

B.5 Dorsilit 7-8-9

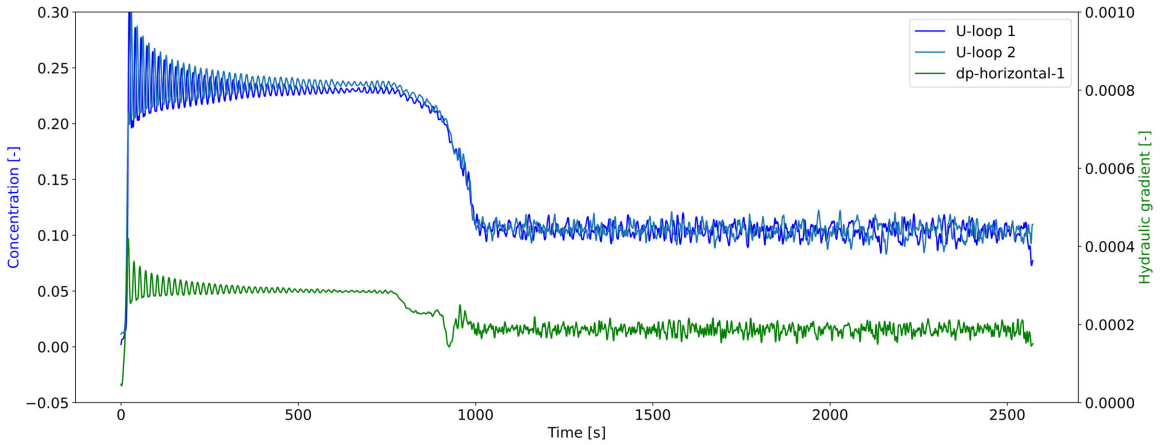

Figure B.5.1: Dorsilit 7-8-9 35v% test.

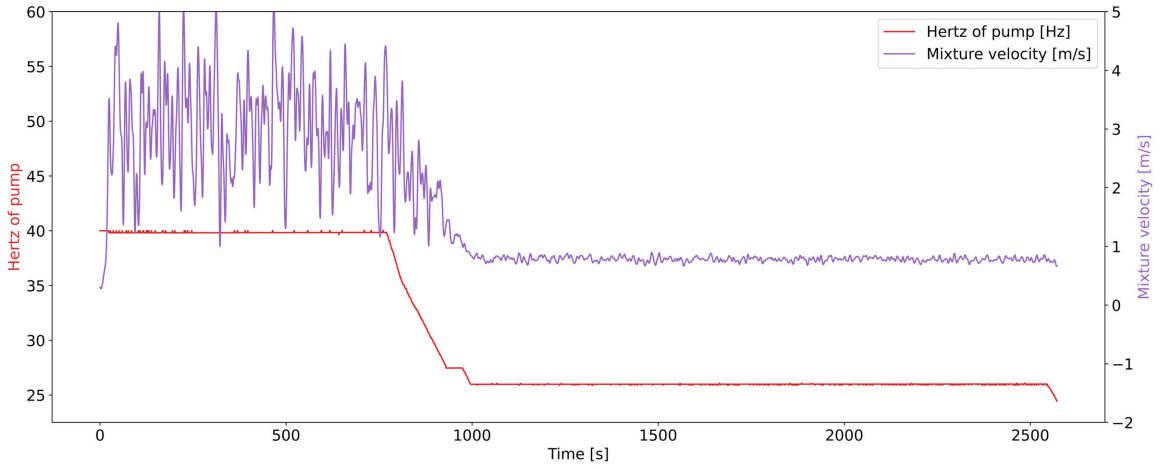

Figure B.5.2: Dorsilit 7-8-9 4 35v% test.

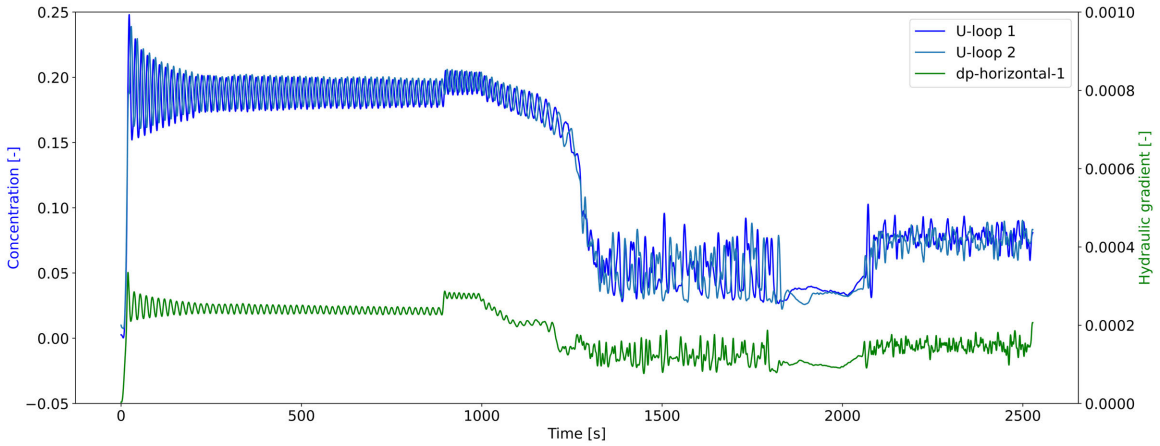

Figure B.5.3: Dorsilit 7-8-9 25v% test, temporary rpm change included.

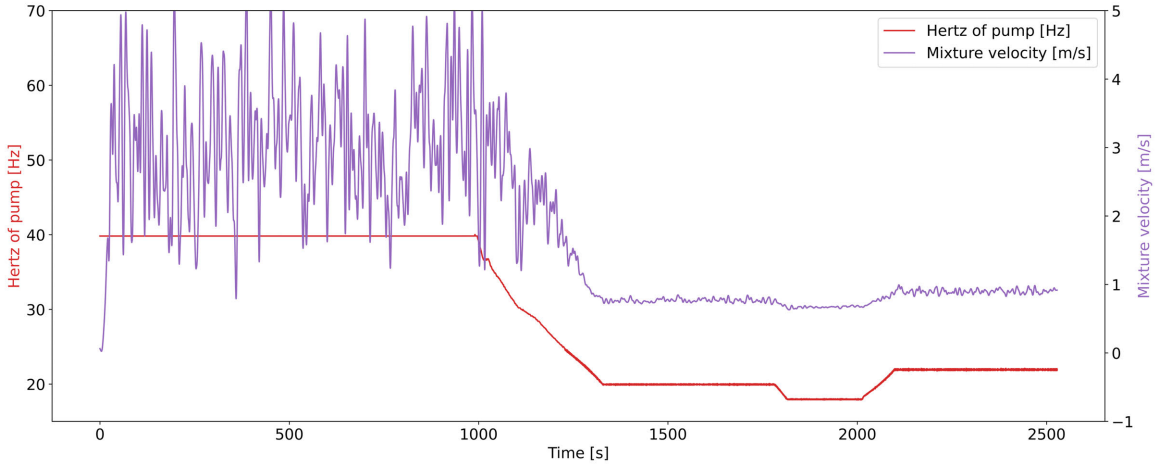

Figure B.5.4: Dorsilit 7-8-9 25v% test, temporary rpm change included.

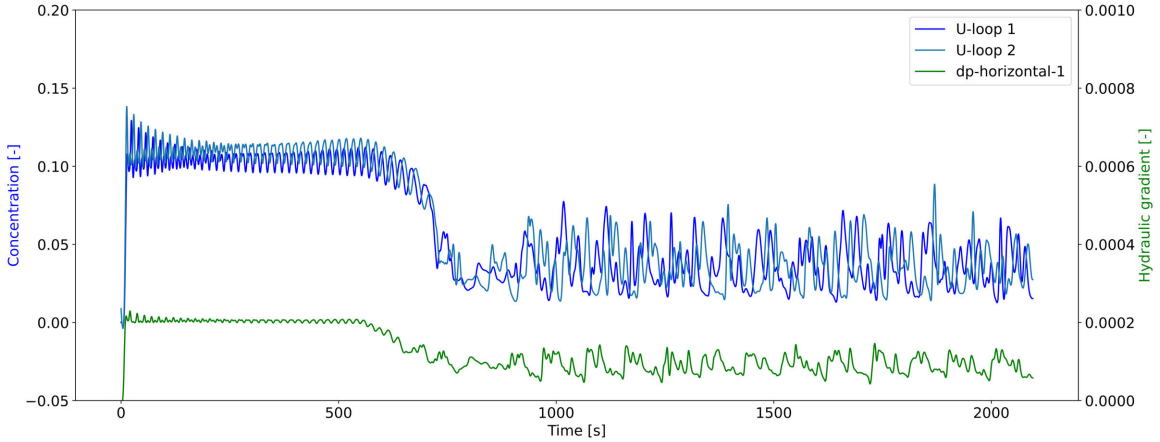

Figure B.5.5: Dorsilit 7-8-9 15v% test.

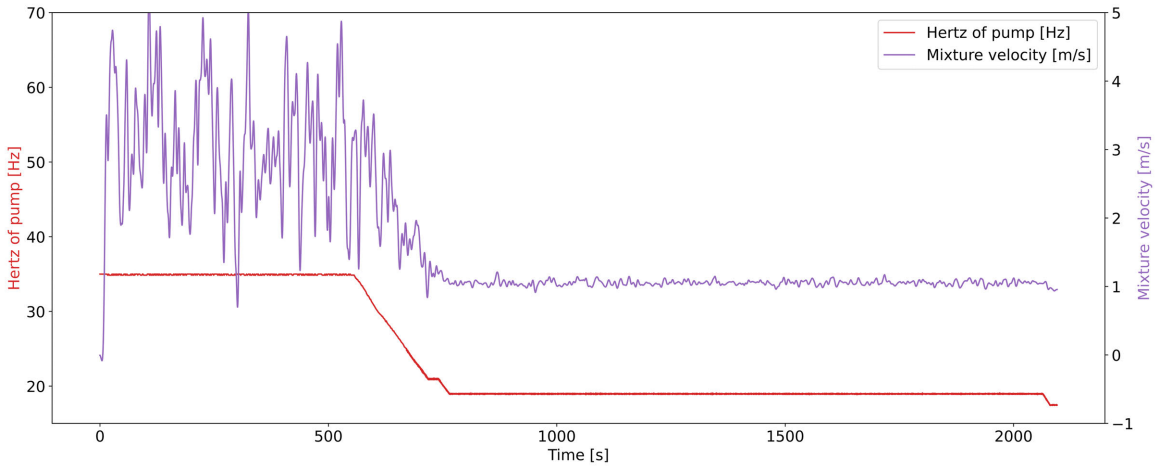

Figure B.5.6: Dorsilit 7-8-9 15v% test.

B.6 Pump curve

Table B.1: Pump curve test 1.

Pressure [kPa]	309.896	311.876	318.102	321.238	324.861	329.725
Mixture velocity [m/s]	5.39982	5.02068	3.18349	1.77062	0.897983	0.2306

Table B.2: Pump Curve test 2.

Pressure [kPa]	311.627	312.623	316.031	320.579	322.11	324.778
Mixture velocity [m/s]	5.33351	5.10617	4.19156	2.57218	1.83987	1.11571

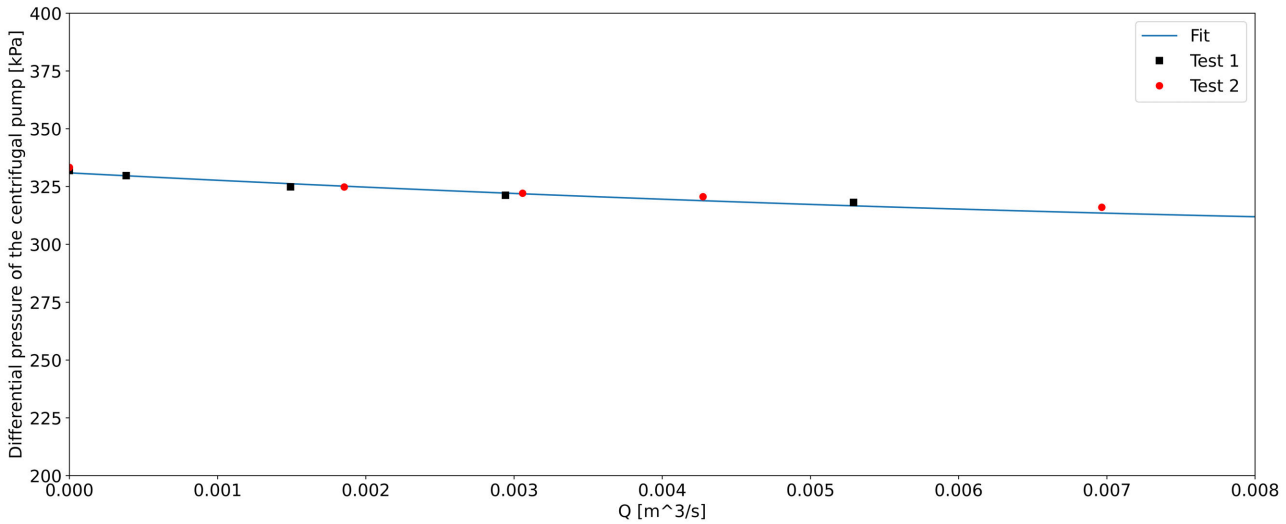

Figure B.6.1: Measured pump curve with the experimental loop.

B.7 Other

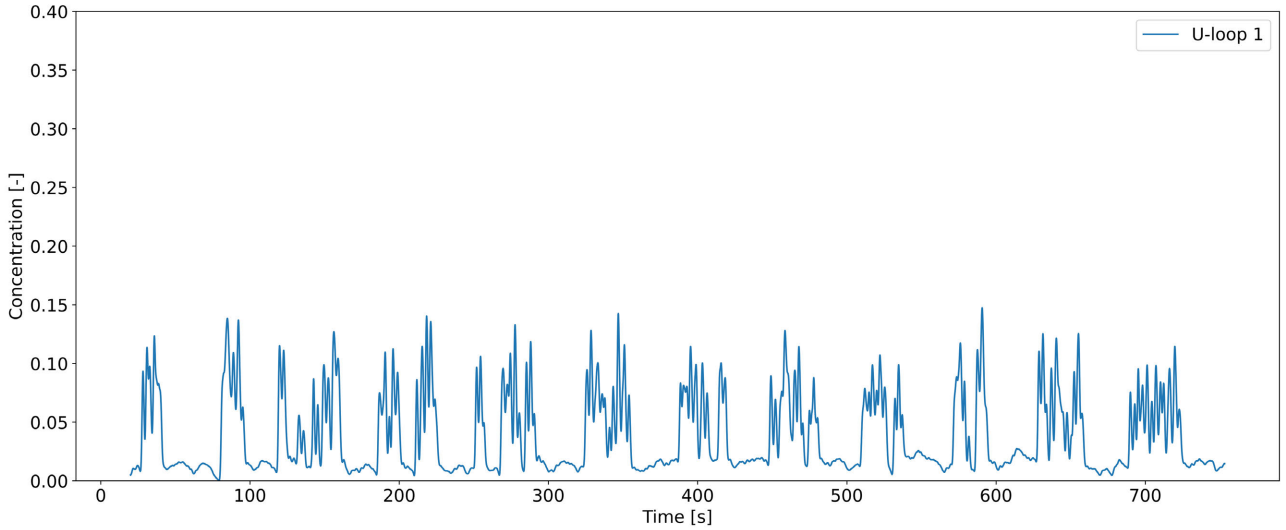

Figure B.7.1: Dorsilit 7 11v%, concentration over time, with multiple density waves and significant concentration gaps.

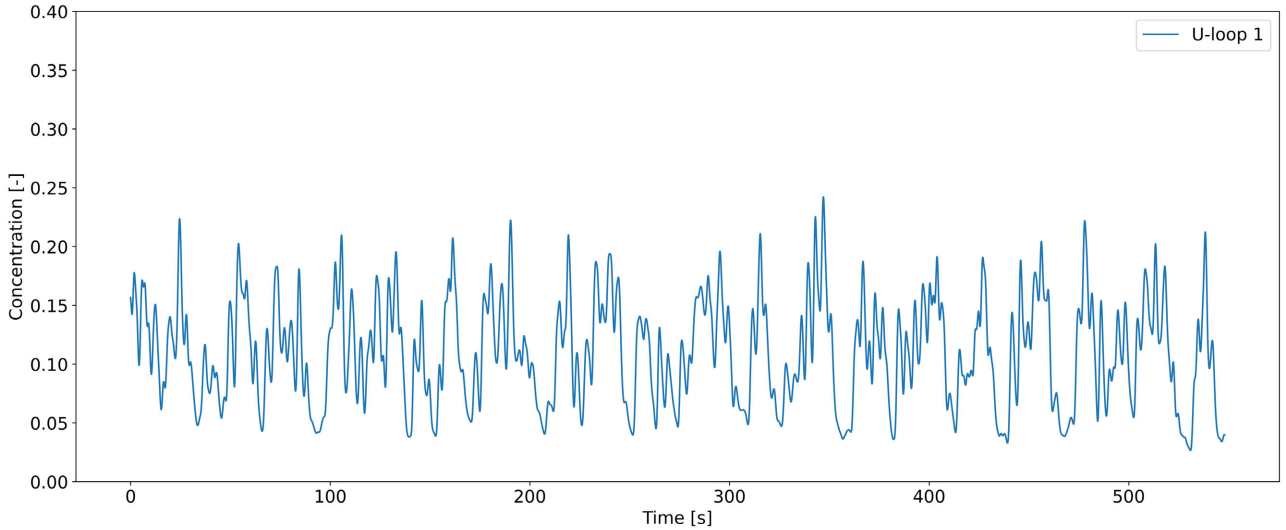

Figure B.7.2: Dorsilit 7 25v%, concentration over time, with multiple density waves.

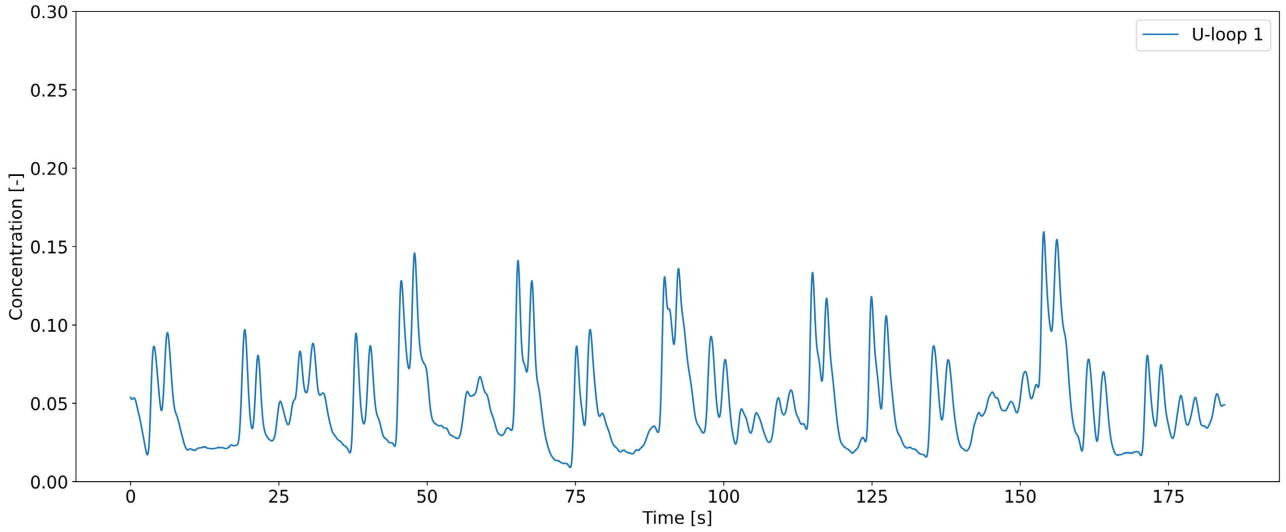

Figure B.7.3: Dorsilit 8 12v%, concentration over time, with multiple density waves and significant concentration gaps.

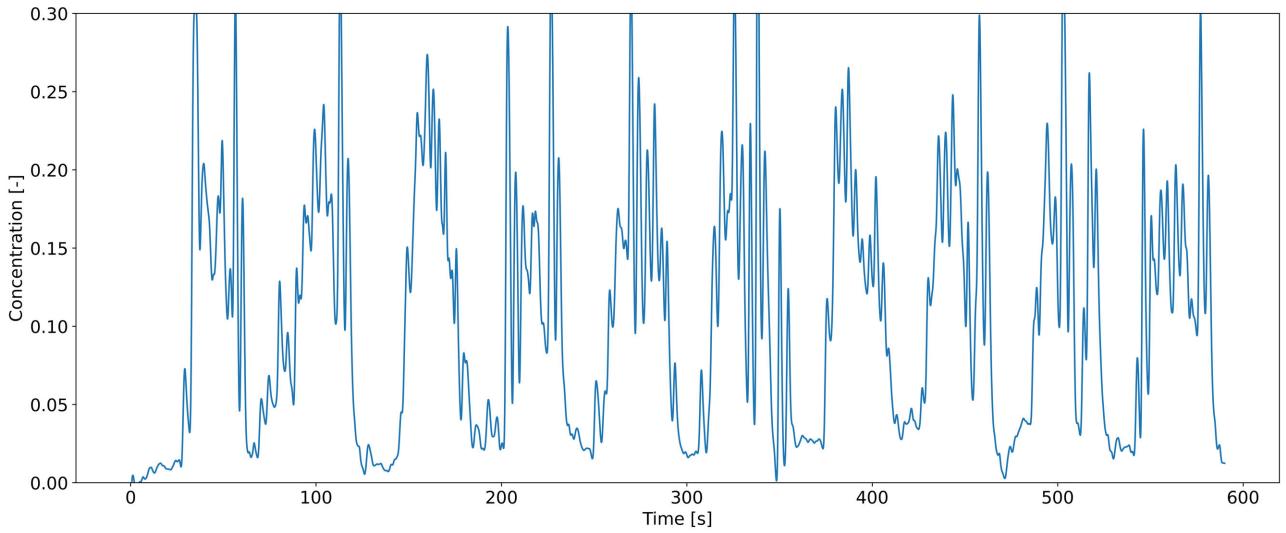

Figure B.7.4: Dorsilit 8 25v%, concentration over time, with multiple density waves.